DSPE MIKRONIEK
2020 (VOL. 60) ISSUE 4
PROFESSIONAL JOURNAL ON PRECISION ENGINEERING

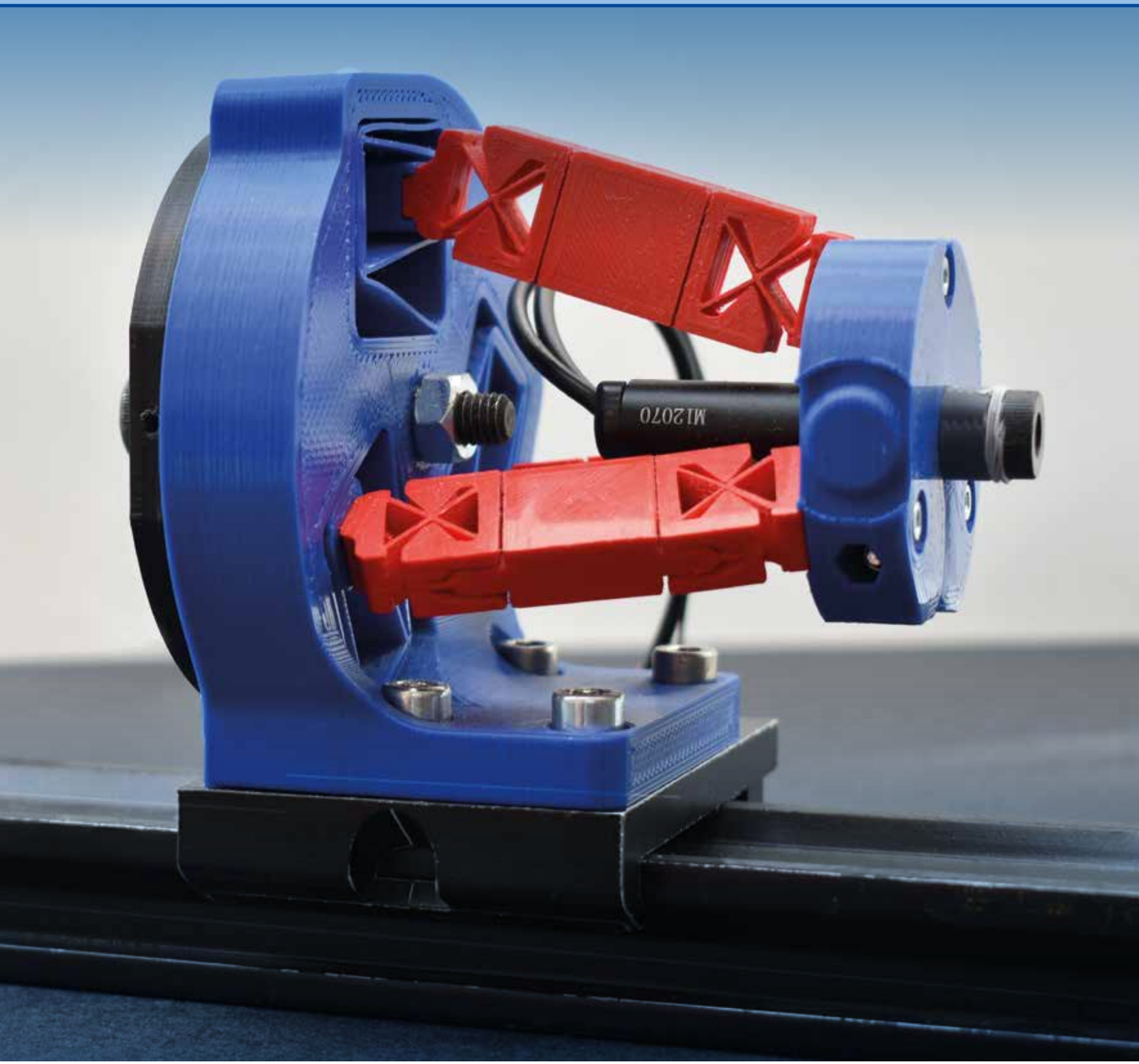

- THEME: MECHANISMS AND METAMATERIALS
- DIRECT OR INDIRECT DRIVE? THAT'S THE QUESTION
- INVESTIGATING THE INDUSTRIAL FEASIBILITY OF FLEXURES
- REPORT OF EUSPEN'S VERY FIRST VIRTUAL CONFERENCE

MIKRONIEK IS A PUBLICATION OF THE DUTCH SOCIETY FOR PRECISION ENGINEERING – WWW.DSPE.NL

PUBLICATION INFORMATION

Objective
Professional journal on precision engineering and the official organ of DSPE, the Dutch Society for Precision Engineering. Mikroniek provides current information about scientific, technical and business developments in the fields of precision engineering, mechatronics and optics. The journal is read by researchers and professionals in charge of the development and realisation of advanced precision machinery.

DSPE
YOUR PRECISION PORTAL

Publisher
DSPE
Annemarie Schrauwen
High Tech Campus 1, 5656 AE Eindhoven
PO Box 80036, 5600 JW Eindhoven
info@dspe.nl, www.dspe.nl

Editor
Hans van Eerden, hans.vaneerden@dspe.nl

Advertising canvasser
Gerrit Kulsdom, Sales & Services
+31 (0)229 – 211 211, gerrit@salesandservices.nl

Design and realisation
Drukkerij Snep, Eindhoven
+31 (0)40 – 251 99 29, info@snep.nl

Subscription
Mikroniek is for DSPE members only.
DSPE membership is open to institutes, companies, self-employed professionals and private persons, and starts at € 80.00 (excl. VAT) per year.

Mikroniek appears six times a year.

ISSN 0026-3699

The cover photo (featuring a spherical mechanism with adjustable centre of rotation) by Irene van Eerden is courtesy of Demcon. Read the article on page 10 ff.

IN THIS ISSUE

THEME: MECHANISMS AND METAMATERIALS

05
Tailored properties
Compliant mechanisms can be designed such that mechanical metamaterials with tailored properties are obtained.

10
Spherical mechanism with adjustable centre of rotation
Deflection of an end-effector using specially designed flexures integrated in the legs of a trapezoidal mechanism.

15
Potential of metamaterials for high-tech systems
The progress in additive manufacturing provides increasing design freedom to overcome hurdles in current mechatronic system design.

21
Kinematic redundancy
Multi-degree-of-freedom parallel mechanisms that retain the desirable properties of conventional parallel mechanisms while having large rotational workspaces.

26
Direct or indirect drive? That's the question
A pragmatic implementation of an (in)direct-drive actuator that is self-guided and compliant in multiple passive directions.

34
Investigating the industrial feasibility of flexures
Design, manufacturing and validation of a long-range flexure mechanism that serves as the elbow hinge in a crank-slider manipulator for a wafer-handling robot.

40
Dynamic balance of finitely stiff mechanisms
A partial balancing solution to counteract the effect of link flexibility in a 2-DoF delta-type robot.

45
Event report – Euspen's very first virtual conference
The euspen Conference – this year a virtual online web-conference – once again attracted high-level interest from the precision engineering community.

FEATURES

04 EDITORIAL
Bas Overvelde, scientific group leader of the Soft Robotic Matter Group at AMOLF, on the potential of mechanical metamaterials with tuneable properties.

33 UPCOMING EVENTS
Including: Precision Fair 2020.

48 ECP2 COURSE CALENDAR
Overview of European Certified Precision Engineering courses.

49 NEWS
Including: DSPE Knowledge Day on Engineering for Contamination Control.

FROM MECHANISMS TO MATERIALS

In engineering applications, the choice to use certain materials depends mostly on their suitability due to their molecular composition. With the arrival of composite materials, material properties no longer only depend on their chemistry, but also on their design. For example, stiff – yet light – materials can be made by carefully layering polymer sheets with different fibre orientations. Still, these materials have fixed properties that do not change over time. To save valuable space, high-tech applications could benefit from materials with tuneable properties, in which material behaviours such as stiffness, permeability and heat or electrical conductivity are tuned on-demand to meet certain requirements. While such materials are yet to appear on the market, the last years have seen an increasing effort from the academic community to develop and design such materials.

One particular class of materials that we are researching in the Soft Robotic Matter Group at AMOLF is called mechanical metamaterials. These metamaterials are designed such that they can exhibit internal shape changes, often the result of distributed mechanisms. The iconic example that kick-started this field is a mechanism consisting only of rotating squares that are placed in a checkerboard pattern and connected at their corners. When triggered, this porous sheet continuously contracts in both directions. From a material point of view, such a mechanism has a negative Poisson's ratio, meaning that it expands transversely under an axial strain; this is a property not often seen in nature. Importantly, the underlying mechanical laws are scale-independent, meaning that such a mechanism can be scaled up to an architectural scale, or scaled down to material sizes where the patterns can no longer be seen with the naked eye.

While this opens up a world of possibilities, the challenge is to come up with structural designs that exhibit interesting – and useful – properties. Here, origami turned out to be a useful source of inspiration. For example, in our group we took inspiration from a modular origami technique called 'snapology', and used it to design reconfigurable cellular metamaterials with tuneable stiffness, porosity, and acoustic properties.

I believe that an important next step in the development of mechanical metamaterials should be application-driven. Opportunities to apply these materials range from prosthetics with active force control, to tuneable photonic systems. For that, there are two directions that need particular attention. On the one hand, we need to be able to design materials with specific and predefined functionalities; in other words, we need to be able to solve the inverse problem of design. This is particularly challenging for these tuneable materials with often nonlinear behaviour. On the other hand, efforts should be directed at developing efficient and cost-effective fabrication strategies. These fabrication strategies will set important constraints on the design of the internal structure.

My hope is that the coming years will see an increasing interest and involvement from industry towards the development of mechanical metamaterials, to explore the potential of these new materials in practice.

Bas Overvelde
Scientific group leader of the Soft Robotic Matter Group, AMOLF
overvelde@amolf.nl, www.overvelde.com

TAILORED PROPERTIES

Mechanical metamaterials are engineered materials whose bulk mechanical properties are determined by their structure. In this way, material properties can be engineered so that they extend beyond what is found in nature. For many mechanical metamaterials, there is a compliant mechanism leading to their unusual bulk properties. Here, we explore the problem of designing these mechanisms such that a metamaterial with tailored properties is obtained.

FREEK BROEREN, VOLKERT VAN DER WIJK AND JUST HERDER

Mechanical metamaterials can be created to have a large range of curious and novel material properties, even extending beyond those found in nature. These range from a negative Poisson's ratio [1] to a stiffness that is unusually high for its weight [2] or even a negative stiffness [3]. This is achieved by altering the material in such a way that the structure, and not the constituent material, is the dominant factor determining the material's bulk properties.

Many mechanical metamaterials rely on the bending of slender parts within the metamaterial structure to obtain these properties. They are often made of a single material, with smartly designed pores to allow for internal deformations. As the predominant internal deformation in these structures is the bending of slender elements, these metamaterials are often referred to as bending-dominated [4].

As these metamaterials deform by the bending of their internal parts, they are very similar to compliant mechanisms. Therefore, when designing mechanical metamaterials, we can make use of some well-known tools for designing compliant mechanisms. Here, we will use the Pseudo-Rigid Body method [5] to design mechanical metamaterials. This method allows us to divide the design process into three distinct steps:

- Firstly, we design a (periodic) linkage that has the desired kinematic properties.
- Secondly, we assign a stiffness to each hinge in the linkage that corresponds to the force-deflection behaviour and/or overall stiffness profile that we want.
- Lastly, we use the techniques from pseudo-rigid-body modelling to convert the linkage, including the hinge stiffnesses, to a periodic compliant mechanism. By tiling this mechanism in two or three dimensions, we obtain a mechanical metamaterial with the desired properties.

In the following, we will mainly look at the first step of this process and investigate how mechanical metamaterials with a specified Poisson's ratio can be designed. For simplicity, we have limited ourselves to static material properties, namely Poisson's ratio and material stiffness, and will only consider planar linkages and thus (quasi) 2D metamaterials.

Furthermore, we have chosen to consider only single-DoF (DoF = degree of freedom) linkages. This approach has two advantages: firstly, it keeps the design and the calculations of the effective properties simpler; secondly, by having a single-DoF mechanism underlying the designed mechanical metamaterial, it will behave more predictably when loaded.

Periodicity

Before we examine the design of a mechanical metamaterial, let us first look at what distinguishes a bending-dominated mechanical metamaterial from a compliant mechanism. Both have specific functions that are determined by the bending of slender elements, so at first glance they seem to be quite similar.

The difference between compliant mechanisms and metamaterials lies in the fact that mechanical metamaterials are designed to be used as materials. They are the building blocks from which other things, such as machine parts or supports, can be made. This means that they must allow for shaping and cutting without losing the designed bulk properties. This is inherently different to (compliant) mechanisms. When a mechanism is cut, or a part is removed, it will have an effect on its properties. In fact, most of the time it will stop working altogether.

In order to allow a metamaterial – actually, a metamaterial-based object – to be sculpted and shaped, the designed bulk properties must be distributed throughout the material (object). This is often achieved by designing them to be periodic. Periodic structures consist of a unit cell, a minimal volume element, that is copied and translated to fill the complete volume of the material. In this way, only a single unit cell needs to be designed to have the desired properties of the bulk metamaterial. The resulting periodic structure can then be cut and shaped to its final shape, as long as the features of the final design are no smaller than the unit cell

AUTHORS' NOTE

Freek Broeren (Ph.D. candidate), Volkert van der Wijk (assistant professor) and Just Herder (professor) are all associated with the Precision and Microsystems Engineering (PME) department of Delft University of Technology (NL). The research presented here was conducted within the framework of the Nano Engineering Research Initiative (NERI).

f.g.j.broeren@tudelft.nl
www.pme.tudelft.nl
www.tudelft.nl/neri

dimensions. The size of the unit cell is determined by the complexity of the design and the accuracy of the manufacturing method used.
When designing a unit cell, care must be taken to allow its properties to be maintained when tiled. When the unit cell is copied and translated, it must be done such that the links at the edges of the unit cells align and that the motion is not obstructed by this coupling. To do this, we design and analyse the unit cell using 'periodic boundary conditions'. These boundary conditions correspond to envisioning the unit cell as lying on a torus, connecting each set of opposite edges. Therefore, each node on an edge must have a corresponding node on the opposite edge and the motions of these nodes will be coupled.

Poisson's ratio as a transmission

The main kinematic property that can be designed in mechanical metamaterials is Poisson's ratio (ν). Effectively, Poisson's ratio is a transmission between two orthogonal directions. When a uniaxial load is applied to a material, most natural materials will expand in the orthogonal directions. The negative ratio between the applied strain and the resulting strain in the orthogonal directions is Poisson's ratio:

$$\nu = -\varepsilon_y / \varepsilon_x$$

The negative sign here indicates that when a material has a positive Poisson's ratio, it will expand in the orthogonal directions, as a response to a uniaxial compression. Most natural materials have a positive Poisson's ratio. For example, rubber has a Poisson's ratio of approximately 0.5, and steel typically has a Poisson's ratio around 0.3.

Mechanical metamaterials can also be designed to have negative Poisson's ratios. This means that when these metamaterials are compressed, they will shrink in the orthogonal directions. Isotropic (meta)materials can have any Poisson's ratio between –1 and 0.5, and values outside this are possible for non-isotropic materials.

Let us now look at how to design this behaviour into a periodic linkage. For this, we take a square patch, which will be our unit cell, and enforce periodic boundary conditions on it. We place the outermost nodes of the linkage on the border of this patch. When the linkage moves, the borders of the patch will move along with the connected nodes, and in this way the height and width of the unit cell change. We will express the changes in the height and width of the unit cell as differential strains:

$$\varepsilon_W = \partial W / W$$

$$\varepsilon_H = \partial H / H$$

Here, H and W are the height and width of the unit cell, respectively, and the strains are denoted by ε. From these strains, we can express Poisson's ratio and, by rewriting this equation, express the transmission between the height and width in terms of this ratio [6]:

$$\nu = -(W/H)\,\partial H / \partial W$$

$$W = CH^{-\nu}$$

Here, C is an arbitrary constant determining the initial ratio between the width and the height of the patch. In our case, $C = 1$, since the initial patch was square. Now that we have this equation, the design of a linkage to serve as the basis for a metamaterial with a desired Poisson's ratio becomes a search for a linkage that follows this transmission function. This problem could be solved using computational methods, for example optimising a linkage to fit this behaviour, but luckily a large body of literature on transmission linkages already exists. Let us look at two examples based on classical transmission linkages.

Poisson's ratio of –1 based on the pantograph

First, we will design a linkage for the most negative Poisson's ratio that can be achieved in an isotropic metamaterial: –1. Substituting this value into the equation, we see that we need:

$$W = H$$

The width and height of the patch should be equal and remain that way when the linkage moves. This can be achieved with a pantograph mechanism (Figure 1). This type of mechanism is well known for preserving shapes and has historically been used to copy drawings and writing. We place a pantograph mechanism inside our square patch, as is shown in Figure 2. Throughout the motion of this linkage, the height and width of our patch will be equal and we will therefore have a Poisson's ratio of –1 for large deformations.

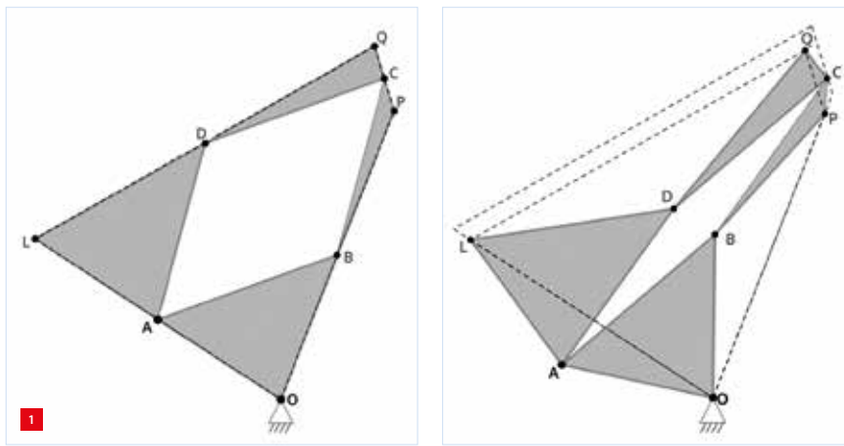

A pantograph linkage preserves the shape spanned by its outer points (O, P, Q, L), while allowing it to scale.

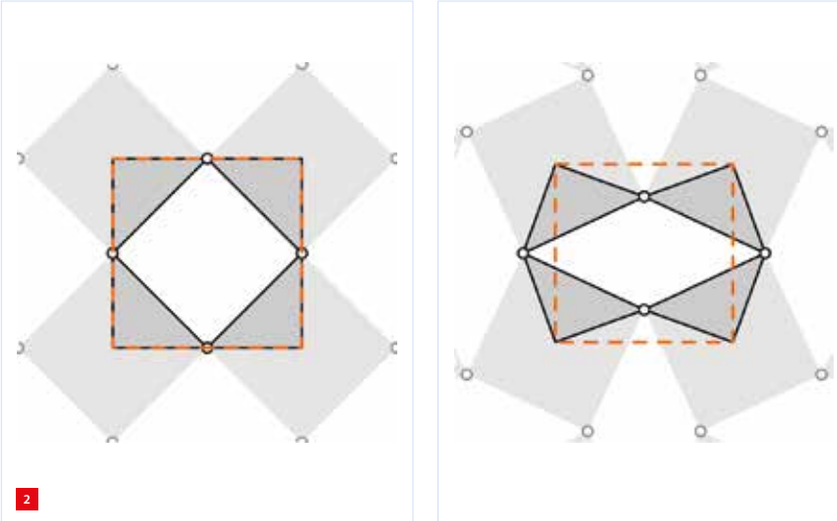

2

We create a unit cell (indicated by an orange dashed line) based on the pantograph such that it allows the unit cell to change its size, but keep its shape.

This structure allows for an easy conversion to a monolithic compliant metamaterial. By replacing the revolute joints by large notch-joints, we obtain the extensively studied 'Holey Sheet' metamaterial shown in Figure 3. Structures such as this have been researched for their ability to become more compact under any applied deformation. This makes them useful in situations where devices have to be placed into tight spaces; for example with stents [7-9]. Also, the compaction under deformations makes these structures exceptional at absorbing shocks, since more of the structure's mass will move towards the impacted area [10].

Poisson's ratio of 1 based on the inversor

What if, however, we want a metamaterial that does the opposite? Can we create a material that, instead of keeping its shape under deformations, preserves its area? In that case, we would need a positive Poisson's ratio of 1, and therefore:

$$W = H^{-1}$$

Such a structure would preserve its area at all times, as $W \times H = 1$. Again, we can find a suitable linkage in

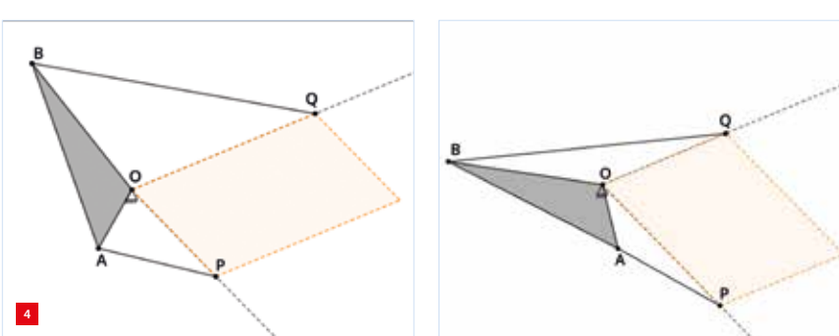

4

The inversor linkage constrains the motions of P and Q such that the product of the distances OP and OQ (the highlighted area) remains constant.

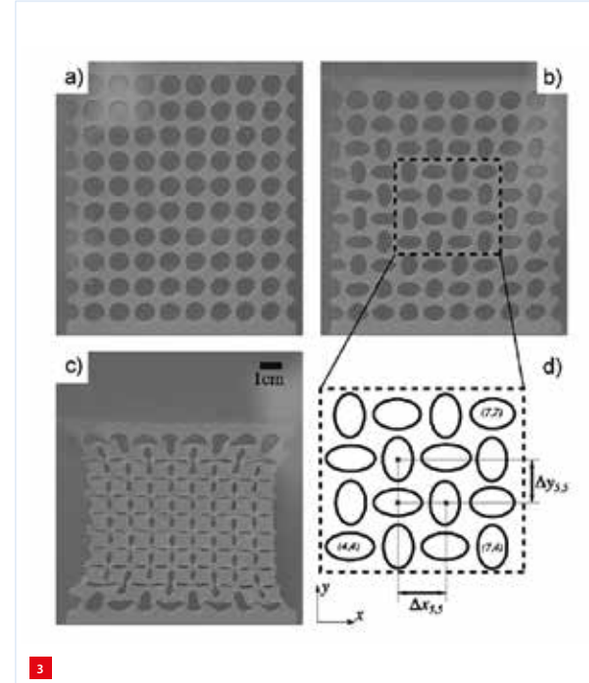

3

A monolithic adaptation of the pantograph-based metamaterial, commonly referred to as a 'Holey Sheet'. Image from [12].

literature: the inversor. We adapt the classical inversor shown in Figure 4, such that the distances *OP* and *OQ* are orthogonal and mirror the linkage to form the tileable linkage shown in Figure 5. This linkage consists of two square bodies that are coupled at their centres with a revolute joint. From these bodies, four sets of two links connect to the sides of the unit cell, creating four coupled four-bar linkages with one collective DoF.

The conversion of this linkage into a monolithic compliant mechanism is slightly more involved because the linkage consists of multiple layers. Here, we have chosen to replace the revolute joints within a layer by slender beams. The square bodies are replaced by hollow cylinders, which are connected by a set of three vertical leaf flexures. The resulting compliant design is shown in Figure 6. This metamaterial has been constructed using 3D printing. When compressed, this metamaterial extends proportionally in the orthogonal directions as is shown in Figure 7. The resulting mechanical metamaterial will preserve its area up to large deformations since, in the original linkage, the product of the distances *OP* and *OQ* is maintained. Therefore, its bulk modulus is substantially higher than its shear modulus and it will resist uniform compression.

Linkages for other Poisson's ratios

As the previous two examples show, Poisson's ratio can be designed in a linkage as a classical transmission between two orthogonal motions. The two examples discussed here have been designed such that the transmission is constant

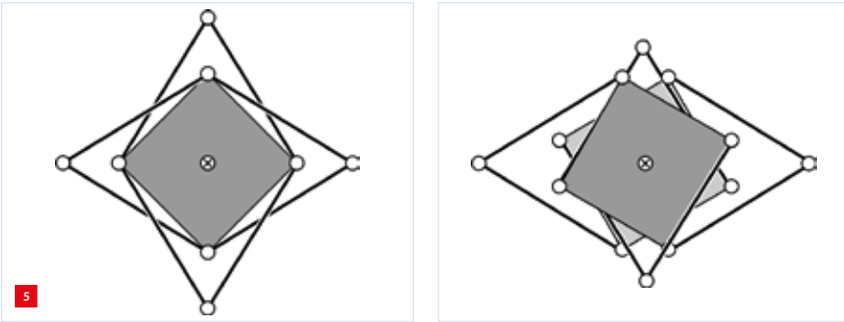

The inversor linkage is copied and mirrored along the horizontal and vertical axes to create a square-tileable linkage to serve as the unit cell for a metamaterial with Poisson's ratio 1.

for the whole range of the linkage's motion. This has the advantage that the resulting mechanical metamaterial has a constant Poisson's ratio up to large deformations. For most applications, however, this is not necessary. In those cases, a linkage could be optimised to achieve the approximate transmission ratio for the relevant deformations around the compliant mechanism's equilibrium only. This gives more freedom to the designer and will likely result in metamaterials that are easier to manufacture.

Stiffness design of mechanical metamaterials

The designs shown here consider only the kinematic properties of the structure and therefore the only material property that is designed for is Poisson's ratio. However, these structures will have a stiffness based on the geometries of the compliant implementations of the joints. By taking the stiffness of these joints into account in the design process, the stiffness of these structures could also be designed.

Furthermore, additional flexible elements that do not contribute to the kinematics, but do contribute to the stiffness, could be added. For instance, in the research by Florijn et al. [14], they used a mechanical metamaterial similar to the pantograph-based design shown in this article to create a multi-stable structure. This was done by adding

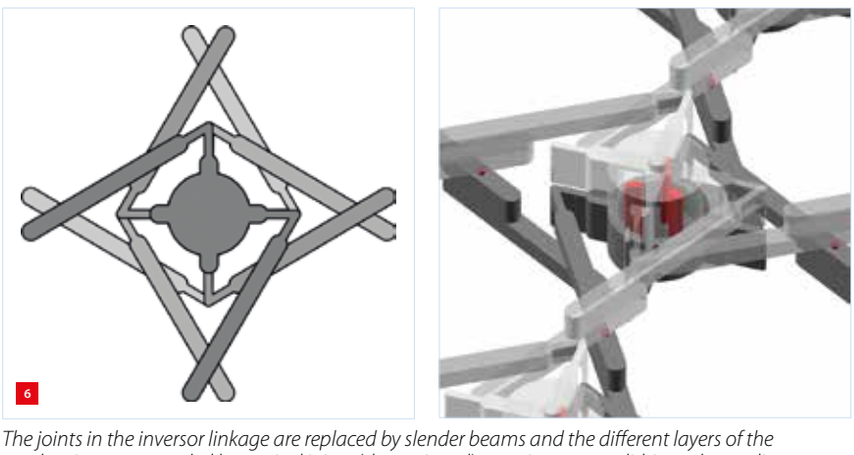

The joints in the inversor linkage are replaced by slender beams and the different layers of the mechanisms are coupled by vertical joints (shown in red), creating a monolithic and compliant metamaterial based on the inversor [13].

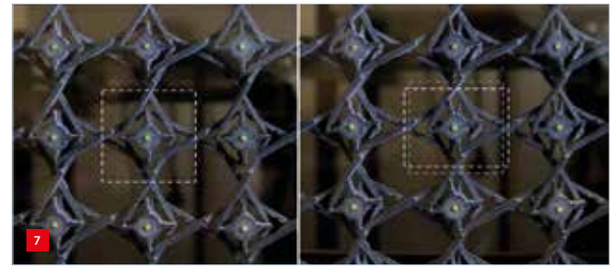

The inversor lattice has been realised experimentally. The left pane shows the initial state and the right pane shows it under 10% compressive strain.

global confinements to the structure. By adding this extra stiffness, they created regions of negative stiffness, where the structure would snap to the next stable state.

Conclusions

Mechanical metamaterials offer a promising route to previously unseen and unavailable material properties. The design process of these novel structures, however, can be difficult and has so far largely depended on the intuition and experience of the designer.

By using techniques from compliant mechanism design, specifically Pseudo-Rigid Body modelling, mechanical metamaterial design can be split into distinct steps, making the process easier to grasp and allowing for a more rational and directed design approach. Instead of having to design the complete structure from the start, the process begins by first constructing a linkage to have the desired kinematic properties. Afterwards, the stiffness of the structure can be designed by assigning stiffnesses to the hinges. Finally, a compliant embodiment of the linkage can be constructed using the replacement rules from the pseudo-rigid-body method.

By using this design process, mechanical metamaterials can be designed to order, tailoring the effective material properties to the intended application. This broadens the range of available material properties and can therefore give more freedom in designing machine parts. The applications of these tailored materials could include self-adapting clamps, adaptable supports or easy-to-place fittings and seals.

For future applications, these methods could also be used to design actuating and sensing components into the metamaterial. In this way, the material from which you make your components could also be used to measure or actuate your machine, allowing for a large degree of function integration.

REFERENCES

[1] X. Ren, R. Das, P. Tran, T.D. Ngo, and Y.M. Xie, "Auxetic metamaterials and structures: a review", *Smart Mater. Struct.*, vol. 27 (2), p. 023001, 2018.

[2] J.B. Berger, H.N.G. Wadley, and R.M. McMeeking, "Mechanical metamaterials at the theoretical limit of isotropic elastic stiffness", *Nature*, 543 (7646), pp. 533-537, 2017

[3] A. Rafsanjani, and D. Pasini, "Bistable auxetic mechanical metamaterials inspired by ancient geometric motifs", *Extreme Mechanics Letters*, 9, pp. 291-296, 2016.

[4] V. S. Deshpande, M. F. Ashby, and N. A. Fleck, "Foam topology: bending versus stretching dominated architectures", *Acta Mater.*, vol. 49 (6), pp. 1035-1040, Apr. 2001.

[5] C. Lusk, "Using Pseudo-Rigid Body Models", in L.L. Howell, et al. (eds), *Handbook of Compliant Mechanisms*, pp. 55-76, John Wiley & Sons, 2013.

[6] F.G.J. Broeren, J.L. Herder, and V. van der Wijk, "On the Synthesis of Periodic Linkages with a Specific Constant Poisson's Ratio", in: Uhl, T. (eds), *Advances in Mechanism and Machine Science, IFToMM WC 2019, Mechanisms and Machine Science*, vol. 73, pp. 249-257, Springer, 2019.

[7] M.N. Ali, and I.U. Rehman, "An Auxetic structure configured as oesophageal stent with potential to be used for palliative treatment of oesophageal cancer; development and in vitro mechanical analysis", *J. Mater. Sci. Mater. Med.*, vol. 22 (11), pp. 2573-2581, 2011.

[8] M.N. Ali, J.J.C. Busfield, and I.U. Rehman, "Auxetic oesophageal stents: structure and mechanical properties", *J. Mater. Sci. Mater. Med.*, vol. 25 (2), pp. 527-553, 2014.

[9] X. Ren, J. Shen, A. Ghaedizadeh, H. Tian, and Y.M. Xie, "A simple auxetic tubular structure with tuneable mechanical properties", *Smart Mater. Struct.*, vol. 25 (6), p. 065012, 2016.

[10] M. Sanami, N. Ravirala, K. Alderson, and A. Alderson, "Auxetic materials for sports applications", *Procedia Engineering*, vol. 72, pp. 453-458, 2014.

[11] I.I. Artobolevskii, *Mechanisms for the generation of plane curves*, Pergamon Press, 1964.

[12] K. Bertoldi, P.M. Reis, S. Willshaw, and T. Mullin, "Negative Poisson's Ratio Behavior Induced by an Elastic Instability", *Adv. Mater.*, vol. 22 (3), pp. 361-366, 2010.

[13] F.G.J. Broeren, V. van der Wijk, and Just L. Herder, "Rational design and experimental characterization of planar mechanical metamaterials with Poisson's ratio of 1", *in preparation*.

[14] B. Florijn, C. Coulais, and M. van Hecke, "Programmable Mechanical Metamaterials", *Phys. Rev. Lett.*, vol. 113 (17), p. 175503, 2014.

3D-PRINTED RCR-SHIFTER

A spherical mount has been designed to align the return optic in a Fizeau interferometer with a laser beam. Faster alignment and a smaller distortion can be achieved by rotating the lens around a remote centre such that the return optic remains aligned with the optical axis of the beam. The design was based on a trapezoidal mechanism with the addition that the remote centre of rotation (RCR) is not fixed, but can be adjusted by changing the orientation of the legs of the trapezoidal mechanism. Deflection of the end-effector of the mechanism is flexure-based, using specially designed flexures integrated in the legs. Measurements on a 3D-printed prototype demonstrated the applicability of the design.

KOEN SMELT

Introduction

Typical goniometer stages have a fixed remote centre of rotation (RCR) distance, which is optimal for lenses with matching focal distance. In that case, the mechanical axis of the return optic can be aligned to the optical axis of the light beam (see Figure 1). If the 'lens under test' is replaced by a lens with another focal length, the stacked gonio-stage is moved closer or further away from the interferometer to reflect the laser beam at the right distance. In that case, the RCR is no longer located at the lens centre, making it impossible to align the mechanical axis of the return optic to the optical axis. To accommodate a range of lenses with different focal lengths, a spherical manipulator is presented, of which the RCR can shift from 45 mm up to infinity (i.e. pure translation). Effectively, this spherical mechanism functions as a stacked gonio-stage with an adjustable RCR. Table 1 lists the main requirements.

The proposed design (Figure 2) consists of three flexure-based legs that connect to the end-effector in a trapezoidal manner. The support lines of these three legs intersect in a common point, allowing for a spherical movement of the end-effector around this point. A radial displacement of the base connections of the legs results in the desired shift of the RCR along the centre-line of the mechanism.

AUTHOR'S NOTE

Koen Smelt is a mechanical engineer at Demcon in Enschede (NL). He performed the work described in this article at Demcon Focal for his M.Sc. work in the Precision Engineering group of the Faculty of Engineering Technology at the University of Twente (UT), Enschede (NL).

koen.smelt@demcon.com
www.demcon.com
www.utwente.nl/en/et/ms3/research-chairs/pe

Table 1
Main requirements for the spherical manipulator.

Range of motion end-effector	±3° (±2 mm lateral motion)
Range distance to RCR	Infinity to 45 mm
Accuracy of spherical motion	5 µm in lateral direction
Accuracy of RCR manipulation	Max. 15% deviation of desired RCR distance
Support stiffness of end-effector	Min. 12 Nm/rad
Torsion stiffness of end-effector	Max. 0.2 Nm/rad
Actuation stiffness	Max. 20 N/mm

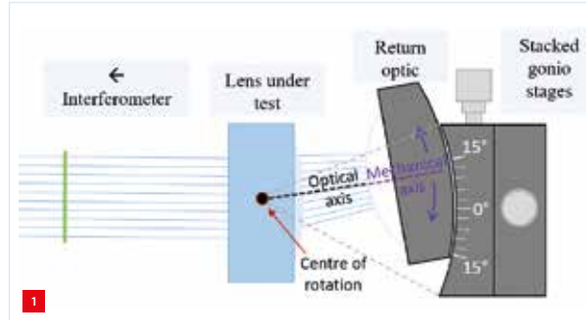

Lens testing with a Fizeau interferometer requires a spherical motion of the return optic to align the mechanical and optical axes. Using stacked gonio-stages to achieve spherical motion, the distance from the end-effector to the remote centre of rotation is fixed. If a lens with a different focal distance is tested, this RCR distance should be adjusted accordingly.
Note: for illustration purposes the angular error (12°) is exaggerated. The expected angular error of the beam is max. 3°.

Design process

After defining the kinematic, stiffness and accuracy requirements for the optical mount, various concepts were generated using a large overview with building blocks containing solutions to different aspects of the mechanism. Six different concepts were created by picking different combinations of building blocks. The first three concepts are based on a set of parallel legs that connect the end-effector to the base. The constraint lines associated with these legs are intersecting in the desired RCR. The other three concepts have an intermediate body.

In this article, concepts 1-3 are explained in more detail (see Figure 3). These concepts use a trapezoidal mechanism with parallel links, which has several benefits compared to the other concepts (4-6). Higher support stiffness is achieved, because the axial stiffness of each link is added up. Mechanisms with a higher support stiffness produce a smaller error when a load is applied perpendicular to the

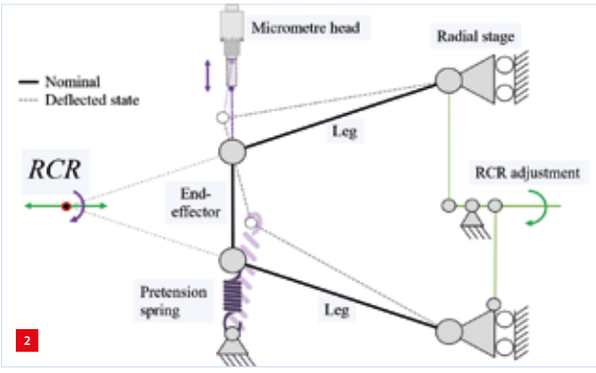

The working principle of the isosceles (legs with equal leg length) trapezoidal mechanism (in 2D) with an adjustable RCR. By pulling the end-effector towards the micrometre head, the end-effector is deflected about the RCR. Varying the orientation of the legs with respect to the radial stages changes the RCR distance.

actuated direction. Furthermore, all legs are manipulated in the same way when the RCR is adjusted, making these mechanisms less complicated.

All concepts were compared using criteria based on the requirements in a concept comparison table. The criteria with the largest weighted value were support stiffness and backlash. Concept 2 is superior in terms of support stiffness. However, the accuracy of the mechanism suffers from stick-slip in the pre-tensioned joints because of friction forces. In concept 3, the folded leafsprings are twisted too much when manipulating the RCR, resulting in a collapse of the support stiffness.

In the end, concept 1 was chosen for the flexure-based legs. Flexure-based spherical movements are less prone to backlash, as flexures have no wearing parts, which makes the movements more accurate [2]. The flexures to move the legs outward in the rotating disk cannot achieve the required range of motion in the given design space. Therefore, the spiral 'pin-in-slot' mechanism of concept 2 is used.

Detailed design

Figure 4 shows the functional model of the detailed concept. In the end-effector a laser pointer is mounted instead of a return optic. The laser was used for validation purposes. Newly developed flexure-based joints are integrated in each leg. These multi-degree-of-freedom flexure joints make use of a cartwheel hinge whose axis intersects perpendicularly with a short leafspring flexure. The legs therefore act as reinforced wire flexures that make up the edges of a spatial isosceles trapezoidal structure. Parallel flexure guides accommodate the radial movement of the base connection points for the RCR adjustment. A spiral guide synchronises the separation of the three legs.

To demonstrate that the chosen concept can accomplish spherical motion, a pseudo-rigid-body model (PRBM) was used to illustrate how the orientation of the legs is changed

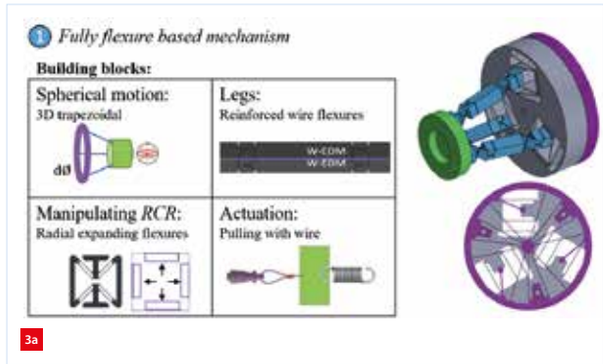

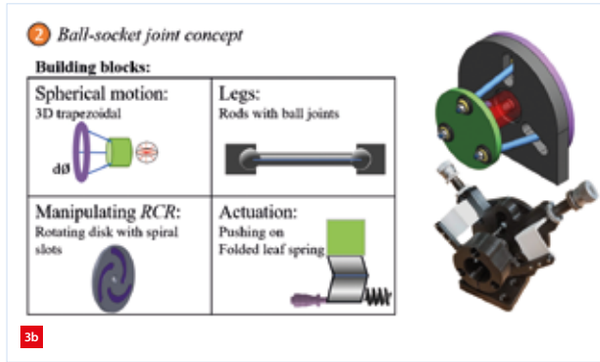

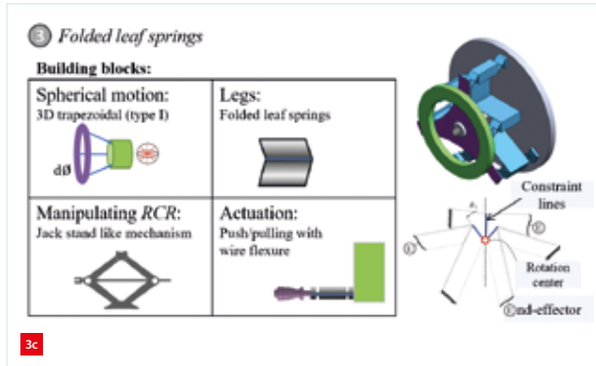

Three design concepts based on a set of parallel legs that connect the end-effector to the base.
(a) Flexure-based trapezoidal mechanism. The legs (blue) are reinforced wire flexures, connecting the end-effector (green) to the base (grey). At the base, the legs move in radial direction using leafsprings. By rotating the purple disk, the RCR distance is adjusted.
(b) Trapezoidal mechanism with conventional ball-socket joints. To eliminate backlash, the ball-socket joints are pre-tensioned by means of a spring (red). Deflection of the end-effector is uncoupled from the micrometers using leafsprings. A functional 3D-printed model of the mechanism is shown in the lower right.
(c) Spherical motion is achieved using folded leafsprings as legs between the green and grey body. The fold lines of leafsprings intersect in the RCR. Tilting the angle of these lines shifts the RCR. Cartwheel hinges allow tilting of the folded leafsprings when the purple body contracts. The concept is based on the large-stroke spherical flexure joint (shown in the lower right figure), developed by the Precision Engineering group at the UT [1].

when the distance towards the RCR is varied. In the PRBM, the flexures at the ends of the legs were replaced by ball joints. The kinematics were derived by means of this rigid-body model. By adding (rotational) spring elements to the joints of the PRBM, it was possible to derive the compliances of the system in the actuation and support [2].

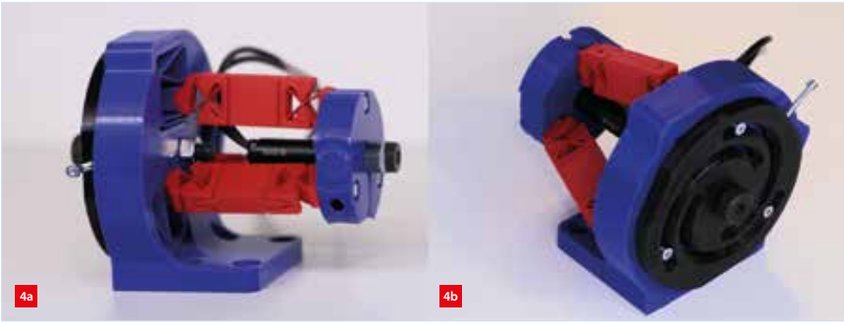

A 3D-printed functional model of the spherical mechanism with adjustable RCR. The legs are red, the spiral guide is black and the base and end-effector holding a laser pointer are blue.
(a) Legs in parallel configuration; the mechanism rotates about RCR at infinity.
(b) Legs in converging configuration; leg orientations are readjusted to rotate about the RCR at 45 mm in front of the end-effector.

As implicitly shown in Figure 5 (and already explicitly illustrated for the 2D case in Figure 2), the RCR is located at the intersection of the three legs in the mechanism. In order to shift the RCR closer or further away from the end-effector, the joints at the base are radially shifted inward or outward. Varying radial distance (s_1), ranging from 22 mm to 33 mm, to transform the mechanism from translating ($R = \infty$) to rotate about the RCR at the minimal distance from the end-effector (R = 45 mm), the legs have to tilt 22°, which requires a joint range of motion of ±11°. Together with the desired travel of the end-effector (±2 mm), the joints in the legs must be able to tilt ±15° in one direction (R_y). Perpendicular to this tilting motion, the joints in the legs should be able to rotate ±2.5° in (R_x) direction to allow for spherical movement as shown in Figure 6.

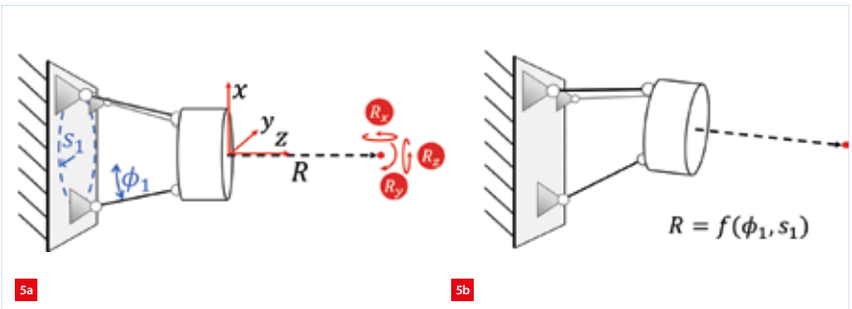

Rigid-body model (RBM) of the mechanism in side view. The RCR distance (R) is a function of the angle of the legs (ϕ_1) in the undeflected state and the pitch circle radius of the joints at the base (s_1).
(a) Nominal state.
(b) Deflected state.

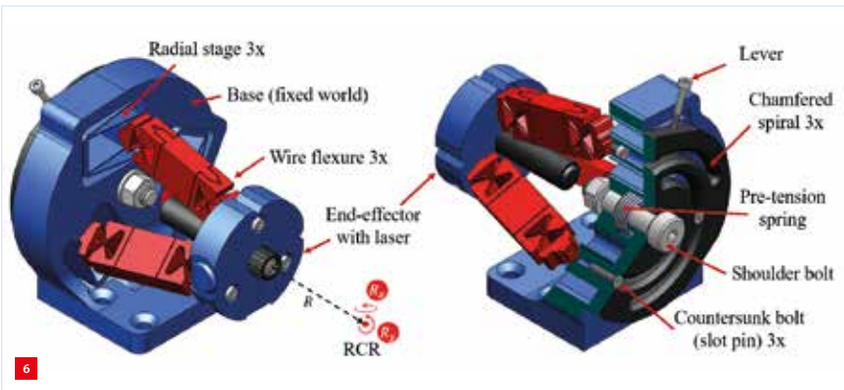

Functional overview of the spherical mechanism without actuators. On the right, the base and spiral disk are partially sectioned to illustrate how pre-tensioning of the spiral disk (black) centres the slot pin in the spiral for a backlash-free manipulation of the legs.

Three radial stages are present in the base to allow the radial movement of the legs, as shown in Figure 6. To prevent parasitic motion and save space, a compound parallel guide is used. By using two sets of antagonistic parallel leafsprings connected at an intermediate body, the parasitic motion of the first set is compensated by the second. In addition, space is saved by slightly angling the parallel leafsprings. These radial stages are actuated by a 'pin-in-slot' mechanism located at the backside of the base.

The actuation of the radial motion of the wire flexure is accomplished by spiralling slots in a rotatable disk, which is attached at the back side of the base. This disk with slots rotates concentrically with the z-axis using a shoulder bolt. The 'pins' are attached to the radial stages and protrude through the spiralling slots. To eliminate backlash in these slots, countersunk screws are used in combination with chamfered edges of the spirals. In order to keep these slot pins and chamfered faces in contact, the disk is pre-tensioned by means of a spring over the shoulder bolt. An additional benefit of this pre-tensioning is that the mechanism is self-locking after adjustment of the RCR distance.

Large-range 3D-printed joint

With the further detailing of a functional 3D-printed model of the mechanism, a new type of compliant cardan flexure has been developed. This compact joint provides a large range of motion in R_y (±15°) and a small range of motion (±2.5°) in the R_x-direction, while providing high axial stiffness in a compact space. The compliances in the legs are concentrated onto two cardan-based flexures with intersecting centres of rotation, as shown in Figure 6.

Since the support stiffness benefits from a lumped instead of distributed compliance [3], a small leafspring hinge (SLSH) and cartwheel hinge (CH) are combined. The CH is responsible for the large deflection in R_y, while the SLSH can cope with the smaller rotation in R_y-direction. It is important that the rotation centres intersect, so that the location of the RCR of the spherical mechanism is the same for tip and tilting motions. The integration of the notch-type hinge into the support of the cartwheel hinge results in a compact cardan joint design. The designed cardan flexure is space-efficient, because the SLSH makes use of the unused space available at the sides of the CH flexure. In addition, the maximal allowable range of motion is physically limited by rigid parts of the joints in order to prevent the flexure from exceeding the yield stress.

To produce these flexures, 3D printing (fused deposition modelling, FDM) is the most suitable production method due to the presence of some undercuts. Other techniques, such as wire-EDM cutting, are feasible but require assembly from multiple parts. The geometry of the cardan joints in the legs was optimised using the mechanical properties of the PLA plastic that was used for the functional model. The range of motion was optimised for the highest axial stiffness.

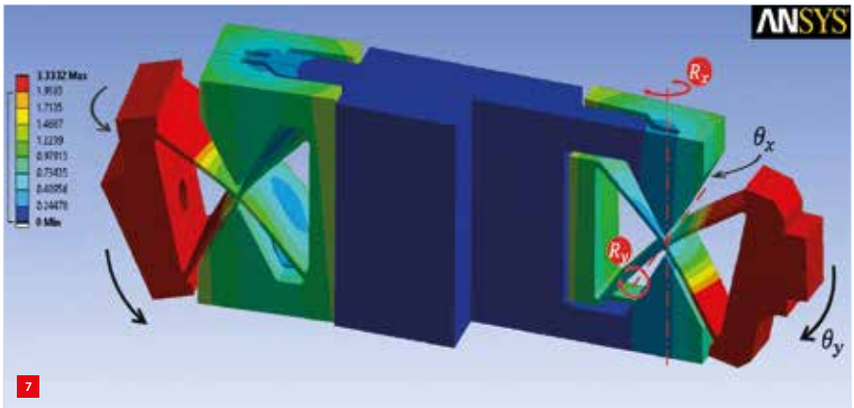

Simulated deformation plot for one of the legs in deflected state, with partial section view on the right. This (3D-printed) part uses two novel flexure-based cardan joints. R_y-rotation has an angular range of 30°. R_x-rotation has a range of 5°. The unused space around the cartwheel hinge flexure is used by a notch-type flexure to make the joints very compact.

Table 2
Comparison of the stiffness values produced by the finite-element model (FEM) and the analytical model. The difference in axial stiffness between the two models is due to the material that connects the two flexural elements having non-zero compliance, which decreases axial stiffness.

	Angular range of motion [°]	Actuation stiffness [Nmm/rad]	Axial stiffness [N/mm]	Thick-ness *t* [mm]	Length *L* [mm]	Width *b* [mm]
Cartwheel hinge flexure	±15	82 (FEM) 75 (analytical)	714 (FEM) 1.411 (analytical)	0.4	18	20
Small leafspring flexure	±2.5	551 (FEM) 427 (analytical)	8.012 (FEM) 11.200 (analytical)	0.8	3	15

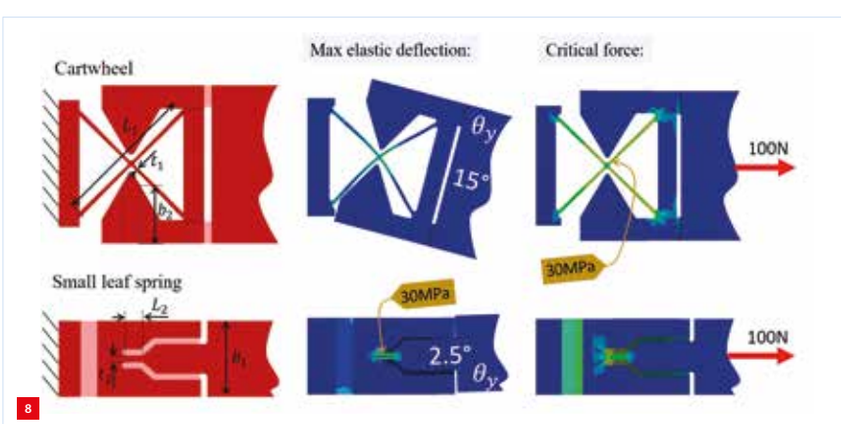

Optimisation of the compliant, fused-filament-fabricated (3D-printed) cardan joint. The tags indicate the maximal allowable stress.
(a) Optimisation variables: lengths L_1 and L_2, thicknesses t_1 and t_2, and body dimensions b_1 and b_2.
(b) Stress plots of the cardan joint with the prescribed range of motion optimised.
(c) Stress plots of maximal allowable axial loading.

Two methods were used for analysing stiffness and range of motion. The first method relied on analytical approximations to predict the stiffness and maximal deflection of the joint using equations known from literature for the cartwheel and small leaf flexure joint [4]. These equations were used for calculating initial lengths. With a finite-element model (FEM) in ANSYS, a more detailed design of the joint as a whole was optimised (Figure 7).

Figure 8 and the corresponding Table 2 present the optimised lengths and resulting design. It was found that the printed legs were able to reach the desired range of motion without failing. However, for FDM printing it is important to keep the anisotropic behaviour of the resulting parts in mind. Layer adhesion limits the yield strength in the height direction to approx. 40% of that in virgin material. Therefore, the legs were printed with the side surface down, so stresses between layers are limited. Other influences on maximal yield strength of the material are print temperature, layer height, infill percentage, porosity and extrusion width [5], [6].

Centre shift

The mechanism was designed for spherical motion around a specified RCR. Ideally, the end-effector stays perfectly oriented towards this point for all motion. However, for this mechanism this is only the case in the initial position due to a kinematic change of the intersection point of the legs (Figure 2), also known as the shortening effect of the legs (see Figure 9). This causes more rotation of the end-effector for a given translation, resulting in a different RCR. This phenomenon is called 'centre shift'.

This centre shift was measured on the prototype by placing a camera sensor at the location of the desired RCR. The aforementioned laser pointer was mounted on the end-effector to illuminate the sensor at the RCR. In the ideal case, the camera sensor does not move during deflection. In practice, it does. Therefore, the change in spot location is taken as a measure for the centre shift. Figure 10 shows the centre shift computed by the kinematic model and measurements on the 3D-printed prototype.

As expected, the centre shift increases with larger deflections and shorter distance towards the RCR. From the experimental validation, it could be determined that the centre shift is much larger for deflections greater than 1.0 mm, up to 2.5 times larger than expected from the

kinematic model. This is due to the finite support stiffness of the mechanism. Since the actuation force is applied at the end-effector and not in-line with the centre of compliance, an additional angular error is introduced, causing a 'diving' motion of end-effector.

Conclusion

An adaptive optical mount was developed. The resulting three-legged, flexure-based isosceles trapezoidal mechanism can perform the spherical motion about an adjustable remote centre of rotation, as needed for the alignment of lenses. Each leg consists of two new cardan joints that combine a cartwheel hinge and a short leafspring hinge for high support stiffness. For deflections larger than 1.0 mm at small RCR distances, the centre shift increases exponentially, whereas the centre shift in the kinematic model increases linearly. With the evaluation of the 3D-printed functional model it was found that the location where the actuators push or pull the end-effector is not optimal. To reduce the amount of centre shift this location is desired to be in the centre of compliance. This location is at the centre of the trapezoid to counteract axial forces in the legs when deflecting. Also, if this design would be realised in metal, the support stiffness would improve as well. Nevertheless, the design fulfils all requirements for the current application of lens testing.

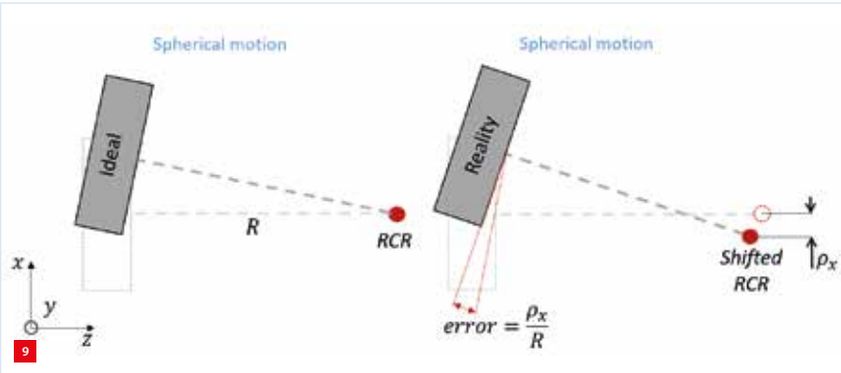

Angular error of the end-effector causing a shift of the RCR. This is mainly caused by the shortening effect of the legs and is noticeable at large deflections.

REFERENCES

[1] M. Naves, R. Aarts, and D. Brouwer, "Large-stroke spherical flexure joint", *Mikroniek*, 59 (3), pp. 17-21, 2019.

[2] M. Wang, "Mechanical and geometric advantages in compliant mechanism optimization," *Frontiers of Mechanical Engineering in China*, 4 (3), pp. 229-241, 2009.

[3] Howell, L.L., and Midha, A., "A Method for the Design of Compliant Mechanisms With Small-Length Flexural Pivots", *J. Mech. Des.*, 116 (1), pp. 280-290, 1994

[4] J. Wu, S. Cai, J. Cui, and J. Tan, "A generalized analytical compliance model for cartwheel flexure hinges", *Review of Scientific Instruments*, 86, p. 105003, 2015.

[5] B. Wittbrodt, and J. Pearce, "The effects of PLA color on material properties of 3-D printed components", *Additive Manufacturing*, 8, pp. 110-116, 2015.

[6] S. Rajpurohit, and H. Dave, "Analysis of tensile strength of a fused filament fabricated PLA part using an open-source 3D printer", *The International Journal of Advanced Manufacturing Technology*, 101, pp. 1-4, 2019.

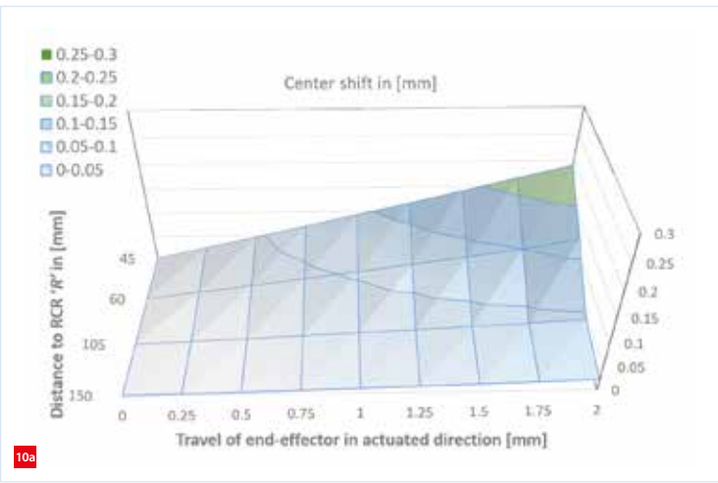

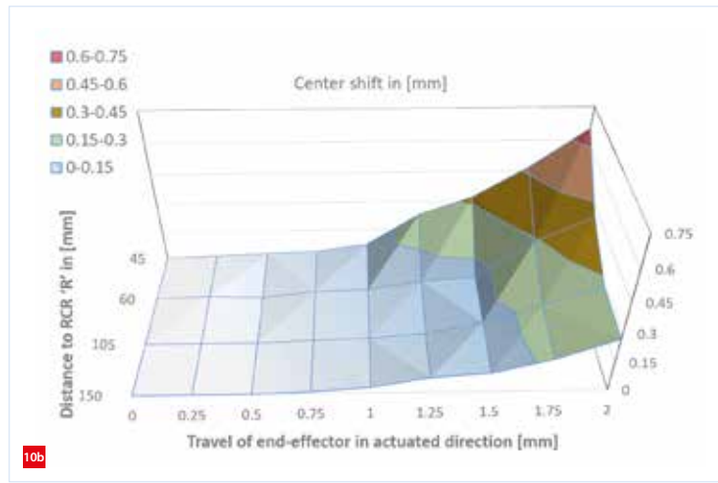

Lateral centre shift of the RCR.
(a) Estimated using kinematics of the rigid-body model.
(b) Determined using the experimental set-up with the functional model.

EXPLORING ADDITIONAL SOLUTIONS FOR FREEFORM MECHATRONICS

Metamaterials is a rapidly developing field of research. It offers the prospect of material properties that do not exist in regular materials and which might be useful for overcoming hurdles in current mechatronic system design. Stimulated by the progress in additive manufacturing (AM) that has enabled fabrication of materials with complex microstructures, system designers have discovered increased design freedom. With metamaterials, even the possibility of distributing material properties has entered the design arena, which might expand the system engineering solution space. Building further on the idea of freeform mechatronics, this opens up new perspectives for applications of metamaterials in high-tech mechatronic systems.

GREGOR VAN BAARS, BASTIAAN FLORIJN, JOOST PETERS, JAN DE VREUGD, FLORIS VAN KEMPEN, SANNE VAN DEN BOOM, EMIEL VAN DE VEN, WOUTER JONKER AND LUUK LUBBERS

This article looks into the potential of metamaterials for high-tech mechatronic systems, building further on the idea of freeform mechatronics presented earlier [1, 2]; see Figure 1. It reports some of the current thoughts and developments so far, merely to inspire the high-tech systems engineering community, and is an invitation to join the developments in this direction. The following sections provide an introduction to the field of metamaterials (summarised from [3]), an assessment of metamaterials potential for mechatronic systems, and short descriptions of a few of our first explorations at TNO.

AUTHORS' NOTE

Gregor van Baars is senior system engineer/project manager at TNO.
All authors are associated with the Opto-Mechatronics department of TNO in Delft (NL), with the exception of Luuk Lubbers, who works in the department of Explosions, Ballistics and Protection at TNO in Den Haag (NL).

gregor.vanbaars@tno.nl
www.tno.nl

Introduction to metamaterials

Metamaterials are artificial materials with properties that may not be found in nature. They derive their properties from their geometry or structure, rather than their composition. See [3] for a more elaborate introduction and references for further reading.

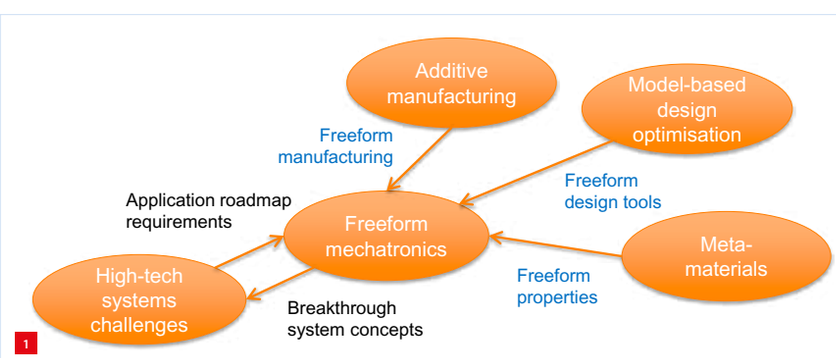

Freeform mechatronics: combining emerging technologies such as additive manufacturing, design optimisation and metamaterials to develop new mechatronic concepts.

Metamaterials were first mentioned in the context of electromagnetics. As early as 1968, Soviet physicist Victor Veselago showed theoretically that he could design materials with a negative refractive index. In retrospect, these materials could be considered optical metamaterials. In 2000, Roger Penrose showed theoretically that materials with negative refractive indices could be used to make perfect lenses, lenses that beat Abbe's diffraction limit. Other examples of electromagnetic metamaterials are: super-absorbing metamaterials, where resonating elements are located in a grid to achieve super-black materials; photonic metamaterials (where certain photons are not allowed to travel through); and cloaking metamaterials, where a metamaterial structure is used to guide light around objects.

Nowadays, almost every branch of physics has their own type of metamaterials. What they all have in common is that by careful architecting of the microstructure (a 2D/3D tiling of repeating unit cells), surprising behaviour on the macrostructure level can be designed. Of particular interest are mechanical metamaterials, where a material's response in terms of deformation is controlled by the design of its microstructure. For example, this means that materials can be designed with a negative Poisson's ratio (auxetic), a vanishing shear modulus or negative compressibility.

Other potentially interesting classes of mechanical metamaterials are nonlinear metamaterials, topological metamaterials and pattern-transforming metamaterials (inspired by the Japanese art of origami). Such (un)folding

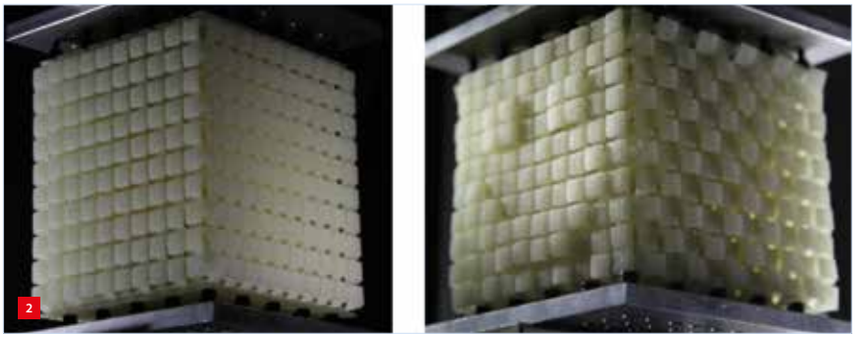

A metacube with specific stacking of cuboid-shaped unit cells (left) generates a smiley-face texture (right) when compressed. (Courtesy of [4])

metamaterials might have interesting applications in deployable structures where compact transport is desired, followed by unfolding to functionality upon arrival in the operational environment.

Other mechanical metamaterials have been developed that harness geometric nonlinearities and elastic instabilities to obtain novel functionalities. For example, in smart morphable surfaces ('smorphs'), elastic instabilities have been used to switch quickly between different wrinkling patterns on a surface. An example of a fully 3D auxetic metamaterial [4] is a stack of cuboid-shaped unit cells, which displays a buckling-induced smiley texture on the surface of the cube (see Figure 2).

Programmable mechanical metamaterials can be made using quasi-2D slabs perforated with a square array of holes. The mechanical response to uniaxial compression of such materials can be controlled by lateral confinement. Depending on the amount of confinement, the material behaves monotonically, non-monotonically with negative incremental stiffness, hysteretically, and non-monotonically again (without pattern transformation); see Figure 3.

Considering the area of vibration control, phononic

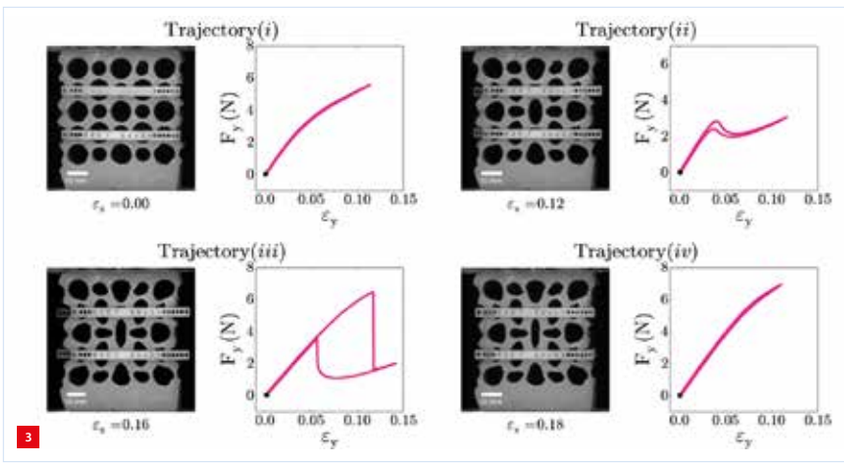

Different material responses of a single piece of material, which can be programmed by lateral confinement (increasing from upper left to lower right).

bandgap structures are interesting. This type of mechanical metamaterials make use of phononic crystals (PCs). In PCs, the material does not fundamentally allow for the propagation of certain lattice vibrations (phonons).

The possibilities and types of metamaterials are expected to increase over the coming years, as this field of research is just emerging and looking to connect to applications.

Assessment of potential for mechatronic systems

From the overview above, it is clear that the field of metamaterials offers an inspiring set of properties. This section will present an initial assessment of the potential value for mechatronic system engineering by attempting to answer the following questions:

- What could it bring?
  How do we envision metamaterials contributing to the development of better systems? Can we exploit new behaviours, properties, etc. such that specifications are met? To what new system concepts might that lead?
- What is needed to capture that?
  How are we going to design the materials and their properties in mechatronic systems such that they behave exactly as we desire? Do we need to use new design, modelling and performance analysis tools? What about new or revised sets of design principles?

Some thoughts and research questions related to what metamaterials could bring to mechatronic systems engineering are:

- Overcoming classical material properties trade-offs.
  For example, will it be possible to simultaneously increase stiffness and damping or introduce progressive nonlinear behaviour?
- Distribution of mechanical properties (stiffness, damping, density) across a construction part.
  This is also denoted as grading properties (Figure 4). Supposing it is possible to tailor mechanical properties beyond conventional (isotropic, homogeneous) materials, which performance bottlenecks will be resolved?
- Directionality of properties.
  For example, thermal conduction in one orientation and thermal isolation in another orientation.
- Switching behaviour.
  For example, a load-dependent response being stiff at high acceleration or force levels and very soft at stand still or constant velocity. Or a material that is flexible under normal conditions, exhibiting extreme stiffening upon impact from the outside.
- Extreme isolation from environmental influences.
  Examples are thermal cloak and vibration isolation achieved by zero-transmission paths to specified performance points

Regarding the question of what is needed to capture the possible benefits of metamaterials, the following remarks can be made:

- Support from optimisation-based design tools will most likely be required.
  We will be confronted with the reverse design problem: if the desired properties are specified, how then to generate the design of the metamaterial structure that delivers these? It will probably be too difficult for the human mind to navigate the increased design space towards optimal designs. Model-based design optimisation can be powerful in finding optimal solutions. The key to success is the proper translation of specifications and boundary conditions into an optimisation problem. This obviously requires deep engineering insight, but also an understanding of the optimisation tools. Also, interpretation of the results will always be required and might lead to new insights (design principles) on what makes sense and what not.
- Modelling and analysis tooling will probably need to be adapted to handle metamaterials.
  As systems engineering depends heavily on design analysis and predictive modelling, these tools should be capable of handling metamaterials and correctly simulating and analysing their behaviour. For example, FEM and modal analysis are not trivial for non-isotropic, graded materials, or for auxetic, nonlinear and switching behaviours.

The thinking process concerning potential applications of metamaterials is just beginning. In this article we discuss high-tech mechatronic systems, but applications for defence (protection of persons and vehicles), building and civil construction, space instruments, and automotive and biomedical (implants) are also interesting. Other applications will surely develop over time.

The following sections present a few investigations and design studies to connect metamaterials and systems engineering.

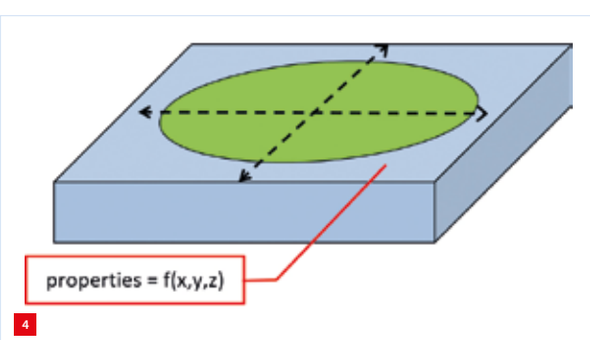

Distribution of part properties across the design volume (blue part).

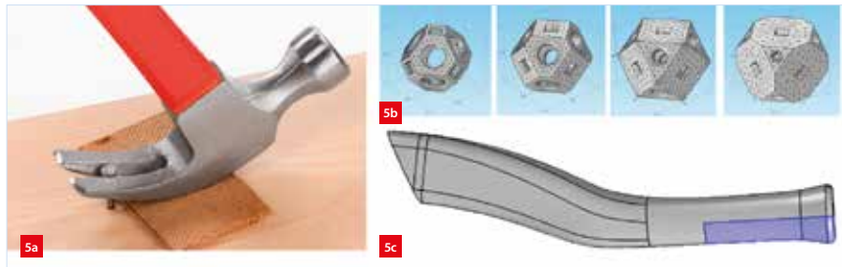

The hammer handle design study case.
(a) The load case of removing a nail.
(b) Available unit cells with increasing density and E-modulus.
(c) Available design volume.

Grading mechanical properties: hammer handle case

To explore the idea of grading material properties, a design study for the simple case of a hammer handle has been performed (see Figure 5).

The starting point was previous work on lightweight unit cells (octahedra) that can be manufactured with AM, and could serve as building blocks for system parts [1, 2]. By giving the unit cells different wall thickness, a different mechanical stiffness and density are obtained at homogenised cell level. By placing different cells across a design volume, the designer has the freedom to play with stiffness and density. This leads to grading of properties and deliberately drops the need for material isotropy and homogeneity; this grading can be seen as a form of metamaterial. Model-based design optimisation (using Comsol) has been carried out to determine which unit cell to put where in the available design volume, while optimising weight and resistance to the load case.

For the hammer handle case, the results are presented in Figures 6 and 7. A bone-like structure can be recognised: dense on the outside and more open on the inside. In terms of resisting the loads, it does not help greatly to put a lot

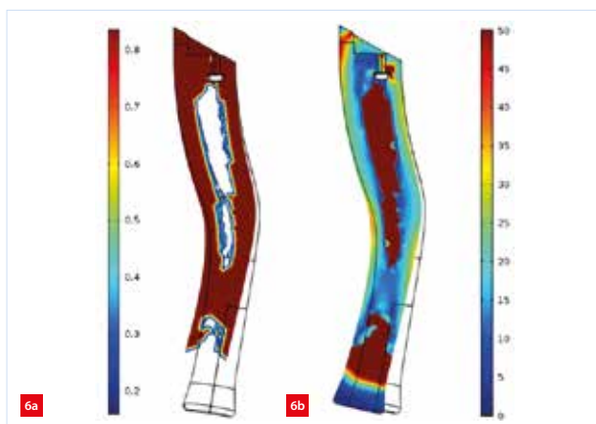

Optimised design result for the hammer handle.
(a) Density distribution (overall 50%).
(b) Von Mises stress at 900 N loading.

Virtual and physical realisation of the hammer handle.
(a) Distribution of different types of unit cells.
(b) 3D-printed cross-section (left) and full version.

of material at the core of the design volume. Stated another way, massive and homogeneous filling of the design volume appears to be sub-optimal. Although a human designer would not be able to produce this exact distribution of cells, the optimisation result can be understood and accepted from an engineering perspective. For demonstration of the result, the hammer handle design has been 3D printed as a cross section (showing the interior structure) and a full version (see Figure 7).
This limited design study is already enough to encourage further research into the metamaterial class of grading towards more serious applications, and more dynamic or even mechatronic settings.

Auxetic structure design study

Mechanical properties of natural/conventional materials span a specific, limited range. A clear example is the Poisson's ratio, which is positive for most materials used in engineering constructions and parts. This means that in practice, engineers are accustomed to materials that contract laterally when axially stretched, or expand laterally when axially compressed. This section will look into the class of auxetic metamaterials that are deliberately designed to have a negative Poisson's ratio.

Auxetic (micro) structures consist of a number of unit cells arranged such that the overall structure expands when stretched and contracts when compressed. Over the years, several new 2D and 3D auxetic cellular structures based on re-entrant, chiral, lozenge and square grids, etc., have been developed. Examples are given in Figures 8 and 9.

Regarding applications, the question is how auxetic behaviour can be of value for systems engineering and mechatronic performance? Perhaps it would be interesting to have the Poisson's ratio equal to zero, such that no lateral contraction or expansion happens under loading, which eliminates cross-talk issues in terms of structural and geometrical stability. Protecting fast-moving objects from damage by exploiting auxetic behaviour for crash buffering and impact absorption might also be an interesting application.

To explore the design and analysis steps associated with this type of metamaterial, an auxetic material has been designed using homogenisation and shape optimisation tools to derive the structure of interest. This means that the structure of the auxetic material has been parametrised (left part of Figure 10) and the shape optimisation algorithm delivered the optimum parameter values for the targeted specifications. For the resulting optimal auxetic design, see the right part of Figure 10. Nonlinear geometric analysis has been done to predict the Poisson's ratio as a function of applied strain. The results (see Figure 11) show that the microstructure has indeed a Poisson's ratio close to –1, only slowly reducing with increasing strain. This enables application in situations where the Poisson's ratio is supposed to be stable under various load levels.

Further research will concern the use of topology optimisation to derive new auxetic structures, tailored to specific design criteria.

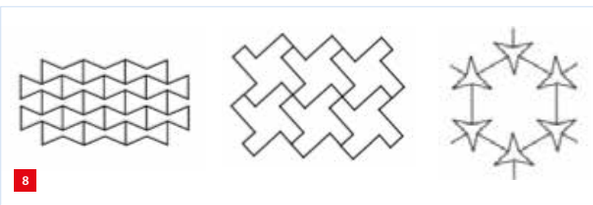

Re-entrant auxetic microstructures.

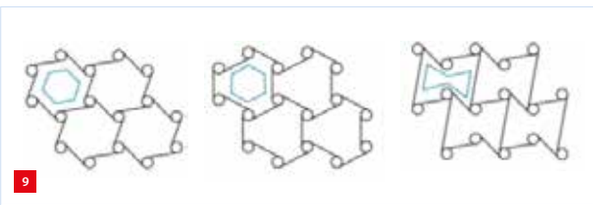

Chiral auxetic microstructures.

Phononic bandgap metamaterial demonstrator

This section presents part of ongoing research for which the intermediate results have been documented in a concept article, to be submitted for publication ([5], expected early 2021). Here, we will present a few insights and highlights as a sneak preview.

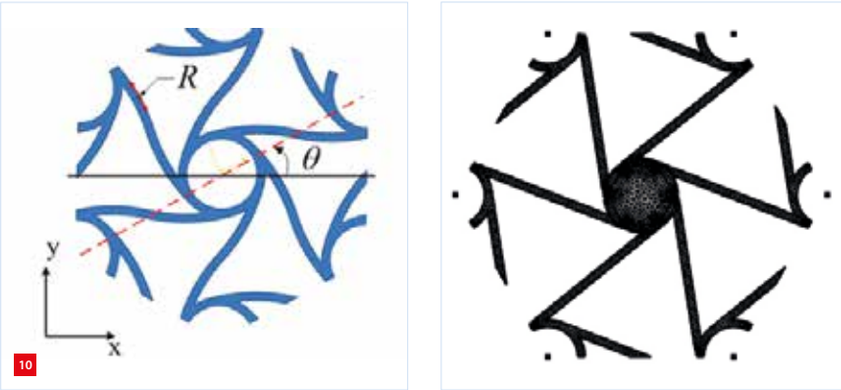

Unit cell of a so-called hexachiral microstructure, with finite-element model representation (Comsol) on the right.

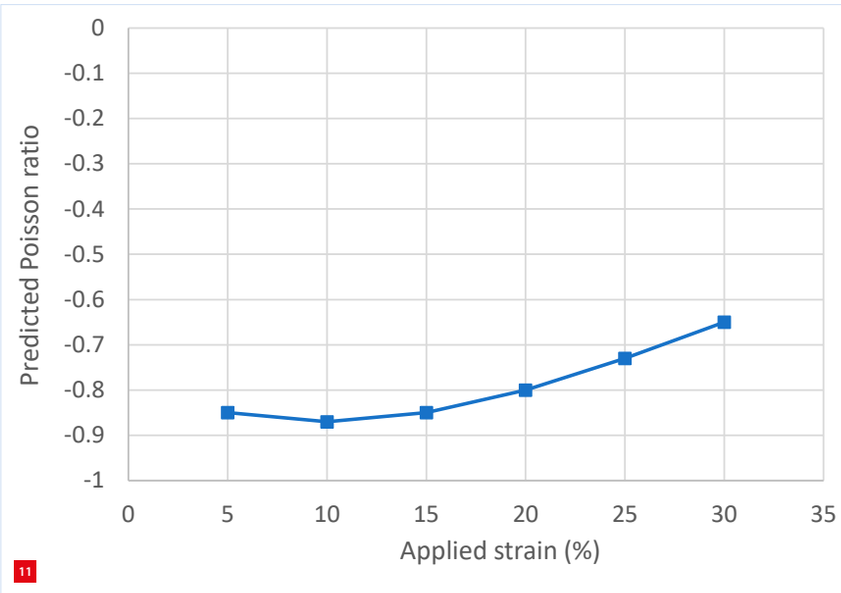

Predicted Poisson's ratio as a function of applied strain (hexachiral structure).

As mentioned in the introduction, mechanical metamaterials that exhibit a phononic bandgap, i.e. phononic crystals (PCs), can be of particular interest in the area of vibration control. The idea is to design the structures in metamaterials such that specific frequency content in vibrational disturbances can be attenuated or rejected. In addition, this could enable the favourable shaping of dynamic behaviour, increasing control bandwidth and ultimately improving closed-loop performance.

Two main categories in PCs can be recognised, based on their working mechanisms:

(i) PCs that derive their bandgap from Bragg diffractions between regions of high density and low density;

(ii) PCs that derive their bandgaps from locally resonant unit cells.

To explore phononic bandgap design and behaviour, we used analytical and numerical models for the design of PCs of both types, and proposed a demonstrator design based on these analyses. Here, only a few results for the Bragg (type i) PC will be presented. The design aspects for locally resonant bandgap metamaterial (type ii) have also been studied and lead to similar results in terms of bandgap. To limit the total size of the demonstrator we restricted the size of the unit cell to 2 cm, and made it out of aluminium, as this is used widely in high-tech and space hardware (Figure 12).

To characterise the complete band structure of PCs with an eigenfrequency analysis it is sufficient to vary the vibrational wave vector k along the boundaries of the so-called irreducible Brillouin zone. (The Brillouin zone is a notion from solid-state physics and involves quantum mechanical theory to analyse periodic structures of unit cells. It is used to solve the wave equation to discover the relationship between frequency and wavenumber for the whole crystal.) The resulting dispersion curves (not shown here) demonstrate a bandgap for frequencies in between 106.5 kHz and 123 kHz.

Next, numerical analyses (using Comsol) have been performed for a phononic crystal demonstrator with a finite crystal with 10×10 unit cells at the middle part of a rectangular aluminium plate. The plate was excited from the left side with a sinusoidal plane wave with driving frequencies below (45 kHz), within (110 kHz) and above (200 kHz) the bandgap. The results are shown in Figure 13.

For the driving frequency inside the bandgap, we observe large deformations at the left side. Only deformations on the order $O(10^{-7})$ are observed at the right side of the crystal. Hence, consistent with the unit cell simulations, elastic waves are not transmitted through the phononic crystal, but are reflected back to the source. For excitation frequencies outside the bandgap, clearly the waves are transmitted to the right side (as expected).

Obviously, bandgap frequencies in the 100-kHz range are too high for mechatronic relevance, but the results of this work illustrate the effectiveness of using analytical and numerical models to design the unit cell structure of a phononic metamaterial. Future work will include 3D modelling of the metamaterials and realisation of the proposed demonstrator designs to further verify the design approach.

Computational design of phononic crystals

To address the reverse design problem for phononic metamaterials, we will look at the computational design (topology optimisation, TO) of phononic crystals in

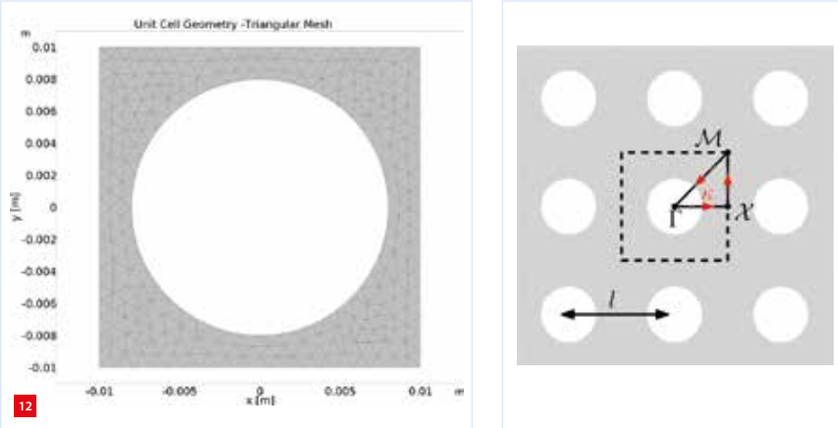

Aluminium-air unit cell with 2 cm lattice size; on the right, a definition of the periodic structure.

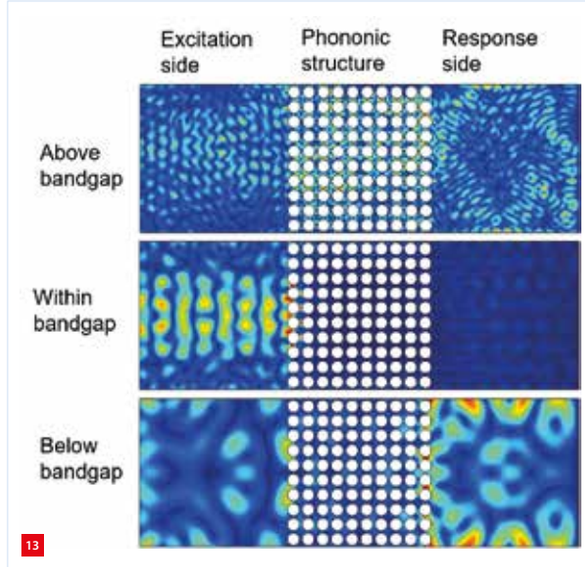

Magnitude of displacements within the phononic crystal demonstrator for three perturbation frequencies. From blue to red displacements increase (different scale for each frequency).

collaboration with Delft University of Technology [6]. Standard density-based TO does not appear to work well because of a 'staircased' (pixelated) and diffuse representation of the material interface. The Interface-enriched Generalized Finite Element Method (IGFEM) [6] is more suitable and provides a smoother boundary description without the need for remeshing.

The benefit of using IGFEM instead of a density-based approach has been demonstrated (not shown here, see for example [6]) in a direct comparison. IGFEM predicts the bandgap more correctly for the same size of mesh. This proof of principle demonstrates that the proposed approach has great potential for the design of metamaterials that interact with waves.

Closing remarks

This article has been a first attempt to explore the potential value of metamaterials for mechatronic systems engineering. The range of new properties, provided by the emerging field of metamaterials, is truly inspiring. However, we are just at the beginning of finding the answer to the question of what they can bring to high-tech applications.

We will continue these explorations, identifying open issues and challenges in the search for meaningful combinations of the emerging field of metamaterials and the well-established field of systems engineering. Suggestions for and joining in this challenge are welcome.

REFERENCES

[1] G. van Baars, "Getting High Tech Systems in Shape and Fit for the Future", *Mikroniek*, vol. 52 (2), pp. 30-36, 2012.
[2] G. van Baars, J. Smeltink, J. van der Werff, M. Limpens, M. Barink, J. de Vreugd, O. Galaktionov, and G. Witvoet, "Additive Manufacturing enabled Freeform Mechatronics for High Tech Systems", *Mikroniek*, vol. 54 (6), pp. 9-15, 2014.
[3] H. Florijn, 'Programmable Mechanical Metamaterials', Ph.D. thesis. Leiden University, 2016, *openaccess.leidenuniv.nl/handle/1887/44475*
[4] C. Coulais, E.Teomy, K. de Reus, Y. Shokef, and M. van Hecke, "Combinatorial design of textured mechanical metamaterials", *Nature*, 535 (7613), pp. 529-532, 2016.
[5] J. Peters, B. Florijn, L. Lubbers, and G. van Baars, "Demonstrator Design for Phononic Bandgap Meta Materials", *in preparation*.
[6] S. van den Boom, R. Abedi, F. van Keulen, and A. Aragón, "Topology optimisation of phononic crystals using an interface-enriched finite element formulation", *in preparation*.

KINEMATIC REDUNDANCY

Multi-DoF parallel mechanisms are used with great success in many applications including flight simulation, robotics, precision mechanisms and machine tools. However, due to parallel kinematic singularities, the mechanical properties of these devices deteriorate when the platform is rotated from its reference orientation and hence their effective rotational workspace is typically very limited. In this article, it is shown that kinematic redundancy can be used to alleviate singularities, thereby extending the rotational workspace of multi-DoF parallel mechanisms. The proposed approach results in mechanisms that retain the desirable properties of conventional parallel mechanisms while having large rotational workspaces.

CLÉMENT GOSSELIN, LOUIS-THOMAS SCHREIBER AND THIERRY LALIBERTÉ

Introduction

In many applications, multi-degree-of-freedom (multi-DoF) devices are used to apply loads to mechanical systems. When stiffness, high-performance dynamics or accuracy are required, parallel mechanisms are typically used for this purpose because they provide a much more efficient use of materials than serial linkages. For example, in a flight simulator, the motion system must support the weight of – and impart accelerations to – a cockpit having a mass of several tons while moving it with six DoFs, which can be done only through the use of a parallel mechanism. One of the most successful architectures of multi-DoF parallel mechanisms is undoubtedly the Gough-Stewart platform (GSP), represented schematically in Figure 1, which was introduced half a century ago in a tire-testing application [1] and has been extensively used in flight simulators and other applications.

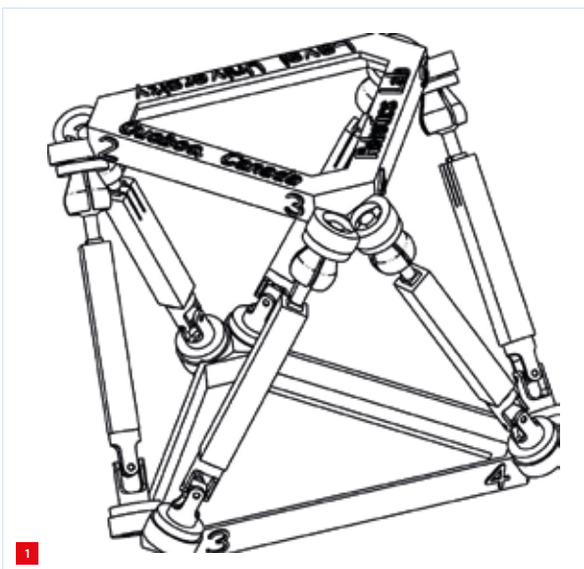

1

Architecture of the Gough-Stewart platform. Each of the six legs connecting the base to the platform contains a passive Hooke joint, an actuated prismatic joint and a passive spherical joint.

As it can be observed in Figure 1, the effectiveness of the GSP is due to the fact that, in this architecture, the links connecting the base to the platform are subjected only to tension/compression loads, which yields high stiffness and accuracy. By controlling the extension of each of the six legs, the position and orientation of the platform can be fully controlled, with six DoFs.

Although many researchers have addressed the geometric optimisation of the GSP (see many references in [2]), the very nature of the device and of the parallel singularities limits its rotational workspace. In practice, tilt angles larger than 45° can rarely be reached. Here, tilting the platform means rotating it with respect to a horizontal axis. It should be noted that the translational workspace is less critical because it can always be increased by scaling up the mechanism. However, scaling the mechanism has no impact on the rotational workspace.

Other multi-DoF parallel mechanisms also suffer from similar limitations. Indeed, combining translational and rotational workspace in a parallel mechanism is clearly a challenge, whereas purely translational (e.g. the Delta robot [3]) or purely rotational (e.g. the Agile Eye [4]) mechanisms are easier to optimise.

A possible approach to alleviate singularities in parallel mechanisms is to introduce redundancy. Two main types of redundancies can be implemented, namely actuation redundancy and kinematic redundancy (see [5] and [6] for literature reviews). The former consists in introducing extra actuators without introducing additional DoFs, while the latter consists in introducing additional actuators and DoFs.

Although redundantly actuated parallel mechanisms have been successfully demonstrated for some applications (see for example [7]), this approach leads to mechanisms in

AUTHORS' NOTE

All authors are affiliated with the Robotics Laboratory of the Department of Mechanical Engineering at Université Laval in Quebec City, Canada.
Clément Gosselin is professor and Canada Research Chair in Robotics and Mechatronics as well as the director of CeRVIM, the Research Centre on Robotics, Computer Vision and Machine Intelligence.
Louis-Thomas Schreiber was a Ph.D. student who graduated in 2019 and who is currently with Robotiq, St-Nicolas, Québec.
Thierry Laliberté is a research engineer in the Robotics Laboratory.

clement.gosselin@gmc.ulaval.ca
robot.gmc.ulaval.ca

which antagonistic forces can appear (the mechanism becomes overconstrained), thereby requiring advanced force control and sensing. In the approach presented in this article, kinematic redundancy is used instead, which yields architectures of mechanisms that retain the characteristics of conventional parallel mechanisms and that are statically determined (no antagonistic forces can be generated).

Revisiting the Gough-Stewart platform

As mentioned above, the GSP is one of the most successful architectures of multi-DoF parallel mechanism due to the axial loading of its legs. In fact, the legs can be considered as a means of applying six pure forces – directed along the legs – to the platform. As a consequence, parallel singularities appear when the Plücker coordinates of the lines associated with the legs become linearly dependent [8]; see the text box.

The question that arises then is: how could redundancy be included in the GSP so that the location and/or direction of the line of action of the forces (axes of the legs) could be actively modified to avoid singular configurations while preserving the axial loading of the legs?
A possible solution is the use of rails to displace the point of attachment of the legs on the base or platform, such as in [9]. However, this solution requires a complex guiding of the rails with large forces acting orthogonally to their axes, leading to inefficient use of materials and actuators. Another approach consists in replacing some of the legs of the GSP with redundant legs, whose architecture is illustrated in Figure 2, as proposed in [10]. In this redundant leg, two actuators are mounted on segments that are connected by a revolute joint. An extra link is mounted on the revolute joint and connected to the platform via a spherical joint.

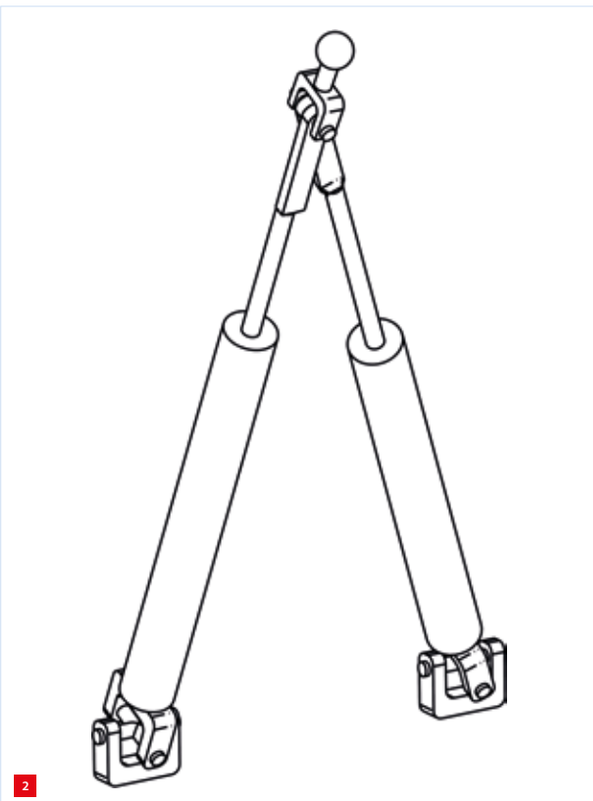

2

Redundant leg connecting the base to a point of attachment on the platform (spherical joint). Such legs can be used to construct a spatial kinematically redundant parallel mechanism because the direction of the link connected to the platform can be controlled.

Plücker coordinates

In a GSP, the Plücker coordinates of the lines defined along the legs play a key role in the kinematic properties. The Plücker coordinates of a line include six components, namely a vector along the direction of the line and the moment of this vector with respect to a reference point. In a regular configuration of the GSP, the six lines are independent. On the other hand, a singular configuration is reached (loss of the rigidity condition) when the six lines are no longer independent. This can be assessed geometrically using Grassmann geometry or analytically by forming a 6x6 matrix containing the Plücker coordinates of the lines.

It can be observed that, in the arrangement shown in Figure 2, all links, including the link connected to the platform, are subjected to tension and compression forces only, thereby preserving the fundamental property of the GSP. The kinematic analysis presented in [10] clearly shows that the line of action of the force applied to the platform by the redundant leg is directed along the link connected to the platform. Hence, it is possible to arbitrarily orient this vector in the plane of the redundant leg by controlling the two actuators, while maintaining the pose of the platform. This can be clearly observed in video [V1]. By controlling the orientation of this link, the geometric arrangement of the corresponding Plücker line is modified, which can be used to avoid singularities.

The next question for the designer is then: is it necessary to replace all six legs of the GSP with the redundant leg shown in Figure 1? The answer to this question is provided in [10], where it is shown that, under certain geometric assumptions, replacing three of the legs of the GSP with redundant legs suffices to alleviate all singularities, yielding a 9-DoF mechanism, referred to as a (6+3)-DoF mechanism to highlight the redundancy.

A CAD model of the prototype of a (6+3)-DoF kinematically redundant parallel mechanism developed at Université Laval based on this concept is shown in Figure 3 and a realisation is shown in Figure 4. In [10], it is shown

3

CAD model of the prototype of a (6+3)-DoF parallel mechanism built at Université Laval. Three of the legs of the original GSP have been replaced with redundant legs. It should be noted that, compared to Figure 2, an upside-down arrangement is used here. Also, the structure supporting the robot has a third leg, which is not shown here for a better visualisation of the robot itself.

that the rotational workspace of the mechanism is greatly increased when compared to the original GSP because the workspace is then only limited by mechanical interferences and joint limits. The platform can easily produce tilt angles of ±80° in all directions (compared to the conventional value of ±45°). Video [V1] shows the prototype that clearly demonstrates these properties.

As mentioned above, the rotational workspace of the kinematically redundant parallel mechanism is greatly increased and limited only by mechanical interferences and joint limits. Therefore, it is important to adjust the joint limits in order to ensure that the potential of the novel device is fully exploited. In particular, the spherical joints at the platform require special attention since conventional spherical joints typically have limited ranges of motion.

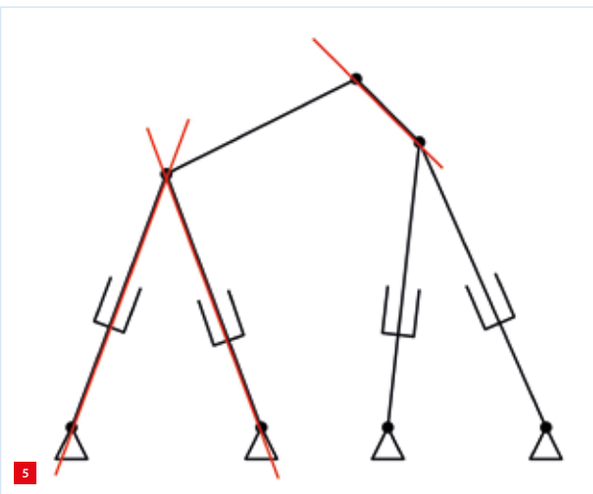

5

A (3+1)-DoF planar kinematically redundant parallel mechanism. The Plücker lines are shown in red. It is easily observed that the rotation of the platform is unlimited with a proper planning of the motion of the redundant leg.

4

Prototype of a (6+3)-DoF parallel mechanism built at Université Laval. It is referred to as the nonapod and can perhaps be considered as the 'Gough-Stewart platform 2.0'.

In order to build the prototype shown in Figure 4, a passive 4-DoF kinematically redundant spherical joint was developed [11]. The joint includes four consecutive revolute joints with intersecting axes. The joint also includes elastic components that keep it away from gimbal lock configurations. It should be noted though, that the elastic components only apply torques to produce the internal motion of the joint and do not affect the force transmission of the spherical joint. These joints have a much larger range of motion than conventional spherical joints while providing a stiffness equivalent to that of Hooke joints. This type of joint could also be used in other mechanisms.

Application to planar parallel mechanisms

The concept of kinematic redundancy described above can be applied to other types of parallel mechanisms. In [12], a planar (3+1)-DoF kinematically redundant parallel mechanism was proposed. In this case, it sufficed to replace one of the three legs of a conventional planar parallel mechanism with the planar equivalent of the redundant leg shown in Figure 2 to alleviate all singularities. The resulting architecture is shown in Figure 5, where the Plücker lines are represented. In this case, the three lines become dependent when they intersect at a common point or when they become parallel. It is easily observed that, with a proper motion planning of the redundant leg, all singularities can be avoided and the rotation of the platform is unlimited.

The redundant DoF of the planar mechanism described can be used to avoid singular configurations. Avoiding certain specific configurations means that infinitely many non-singular configurations remain available. Therefore, the extra DoF can be used for other purposes, or simply to optimise the kinematic or dynamic behaviour of the robot. In the planar robot described above, the extra DoF can be used to operate a gripper. Indeed, the extra DoF can be

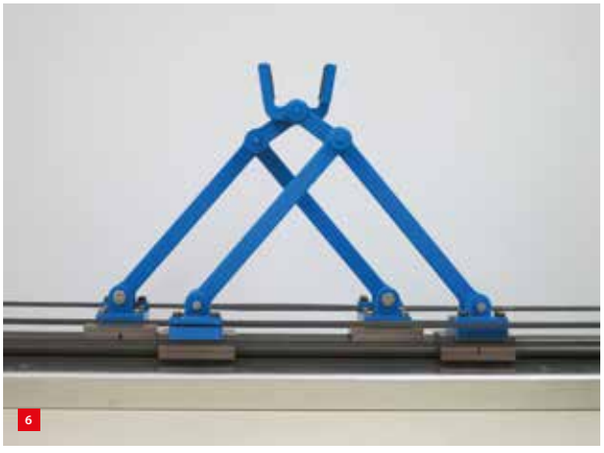

Prototype of a (3+1)-DoF planar parallel mechanism built at Université Laval. This prototype provides unlimited rotational capability of the platform. In a variant of the mechanism, the platform and redundant link can be used as a gripper operated from the base actuators, as demonstrated in the video [V2].

associated with the revolute joint connecting the redundant leg to the platform, which can be mechanically connected to a gripper.

A prototype of a planar (3+1)-DoF kinematically redundant parallel mechanism was designed and built at Université Laval to demonstrate the concept. The prototype, shown in Figure 6, uses fixed prismatic actuators and constant-length rigid legs but the kinematics are very similar to that of the robot illustrated in Figure 5. Video [V2] demonstrates the prototype, including the operation of a gripper from the base actuators, which can be a great advantage for agile robots.

Application to SCARA-type parallel mechanisms

Another class of popular and useful motions are the SCARA motions (or Schönflies motions), which include 3-DoF spatial translations plus rotations around a fixed direction. Four-DoF SCARA robots are very common in industry because many tasks can be performed with this motion pattern. Parallel SCARA robots have been developed before, but it is not easy to find a mechanical architecture that provides fully parallel actuation and unlimited rotation capability.

In [13], kinematic redundancy was applied to the SCARA-type motions and a (4+1)-DoF parallel mechanism was proposed. The fully parallel robot provides the SCARA motions and unlimited rotation around a fixed direction by using a fifth DoF. A CAD model of the robot is shown in Figure 7. It can be observed that the robot consists essentially of two planar subsystems composed of four actuators with parallel axes which provide the unlimited rotation by using a crank-type motion. These subsystems are articulated so that they can be moved in the direction orthogonal to the planar motions using a fifth actuator.

A prototype is shown in Figure 8. It can be observed that the general layout of the robot is very similar to that of a conventional serial SCARA robot, i.e., the actuators can be mounted on a common post, yielding a very compact footprint. This observation highlights another advantage of kinematic redundancy, namely that it makes it possible to significantly change the form factor of a parallel robot. A video demonstrating the prototype of a (4+1)-DoF kinematically redundant parallel robot is available [V3].

Conclusion

Multi-DoF parallel mechanisms that include a combination of translational and rotational DoFs are known to generally have limited rotational workspaces due to parallel singularities. This is especially true for 6-DoF mechanisms.

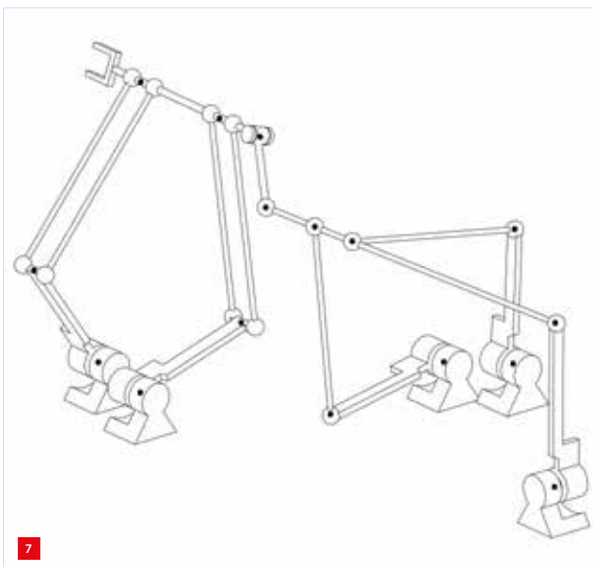

CAD model of the prototype of a (4+1)-DoF kinematically redundant parallel mechanism producing the SCARA motion, showing the arrangement of the links and joints.

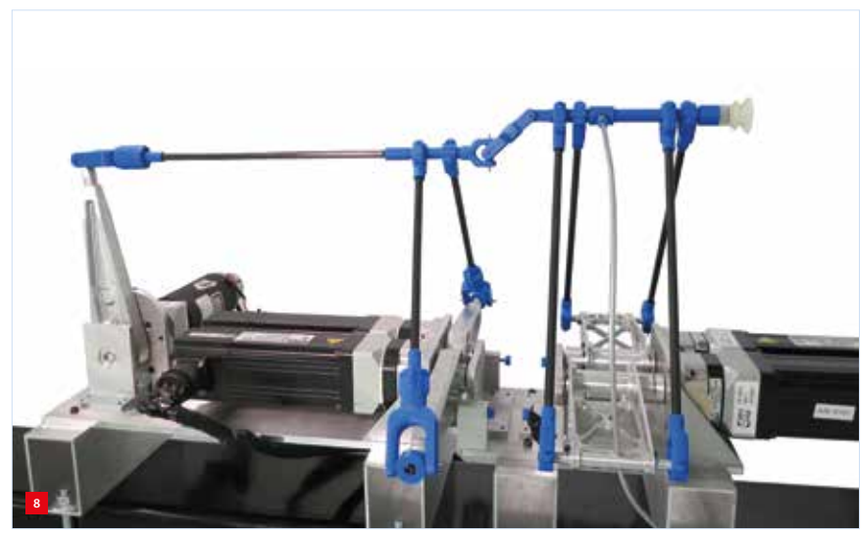

Prototype of a (4+1)-DoF kinematically redundant parallel mechanism producing the SCARA motion, developed at Université Laval.

In this article, it was shown that kinematic redundancy can be used to control the geometric distribution of the links and joints, thereby avoiding singularities and extending the workspace. One key issue is to introduce kinematic redundancy while preserving the desirable properties of parallel mechanisms such as force transmission capabilities, stiffness, accuracy and others.

It was demonstrated that the kinematically redundant leg proposed in [10] can be used to modify the GSP and greatly extend its workspace while preserving its fundamental properties and force transmission capabilities. It was also shown that the approach can be applied to planar and SCARA robots. Three prototypes were shown to illustrate the three types of robots discussed in the article. In the planar case, the kinematic redundancy was used to operate a gripper using the base actuators. (6+3)-DoF spatial kinematically redundant parallel mechanisms that include the operation of a gripper from the base actuators have also been developed and video demonstrations of these robots will soon be available.

REFERENCES

[1] Gough, V.E., and Whitehall, S.G., "Universal tyre test machine", *Proceedings of the FISITA Ninth International Technical Congress*, pp. 117-137, 1962.

[2] Merlet, J.-P., *Parallel robots*, Springer Science & Business Media, 2006.

[3] Clavel, R., "Conception d'un robot parallèle rapide à 4 degrés de liberté", Ph.D. thesis, EPFL, Lausanne, Switzerland, 1991.

[4] Gosselin, C., and Hamel, J.-F., "The agile eye: a high-performance three-degree-of-freedom camera-orienting device", *Proceedings of the IEEE International Conference on Robotics and Automation*, pp. 781-786, 1994.

[5] Luces, M., Mills, J. K., and Benhabib, B., "A review of redundant parallel kinematic mechanisms", *Journal of Intelligent & Robotic Systems*, vol. 86 (2), p. 175-198, 2017.

[6] Gosselin, C., and Schreiber, L.-T., "Redundancy in parallel mechanisms: A review", *Applied Mechanics Review*s, vol. 70 (1), pp. 010802-1-15, 2018.

[7] Harada, T., and Nagase, M., "Impedance control of a redundantly actuated 3-DOF planar parallel link mechanism using direct drive linear motors", *IEEE International Conference on Robotics and Biomimetics*, pp. 501-506, 2010.

[8] Merlet, J.-P., "Singular configurations of parallel manipulators and Grassmann geometry", *The International Journal of Robotics Research*, vol. 8 (5), pp. 45-56, 1989.

[9] Bande, P., Seibt, M., Uhlmann, E., Saha, S.K., and Rao, P.V.M., "Kinematics analyses of Dodekapod", *Mechanism and Machine Theory*, vol. 40 (6), pp. 740-756, 2005.

[10] Gosselin, C., and Schreiber, L.-T., "Kinematically redundant spatial parallel mechanisms for singularity avoidance and large orientational workspace", *IEEE Transactions on Robotics*, vol. 32 (2), pp. 286-300, 2016.

[11] Schreiber, L.-T., and Gosselin, C., "Passively driven redundant spherical joint with very large range of motion", *ASME Journal of Mechanisms and Robotics*, vol. 9 (3), pp. 031014-1-10, 2017.

[12] Gosselin, C., Laliberté, T., and Veillette, A., "Singularity-free kinematically redundant planar parallel mechanisms with unlimited rotational capability", *IEEE Transactions on Robotics*, vol. 31 (2), pp. 457-467, 2015.

[13] Schreiber, L.T., and Gosselin, C., "Schönflies Motion PARAllel Robot (SPARA): A kinematically redundant parallel robot with unlimited rotation capabilities", *IEEE/ASME Transactions on Mechatronics*, vol. 24 (5), pp. 2273-2281, 2019.

VIDEO

[V1] (6+3) Dofs Kinematically Redundant Parallel Mechanism, *www.youtube.com/watch?v=Bf_1pUyjNiM*

[V2] Singularity-Free Kinematically Redundant Planar Parallel Mechanism, *www.youtube.com/watch?v=_vp1ELEtDN4*

[V3] Schonflies motion PARAllel robot (SPARA), a Redundant Parallel Robot with Unlimited Rotation, *www.youtube.com/watch?v=B2BvrgSETD8*

DIRECT OR INDIRECT? THAT'S THE QUESTION

What if it is possible to create an indirect-drive actuator with the benefits of a direct drive? Typical struggles in actuator selection are to balance upsides, such as high force, with the downsides of additional mass, volume and availability. Adding a transmission has its own downsides, such as friction, backlash and hysteresis. But what if a gear ratio can be created with the aid of flexure mechanics, eliminating all these downsides? How does one deal with the parasitic movements, the own guiding stiffness, dynamics and motor choice in a static use case? Here, a pragmatic implementation is presented of an (in)direct-drive actuator that is self-guided and compliant in multiple passive directions to be used in a steady-state multi-axis kinematically coupled system. Stiffness is dominant and accelerations are low, putting the linear motor outside its comfort zone of merely high-dynamic motion.

NIELS KOENRAAD, FRANK SPERLING AND PETER KLEIN MEULEMAN

Load case

Before diving into the principles of direct versus indirect drive actuation it is essential to fully define the load case at hand. This consists of a large mass (> 100 kg) that needs to be actuated in two degrees of freedom (DoFs), i.e. in the *x*- and *y*-direction. A third DoF, the rotation around *z*, needs to be constrained either passively or actively. Theoretically, this can be done by using an intermediate body or another construction element like a bellow, which in turn will introduce its own dynamics and increase the overall complexity. This direction is therefore actively constrained by a third actuator instead. This has as an extra benefit that two actuators (y_1 and y_2) can be used for the *y*-direction (and *Rz*), which for various reasons provides significantly more stiffness in the actuation direction. This in turn possibly allows for the use of the same actuator type for all three positions (one ~~size~~ 12NC fits all).

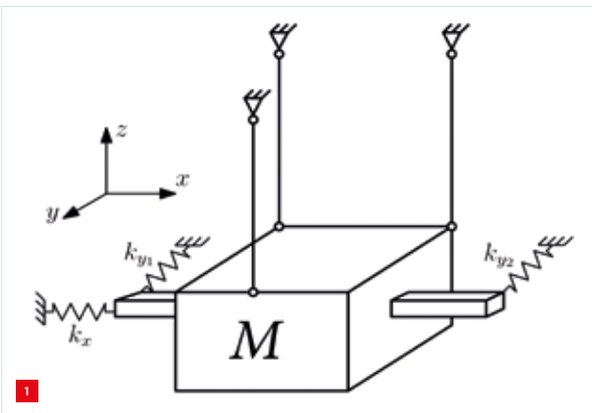

Load guided and passively constrained using flexure mechanics leaving three actively controlled DoFs.

A schematic depiction of the load case is shown in Figure 1. The mass is suspended from the top by three flexible elements that together constrain it in *z, Rx, Ry* and allow for movement in the other DoFs. The actuators are represented by a spring with servo stiffness k_x, k_{y1} and k_{y2}, respectively, with one *y*-actuator on each side to also control *Rz*, and a single *x*-actuator on the right side. From this layout it is apparent that the actuators need to be able to cope with movements perpendicular to the actuator direction: firstly, the functional stroke of the other actuators (millimeter range) and secondly, the parasitic move of the flexure mechanics (tens of microns).

The load will be moved with low acceleration to setpoints where it will remain stationary for long periods of time. During this time, the main function of the actuators is to suppress disturbances from the environment, such as floor vibrations and any flow disturbances to keep a steady position (i.e. trajectories of < 100 µm, < 0.5 Hz). Flexure mechanics can maintain a stable position and enable submicron movements without hysteresis or (local) wear. This will result in a system with high actuation stiffness and low acceleration forces.

In trying to identify and verify all dynamics and mechanics, a functional model (fumo) was made of the load as well as for the different actuator concepts that will be discussed in this article. This fumo is shown in Figure 2, where a mass is suspended from four rods rather than three, yielding an over-determined system. This results from the optimisation process between eigenmodes, actuation stiffness, stresses

AUTHORS' NOTE

Niels Koenraad (system architect), Frank Sperling (director of technology) and Peter Klein Meuleman (lead mechanical engineer) all work at Nobleo Technology, an engineering company based in Eindhoven (NL).

niels.koenraad@nobleo.nl
www.nobleo.nl

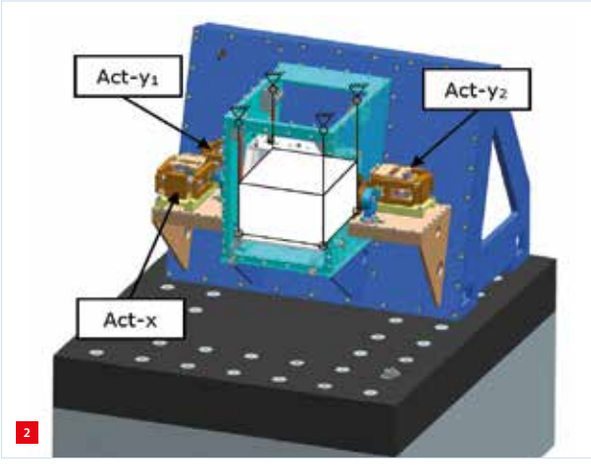

2

Functional model set-up with the load suspended from four rods and actuated by three actuators, one for the x-direction and two controlling the y- and Rz-direction together.

and more that yielded major benefits at the cost of being overdetermined, which to a great extent can be solved in the manufacturing and assembly process. In addition, three actuators that will actuate the mass can be seen in Figure 3, showing their layout with respect to the load itself.

Direct vs Indirect drive

With the load case defined, an actuator can be selected. To sum up: a static use case with little to no peak forces, with parasitic movements in the same order of magnitude as the actuation stroke itself, micron-level movements, no wear, no friction and the ability to suppress high disturbance forces. To add one more requirement not related to the load case per se but to the overall architecture, there is a limited voltage supply (V_{bus} < 30 V) and current (I_{rms} < 3 A). Given this description a logical choice is a direct-drive actuator, which certainly eliminates wear and friction but does not necessarily make it suitable for static use and parasitic movements. Furthermore, it is not so trivial how this choice will affect the capability to suppress disturbances. An alternative might be the indirect drive, but this obviously has drawbacks.

Direct drive

A direct-drive actuator is simply a motor directly connected to the load. For linear motion this is typically in the form of a voice-coil or linear 3-phase motor. The latter is the most suitable in this case, since a voice-coil is constrained in two DoFs by its airgaps, whereas the 3-phase motor is only limited in one DoF. The result is a simple solution with a motor directly fixed to the mass and the stator fixed to the force frame, with only a connecting element, i.e. the servo stiffness k_p as shown in Figure 4. The parasitic movements of one actuator will cause the coils of the perpendicular actuator to move out of the magnet yoke by a few millimeters, resulting in motor constant loss and an additional increase of the complexity of the sensor system. Here, an optical encoder is used to determine the actuation position, which requires a large lateral tolerance for the perpendicular motion

So far nothing is insurmountable, but another issue is the required force (> 100 N) that will have to be created with the limited amplifier supply. For this concept the only possibility to increase force is by increasing the motor size. This is a somewhat inefficient process, because larger motors produce more N^2/W but will see less and less of their potential used. For example, the design might end up with a 500-W motor for a 100-W application simply because there are no other knobs to turn.

Indirect drive

In a lot of applications, fitting a transmission such as a planetary gear, toothed belt or spindle to the actuator is a solution that will make it possible to create high forces (or torques) with a relatively small motor. This typically has drawbacks, the worst being backlash (i.e. play) and friction, which make it especially ill-fitted for an application where submicron positioning is required. An alternative approach is to create a lever using elastic elements, where the distance

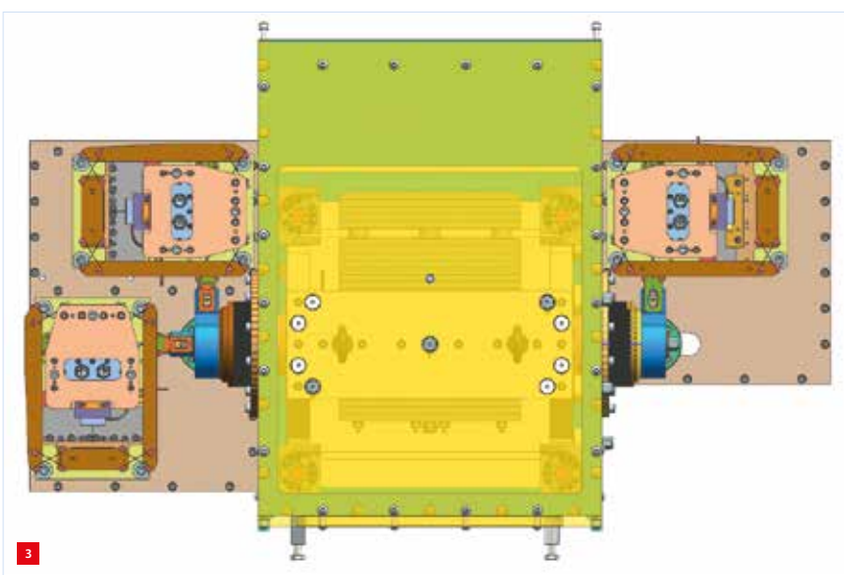

3

Top view of the functional model with the actuator lay-out clearly visible. The bottom left actuator controls the x-direction, the top left and top right actuators control the y-direction and Rz-rotation together.

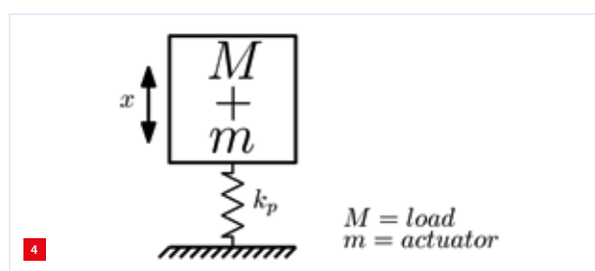

4

Direct-drive actuator connected to the load, resulting in a servo stiffness to the fixed world and a load mass (M) that is increased by the actuator mass (m).

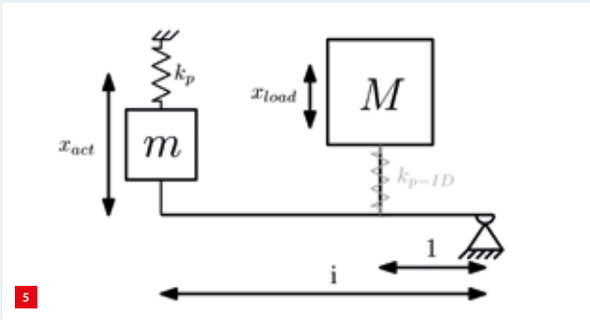

Indirect-drive actuator connected to the load via a gear ratio of 1:i, with stroke and force being scaled by this ratio. Stiffnesses drawn here are the servo stiffness, k_p, and that same stiffness scaled on the load side, $k_{p\text{-}ID}$. Stiffnesses omitted from this drawing are the gear stiffness and load stiffness, which are important to keep in mind for the force budget and will be discussed in the optimisation of the gear ratio itself.

of the motor to the (elastic-) pivot point and that of the load to the pivot point determines the gear ratio, as shown in Figure 5. The force output of the actuator can now be influenced by both the motor size and the gear ratio.

For this to work, a pivot point needs to be created that allows motion and guarantees sufficient stiffness. Additionally, this will have both upsides and downsides regarding the dynamics and control of the complete system. The creation of this pivot point and (optimal) lever will be discussed in the next section. First, a less trivial benefit will be discussed, that of the impact on the servo stiffness.

Servo stiffness amplifier

The main function of the actuator is to suppress disturbances from the environment. This requires a high servo bandwidth or rather high servo stiffness. The disturbances, the dynamics of the load and the stiffness of the reaction path (k_{fp}) are a given, so the last variable in the equation is the actuator itself. Figure 6 shows the load with both the direct-drive (grey) and the indirect-drive (black) actuator, for the first of these the achievable bandwidth will be dictated by the dynamics of the load (which will be negatively influenced by the additional motor mass, because the actuator mass is fully supported by the flexure mechanics of the load). For ease of argument, m is identical for the direct and the indirect drive. The servo stiffness of the direct drive is then:

$$k_p = k_{p\text{-DD}} = (M + m)(2\pi \cdot f_{bw\text{-DD}})^2$$

Note: the reaction path is the force path from the static part of the motor to the 'fixed' world, whereas the action path is that of the moving part of the motor to the load. Their superposition yields the overall dynamics typically shown in a Bode plot.

Assuming the load mass >> motor mass, there is little left to do on the actuator side in terms of dynamics. For the indirect drive, on the other hand, one additional variable, namely the gear ratio 1: i, opens up a field of possibilities:

$$k_p = (M/i^2 + m)(2\pi \cdot f_{bw\text{-ID}})^2$$

$$k_{p\text{-ID}} = k_p \cdot i^2 = (M + m \cdot i^2)(2\pi \cdot f_{bw\text{-ID}})^2$$

By increasing either the motor mass or the gear ratio, the servo stiffness as 'felt' by the load can be increased. Additionally, in contrast to the direct-drive case, this actuator carries its own weight (literally) by its own linear guiding, meaning that it will have little effect on the load dynamics. Of course, there is no such thing as a free lunch; additional mass will have to be moved and the own guiding and mass will introduce its own dynamics that might become dominant instead of the load dynamics. Under the hypothesis that this is not the case (i.e. drive train and guiding are infinitely stiff), the potential of this additional variable will be demonstrated, assuming a motor mass of 3 kg for both types of actuators, a 100-kg mass, a bandwidth of 25 Hz and a gear ratio of 1:5.

$$k_{p\text{-DD}} = 2.5 \cdot 10^6 \text{ N/m}$$

$$k_{p\text{-ID}} = 4.3 \cdot 10^6 \text{ N/m}$$

$$k_{p\text{-ID}} / k_{p\text{-DD}} = 1.7$$

Thus, introducing a gear ratio does not only amplify the force output but the servo stiffness as well. The above example is merely theoretical and in practice increasing the servo stiffness will prove to be more unruly, partly because stiffnesses like k_{lever} and k_{fp}, which have not yet been discussed, will play a role in the design of the indirect-drive actuator.

Action and reaction path dynamics

An additional differentiator between the two types of actuators are the relative amplitudes of the action path with respect to the reaction path (i.e. the amplitude difference).

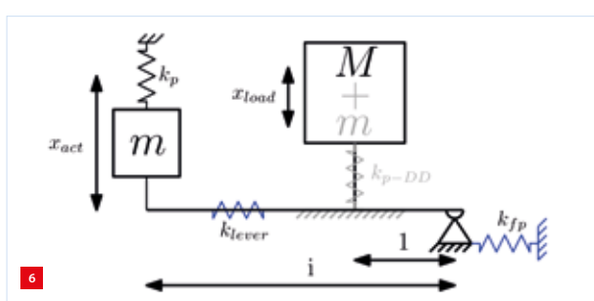

The combined result of a direct-drive (grey) and indirect-drive (black) system can be seen here, with the relevant mechanism stiffnesses (blue) that were omitted from the earlier figures. These stiffnesses become relevant when looking at the action/reaction path dynamics, because in reality the hinge (on the right) is not a 'fixed' world, but a relatively large mass with its own dynamics that may influence the load.

In Figure 7, the action, reaction and total dynamics (force-to-displacement) of the direct-drive actuator in the total system (load and environment) is plotted. This shows that at higher frequencies (> 100 Hz) the reaction path becomes dominant and will limit the maximum achievable bandwidth. However, these reaction path dynamics are often beyond the scope of the design, so limited influence can be exerted on them.

Figure 8 shows the same transfer functions for the indirect-drive actuator in the total system. Here, the reaction path is not dominant due to the higher relative amplitudes of the action path with respect to the reaction path. From a motor perspective, this can be intuitively explained by the load mass being reduced by the square of the gear ratio, resulting in a 'lifted' action path (see absolute numbers of magnitude in Figures 7 and 8). However, the reaction path is lifted too, because there has to be a force balance (e.g. 1 N on motor side is 5 N on load side) that results from the pivot point taking a large share of this balance. Since this effect is linear, there is ultimately a gain in the relative amplitudes. Here, the achievable bandwidth is limited by the dynamics of the actuator itself, more specifically the introduced compliancy of the drivetrain stiffness (i.e. the stiffness of the lever is not infinite as was hypothesised in the previous subsection).

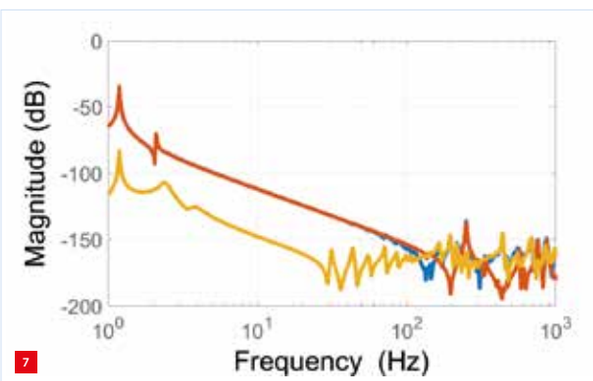

Direct-drive and load dynamics, action (red), reaction (yellow) and total path (blue) transfer functions (force-to-displacement) plotted in a Bode magnitude diagram.

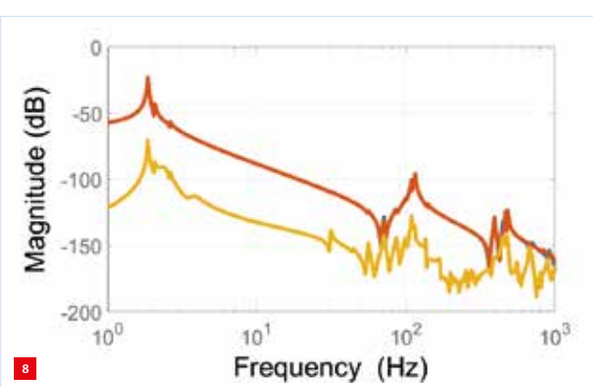

Indirect-drive and load dynamics, action (red) reaction (yellow) and total path (blue) transfer functions (force-to-displacement) plotted in a Bode magnitude diagram.

Whether this is an advantage or not depends on the design scope. When all dynamics in the action and reaction path are in control it might not be necessary to decouple the two. However, as in most cases, only part of the design is within scope here. In this case, this concerns the actuator and the load design; other dynamics are out-of-control and uncertain. The decoupling of the reaction path from the action path is therefore considered as a benefit here, since this makes it more insensitive to frame dynamics.

Pros and cons

To sum up, Table 1 lists the pros and cons of both drive concepts for this use case. Some characteristics will turn out better or worse in a different load case. To further analyse the differences between the direct- and indirect-drive concepts for this load case, both concepts have been designed, built and tested.

Design

The following designs for the direct- and indirect-drive actuators are functional models and lack the details and maturity of a prototype. However, given that both concepts have been developed to this level, they provide a fair comparison. The design of the direct-drive actuator (Figure 9) consists of few elements, namely: motor(s), encoder(s), a body (i.e. moving platform) holding both motor and encoder, and the fixed world. In both actuators, the 'fixed world' holds the coils and is actively cooled to limit the motor temperature. The 3-phase motor shown here consists of two motors that are – parallelly – electrically connected, making it a single motor for the amplifier. For this to work, the alignment of the coils with respect to the yokes and with respect to each other is important, since misalignments will result in motor constant losses. However, this is a cosine effect, so small misalignments (a small percentage of the magnet pitch) are acceptable. A double encoder system is

Table 1
Pros (+) and cons (–) of the direct-drive and indirect-drive concept.

Direct drive	Indirect drive
+ Low part count	– Complexity / internal guiding
– Control bandwidth limited by reaction path dynamics	+ Insensitive to reaction path dynamics
+ High drivetrain stiffness	– Additional mechanics in drivetrain
	+ Parasitic movements can be decoupled from motor
+ Inherently linear and backlash- and hysteresis-free drivetrain	
– Force requirements determine motor size	+ Motor size and gear ratio can be tailored to force requirements (more knobs to turn)
– Dynamic stiffness function of servo stiffness only	+ Dynamic stiffness function of servo stiffness and gear ratio

Gear ratio

When working with a gear ratio that is accomplished with the use of an elastic lever, not every ratio is beneficial for the force budget. Increasing the ratio will reduce the required motor force to move the load. However, this yield diminishes as the ratio increases and will flatten out after a certain ratio has been reached. In contrast, the motor force required to move the actuator itself will increase proportionally, eventually leading to a system where more force is required to move the actuator than the load itself. In Figure 11a two additional stiffnesses are shown, k_{gear} and k_{load}, representing the stiffness of the load and actuator in the actuation direction, respectively. Figure 11b shows the trade-off between the linear and nonlinear effects. For this particular case, a ratio of 1:5 was chosen as an optimum, also taking into account volume, stresses, dynamics, etc.

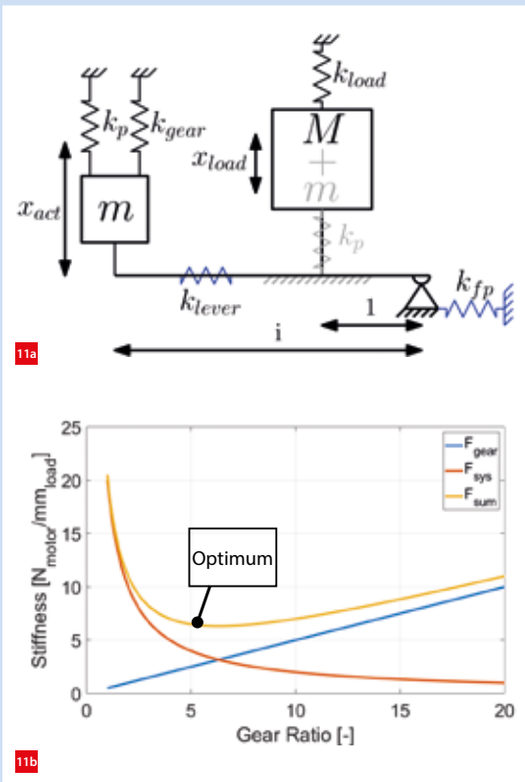

Finding the optimal gear ratio for the force budget.
(a) The system with stiffnesses on the load side (k_{load}) and on motor side (k_{gear}).
A ratio is chosen that results in the lowest motor force.
(b) The optimisation in the graph with the exponential curve of increasing the ratio for load stiffnesses, versus the force required to compensate the linear increase in motor stiffness, due to the increasing stroke on the motor side.

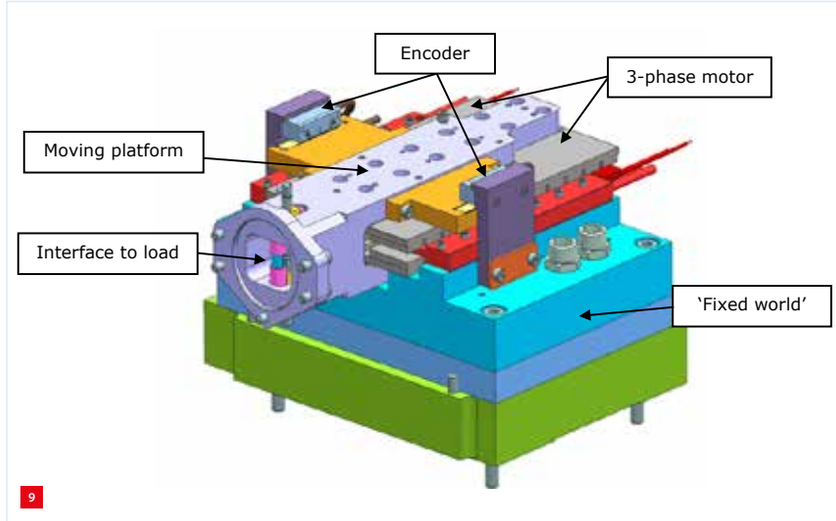

Direct-drive functional model design, with the two encoders enabling 'virtual encoder placement' along the central axis. Coil-to-magnet positioning depends on the frame/system environment.

present in this motor, so that the encoder can be on either side of the motor or virtually in the middle. This is not of significance for the actuator discussion and will not be elaborated in more detail here.

The design of the indirect-drive actuator requires a more elaborate explanation. It is obvious from Figure 10 that this design is more complex than its counterpart. As in the previous concept, this one also contains a motor, encoder, moving platform and fixed base. Additionally, there is the lever, the elastic pivot point(s) in the form of a cross-spring hinge and an interface rod. In this design a ratio of 1:5 is used (the optimisation is presented in the text box). Here, the rear body (or lever) acts as the force transfer and transmission. The front body (or support arm) does neither and only functions as an additional support pillar to complete the parallelogram shown in the next section; because of this it can be much leaner than the functional lever, if permitted by the dynamics.

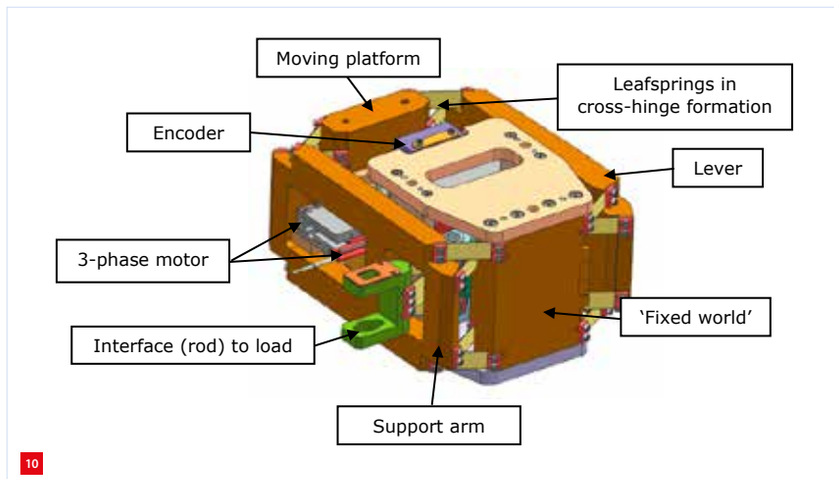

Indirect-drive actuator functional model design.

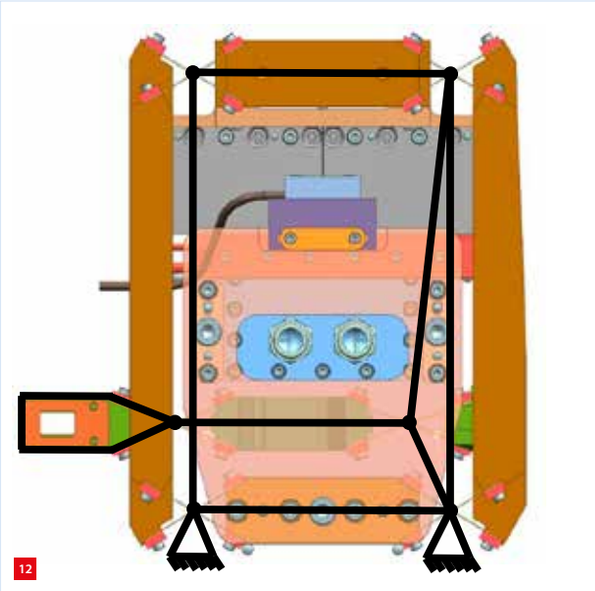

12

The indirect drive as a parallelogram fulfils the same function as the simpler seesaw but with some practical benefits. In this top view of the actuator, the virtual hinges of the 'skeleton' (black) coincide with the pivot points of the cross-leafspring hinges. The connecting mechanics are shown as rigid bodies connecting the pivot points.

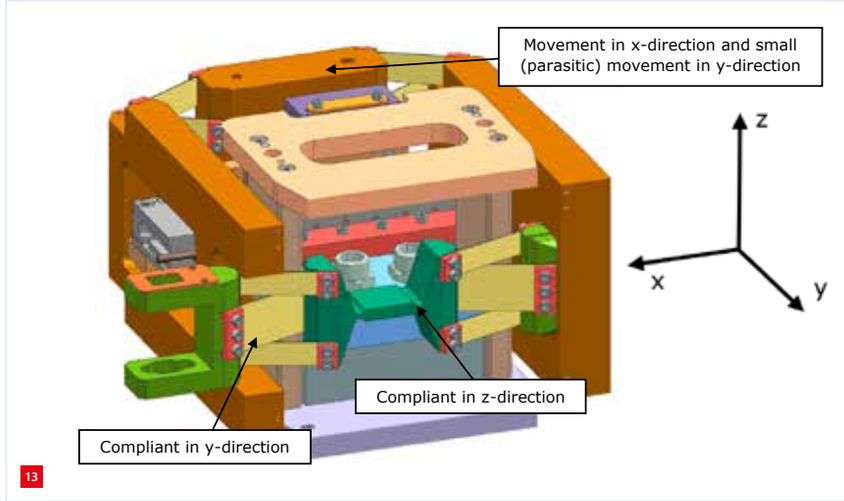

13

Section of the indirect-drive actuator, showing that the interface rod is compliant in two DoFs (y and z), decoupling the parasitic load movements from the motor.

Parallelogram

To create a functioning indirect drive the simple seesaw from Figure 5 was elaborated into a parallelogram as shown in Figure 12. The pivot points are in the centre of the cross-spring flexure and the moving platform is situated further from the fixed base hinges than the connecting interface rod. In fact, this difference in distance is 1:5, creating the intended ratio. From this image it can also be deduced why the support arm (left) has no function as a lever or force transmission: as the interface rod protrudes through this arm it is not in the force path. The movement of the parallelogram is not perfectly linear, but instead describes an arc with a radius equal to the lever length. Because of this, the magnet will move laterally over the coil as a function of the actuation position. This effect is smaller than the parasitic movements induced by the load.

Interface rod

The lateral movement of the magnets with respect to the coil will be smaller than 1 mm, whereas in the original load case – and this is what the direct drive has to cope with – there is a parasitic movement up to 4 mm. The interface rod is compliant in two DoFs as shown in Figure 13, the leafsprings being compliant in the *y*-direction and the middle body in the *z*-direction. This allows the load to move in two directions and also allows for the parasitic movement of the flexures of the load in the *z*-direction. This completely decouples these parasitic movements from the motor and will only result in a small force.

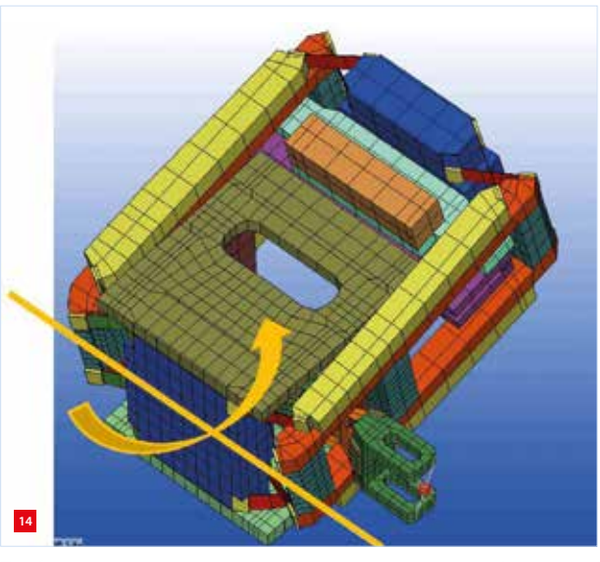

14

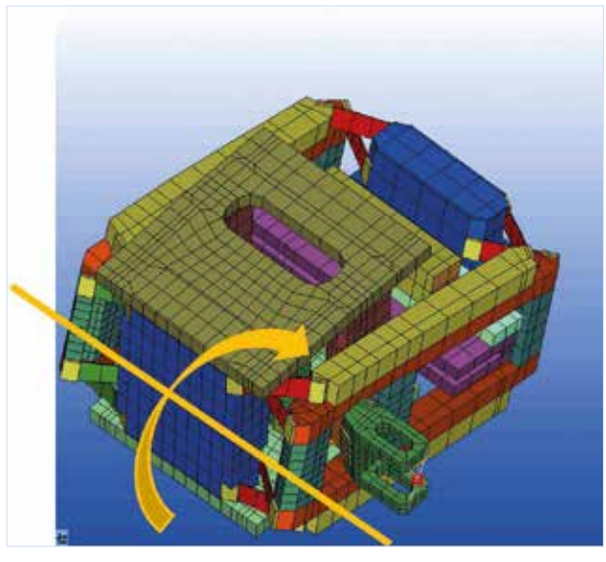

The first eigenmode is the motor rotating around the x-axis (orange line).

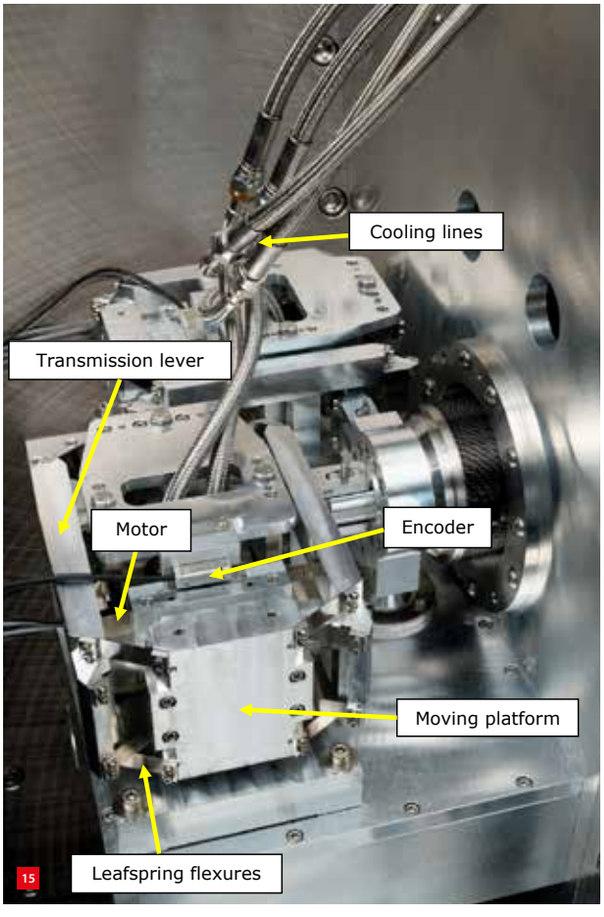

Realisation of the indirect drive actuators, here showing two identical actuators for x and y.

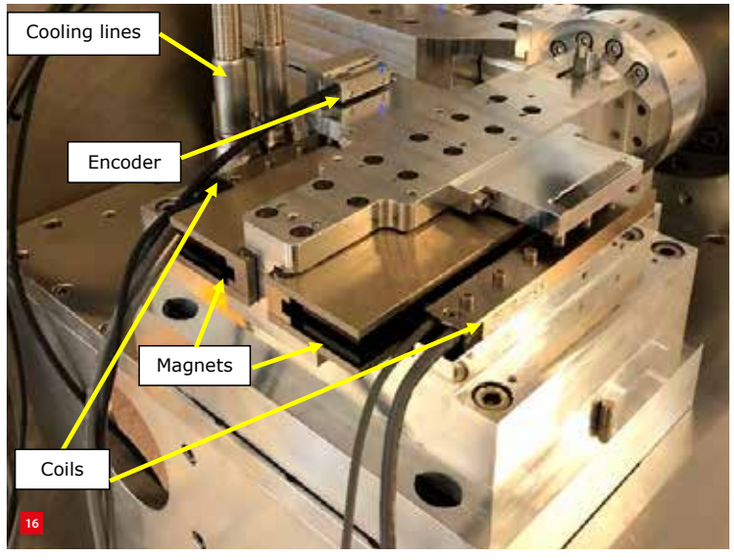

Realisation of the drive actuators, here showing the actuator for the x-direction.

Dynamic considerations

To understand the geometry of the indirect drive it is necessary to consider the dynamics of the actuator. In the section on the servo stiffness of the actuators, the dynamics of the indirect drive were assumed to be infinitely stiff. In reality this is obviously not the case, nor do they need to be; they just have to be non-critical for the overall system. For the parallelogram implementation there are two parasitic eigenmodes that deserve some attention, the first being the rotational mode around the base as shown in Figure 14. The motor mass is a given, as is the arm on which it sits, so what remains is to increase the stiffness of the arms; this explains the height of these bodies as well as the wide placement of the leaf springs. In the second eigenmode the load and the motor move in anti-phase; this is due to the limited drive train stiffness and is a direct consequence of an indirect-drive concept. This can be improved, i.e. raising the frequency of the second eigenmode, by tuning the stiffness of the lever and the interface rod, and has been here to the point where the second eigenmode is no longer a limiting factor.

Lastly, there is an eigenmode that is not necessarily inherent to the parallelogram configuration but to the type of flexures. In the case of a normal reinforced leafspring, there is little to no lateral stiffness, but there is significant mass in the middle of the flexure. This typically starts resonating at much lower frequencies than when used with cross-spring flexures, because these do provide the lateral stiffness. This explains why the design described here contains cross-spring flexures.

Realisation and conclusion

Figures 15 and 16 show the realised functional models of the actuators, on which much of the data and insights discussed in this article are based. Returning to the initial question: direct or indirect drive? The answer to this is more nuanced and less trivial than common practice may suggest. In this specific case it was shown that even though direct drive is definitely not infeasible, indirect drive does have some clear and non-intuitive advantages, making it the clear winner for this case.

UPCOMING **EVENTS**

Please check for any rescheduling, online reformatting or cancellation of events due to the coronavirus crisis.

15-18 September 2020, Geneva (CH)
EPHJ Exhibition
Technological innovation and expertise in the watchmaking and jewellery, microtechnology and medical technology sectors.

WWW.EPHJ.CH

Virtual event

22-25 September 2020
e-Micronora
Microtechnology trade fair, featuring thematic webinars and pitch sessions by experts, b2b meetings and technical, innovative videos by 2021 Micronora exhibitors (21-24 September 2021, Besançon, France).

WWW.MICRONORA.COM/E-MICRONORA

24 September 2020, Den Bosch (NL)
Dutch System Architecting Conference
This third edition features system architecting as a distinguishing discipline in the development and commercialisation of complex systems, products and machines.

WWW.SYSARCH.NL

29 September 2020, Eindhoven (NL)
DSPE Knowledge Day Contamination Control
DSPE event on Engineering for Contamination Control. See also page 49.

WWW.DSPE.NL/EVENTS/AGENDA

6-8 October 2020, Braunschweig (DE)
Special Interest Group Meeting: Structured & Freeform Surfaces
Focus on research in replication techniques, structured surfaces to affect function, precision freeform surfaces, large-scale surface structuring, surfaces for nanomanufacturing and metrology.

WWW.EUSPEN.EU

Virtual event

19-23 October 2020
35th ASPE Annual Meeting
Virtual meeting of the American Society for Precision Engineering, introducing new concepts, processes, equipment, and products while highlighting recent advances in precision measurement, design, control, and fabrication.

WWW.ASPE.NET

20 October 2020, Veldhoven (NL)
Vision, Robotics & Motion
Network event on flexible, reliable, safe and fast manufacturing as facilitated by automation, robotics, machine vision and motion control.

WWW.MIKROCENTRUM.NL

29 October 2020, Veldhoven (NL)
Technology for Automotive 2020
Organised by RAI AutomotiveNL and Mikrocentrum, combining the Automotive Congres and the AutomotiveNL Supplier Day. Topics include green & smart mobility, manufacturing & logistics and materials & design.

WWW.TECHNOLOGYFORAUTOMOTIVE.COM

4 November 2020, Bussum (NL)
National Contamination Control Symposium
Event, organised by VCCN (Dutch Contamination Control Society), comprising a lecture programme, tutorials and an exhibition.

WWW.VCCN.NL

16-18 November 2020, Veldhoven (NL)
Special Interest Group Meeting: Precision Motion Systems & Control
The first edition of this SIG Meeting is organised prior to and partly in parallel with the Precision Fair 2020 (see below).

WWW.EUSPEN.EU

18-19 November 2020, Veldhoven (NL)
Precision Fair 2020
Twentieth edition of the Benelux premier trade fair and conference on precision engineering, organised by Mikrocentrum.

WWW.PRECISIEBEURS.NL

26 November 2020, Utrecht (NL)
Dutch Industrial Suppliers & Customer Awards 2019
Event organised by Link Magazine, with awards for best knowledge supplier and best process & parts supplier, and the Best Customer Award.

WWW.LINKMAGAZINE.NL

Virtual event

3-4 December 2020, Utrecht (NL)
International MicroNanoConference 2020
A wide range of technologies are presented, covering fields such as Health & Life science, Agro & Food, Sustainability & Energy, and Manufacturing & Engineering.

WWW.MICRONANOCONFERENCE.ORG

2 February 2021, Veldhoven (NL)
CLEAN 2021
This theme day, organised by Mikrocentrum, provides an expert's view on cleanliness, focusing on design, production, assembly and packaging.

WWW.MIKROCENTRUM.NL

March 2021, UK
Lamdamap 2021
Fourteenth edition of this event, focused on laser metrology, coordinate measuring machine, and machine tool performance.

WWW.EUSPEN.EU

INVESTIGATING INDUSTRIAL FEASIBILITY OF FLEXURES

Elastic hinge mechanisms (flexures) exhibit no friction or play, which makes them suitable for accurate, clean applications such as positioning in a vacuum. This article presents the design, manufacturing and validation of an elastic hinge mechanism that serves as the elbow hinge in a crank-slider manipulator, which is applicable industrially as a rotation point in a wafer-handling robot. The main challenge was to achieve a large rotation angle without the loss of support stiffness. The design, comprising four Ti-6Al-4V leafsprings, was shown to meet the required specifications. With regard to the eigenfrequencies, the simulations and experiments agreed within 10%.

STEF VAN HAAREN, JAAP BRAND AND DANNIS BROUWER

AUTHORS' NOTE

Stef van Haaren (factory engineer) and Jaap Brand (system architect) work at VDL ETG.
Dannis Brouwer is professor in the chair of Precision Engineering at the University of Twente, Enschede (NL). Last year, Brand was appointed as a (part-time) fellow in this chair.
Van Haaren performed the work described in this article at VDL ETG for his M.Sc. work in the Precision Engineering group.

stef.van.haaren@vdletg.com
www.vdletg.com
www.utwente.nl/en/et/ms3/research-chairs

Introduction

Cluster tools are robots that are used in chip manufacturing processes, where a wafer must be handled after each process step. The tool consists of a vacuum chamber with several process chambers connected to it. A wafer handler transports the wafer from one process chamber to another. Wafer-handler robots are often based on a SCARA (selective-compliance-articulated robot arm) principle [1].

At Eindhoven University of Technology (NL) there is a new wafer handler under development. It is based on a crank-slider manipulator, comprising three rotation points (shoulder, elbow and wrist hinge) and two arms (upper and lower arm); see Figure 1. The end-effector is actuated by the lower arm and is supported in five directions (x, z, R_x, R_y and R_z) using seven active pre-tensioning magnetic bearings [2]. These bearings are able to actuate the carriage in both the positive and negative direction. A membrane in the wrist joint between the lower arm and the end-effector decouples the lower arm from the end-effector in three directions (z, R_x and R_y). Figure 1 shows the motion of the membrane in these three directions.

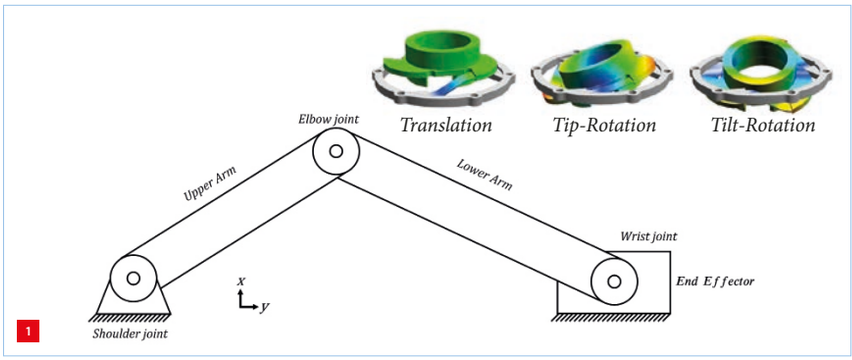

Schematic view of a crank-slider mechanism and visualisation of a membrane releasing three overconstraints.

In a vacuum environment, this robot is not allowed to generate or release any particles, nor are its rotation joints. Designing a flexure-based rotation joint reduces the risk of contamination through particles; flexure mechanisms do not generate or release particles when they move. As mentioned above, flexure mechanisms are suitable for use in applications demanding high repeatability, reproducibility and cleanliness. No lubrication is required and no particles are generated, as movement is based on elastic deformation only.
Unfortunately, flexure mechanisms suffer from a major disadvantage: their complexity in terms of design and manufacturability rapidly increases at large flexure deflections, as high support stiffnesses are then required. Figures 2 and 3 show examples of complex flexure mechanisms that have high support stiffnesses at large flexure deflections.
As far as is known, an elastic hinge mechanism with a large deformation angle, i.e. with more than 60° deflection, has never been made industrially applicable and tested. Hence, this research aims to prove the industrial applicability of elastic hinge mechanisms with a large rotation angle, on the basis of the aforementioned wafer handling application. The objective is to design, manufacture and validate an elbow hinge based on flexures.

Requirements

The crank-slider mechanism should meet the requirements listed in Table 1. The maximum forces on the magnetic bearings in the end-effector are limited. This is why actuation stiffness of the flexure mechanism may not exceed 0.9 Nm/rad. Accelerations (< 2.1 m/s^2) of the robot and forces on the elbow hinge are moderate. Therefore, the stiffness requirement for a minimum parasitic (or unwanted) eigenfrequency of 100 Hz is the most important one. It only holds in the fully extended position, in which the wafer is transported to and from the wafer handler.

Table 1
Requirements on the flexure-based crank-slider mechanism.

Description	Requirement		Remark
	min	max	
Carriage range of motion (mm)	330		Third-order motion profile
Cycle time (s)		1.05	From retracted to extended position
Carriage mass (kg)		1.5	Vertically supported by magnetic bearings
First parasitic eigenfrequency (Hz)	100		In fully extended position
Containment radius (mm)		410	Smallest radius in which wafer handling robot can rotate while fully retracted
Magnetic bearing load (N)		5	Due to flexure stiffness and (de)acceleration
Cycles	$75 \cdot 10^6$		From retracted to extended position
Environmental pressure (mbar)	$1 \cdot 10^{-6}$	$1 \cdot 10^{-5}$	
Environmental temperature (°C)	22	22	
Box z-dimension of design from shoulder to wrist (mm)		50	Limited by load lock
Setpoint error extended position (mm)		0.1	

Method

An important and useful tool for flexure design is SPACAR, a nonlinear, multibody, finite-element software package developed at the University of Twente [5]. With SPACAR, it is possible to calculate stiffness and stresses occurring during large deformations of flexures rapidly. Within SPACAR, the nonlinear behaviour of elastic mechanisms at high deformation is described by analytical expressions.

Various flexure concepts have been developed and calculated in SPACAR. A fair comparison between these different concepts was made using a number of design criteria: installation size of the hinge, drive stiffness and occurring stresses. In order to arrive at suitable dimensions for the chosen concept, the complete flexure-based crank-slider manipulator was then modelled in SPACAR. With this model, the elbow hinge could be dimensioned to meet the requirements of Table 1. In this model, the upper and lower arm are considered to be infinitely stiff.

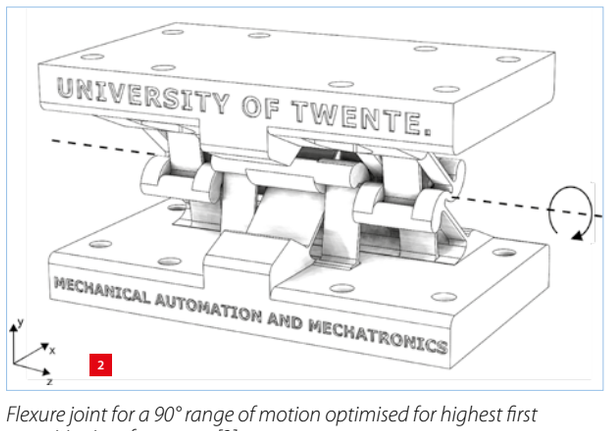

Flexure joint for a 90° range of motion optimised for highest first parasitic eigenfrequency [3].

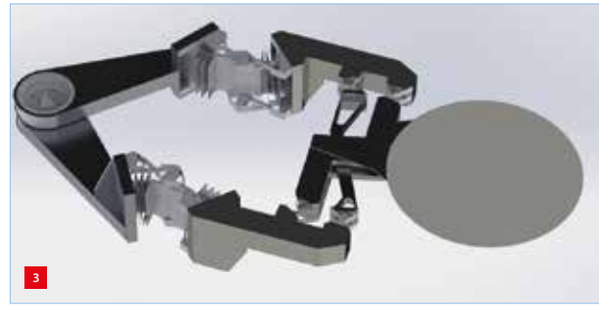

SCARA-robot with two elbow and four wrist flexures [4].

A CAD model was then created based on the SPACAR model. Design details, such as connections between different parts, have been elaborated and the arms were designed as well. As a next step, the complete and realistic CAD model of the flexure-based crank-slider manipulator was modelled in Ansys WorkBench, in order to verify that the CAD model of the hinge matches the SPACAR model. More importantly, it enabled the eigenfrequencies of the mechanism and stresses in the hinge to be calculated. These were slightly different from the calculated values in SPACAR, because it is easier to approximate reality in Ansys WorkBench. Finally, the eigenfrequencies of the flexure-based robotic arm have been validated in practice and compared with Ansys simulations.

Flexure mechanism design

Using various flexure concepts, it is possible to develop a structured design process for flexure mechanisms. The main goal is to develop a flexure concept that has high support stiffness when it is subjected to large deformations. Secondly, the design of the flexure mechanism should remain low in complexity. This will increase manufacturability, which is important as the mechanism has to be industrially feasible. For some time now, additive manufacturing has offered the possibility of manufacturing metal components with high design complexity. However, the fatigue life of these components is not yet on the same level as that of flexures made with more conventional technologies, such as wire-EDM [6].

Figure 4 shows the first design iteration, with a cross hinge serving as a starting point. Adding a third leafspring increases stiffness. Reinforcing the inner leafspring with ribs increases torsional stiffness. However, the outer leafsprings can also be replaced with two serially stacked cross hinges. This in particular increases the translation stiffness on

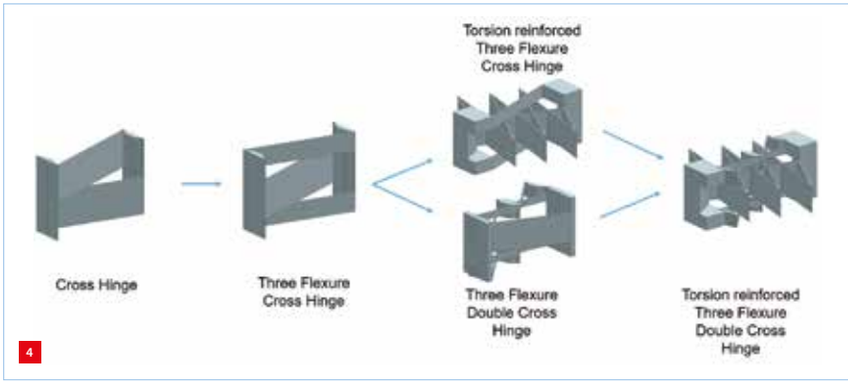

First flexure concept iteration.

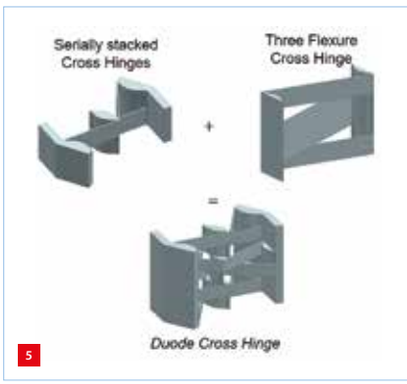

Second flexure concept iteration.

Third flexure concept iteration.

deflection, as well as the critical buckling load. Optimal stiffness can be achieved by combining both reinforcements. Unfortunately, this results in a very complex design, although the support stiffness is very high. This concept has been implemented by Naves [3] and Barels [4] (see Figures 2 and 3, respectively).

In the second iteration, the starting point is a Three Flexure Cross Hinge (cross hinge with three leafsprings). Replacing all leafsprings with two serially stacked cross hinges increases the support stiffness significantly. Unfortunately, this results in a complex concept that includes twelve leafsprings (Figure 5). Therefore, the same has been done in Figure 6, but now with a cross hinge with two leafsprings serving as a starting point. This reduces the final complexity, while keeping the support stiffness high enough. This Quad Cross Hinge concept was ultimately selected because of its high support stiffness with respect to its relatively limited design complexity.

Dimensioning flexure mechanisms

After the concept of the flexure mechanism had been selected, it had to be dimensioned. Using a parametrised design, the influence of parameters on stiffness was studied. For parametrisation, a Three Flexure Double Cross Hinge flexure concept (Figure 7) was selected, as it contains all possible design parameters. This concept consists of a cross hinge with three leafsprings. The two outer leafsprings have been replaced by two serially stacked cross hinges. This concept features all the design variables that other concepts also have. Here, ϕ represents the angle (xy-plane) between the inner and outer layers, whereas ψ represents the angle (xy-plane) between the leafsprings of the cross hinge in the outer layers.

Using a sensitivity study, the influence of each design parameter on the support stiffness of the Quad Cross Hinge flexure concept was studied. Support stiffness is the stiffness in directions other than the actuation direction (K_z in this application). Intuitively, it can already be seen that a smaller angle ϕ will result in dominant translation stiffness in y-direction, while translation stiffness in x-direction will drop.

Figures 8 and 9 present the influence of design parameters ϕ and ψ on the support rotation stiffness along the x- and y-axis, respectively. The nonlinear influence of these design parameters on the support stiffness is shown. Next to that, the figures show the compromise required between the support stiffnesses in two directions when choosing values for ϕ and ψ: an optimal rotation stiffness K_x results intrinsically in low stiffness K_y. As the elbow joint in the crank-slider mechanism requires an as-high-as-possible rotation stiffness along both the x- and the y-axis, a value of 50° to 60° for the ϕ and ψ angles was selected. This compromise is the same for other concepts featuring the design parameters ϕ and ψ, for example the Three Flexure Double Cross Hinge.

In the same way, values for the other design parameters have been selected. The only difference is the linear influence of the remaining design parameters on support stiffness. Finally, some design parameters are constrained by the allowable box dimensions (e.g. height in z-direction of the flexure mechanism).

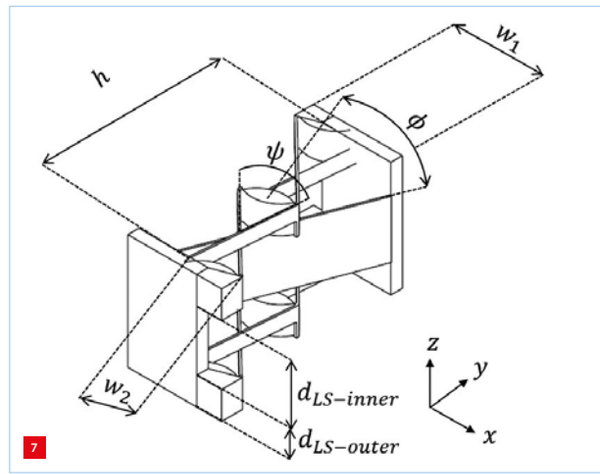

Parametrised design of a flexure mechanism.

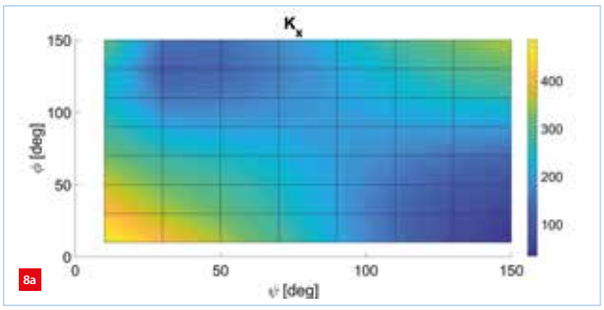

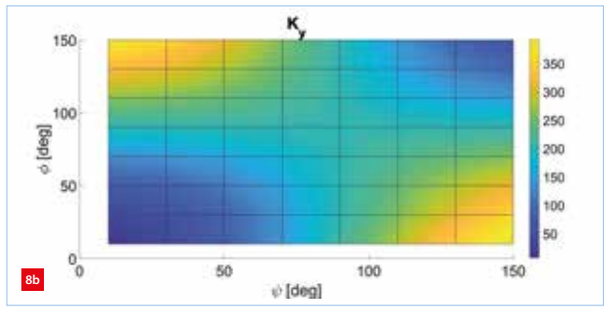

Influence of ϕ and ψ on support rotation stiffness (in Nm/rad).
(a) K_x.
(b) K_y.

Detailed design

Figure 9 presents the design of the flexure-based elbow hinge. The two orange flexures are identical, as are the two blue ones. The flexure mechanism is based on the Quad Cross Hinge concept, shown in Figure 6.

Figure 10a depicts the exploded view of the flexure-based robot arm. The leafsprings, manufactured by milling and wire-EDM, are fixed to the arms using two bolts and two dowels. The orange and blue leafsprings are attached to each other at the intermediate body. The upper and lower arm are based on an H-profile. Stiffness is increased with the aid of lids.

Figure 10b depicts the realisation of the produced robot arm. The shoulder and wrist shafts (purple and light blue, respectively) connect the arms to the shoulder and wrist joint, respectively, and are glued to the arms using epoxy glue Araldite 2030. This glue provides high stiffness and exhibits low outgassing, making it suitable for use in a vacuum, as shown by several examples from, for instance, ASML. Outgassing is minimised by keeping the glue gap as small as possible.

The flexure-based crank-slider manipulator should last a minimum of 75 million cycles; see Table 1. This means that the leafspring fatigue stress is important and should be high, while the elasticity modulus should remain low in view of the stresses that occur. Figure 11 shows the fatigue stress (i.e. endurance limit) and elasticity modulus (i.e. Young's modulus) of various materials. Both Ti-6Al-4V, a titanium alloy with a high strength-to-mass ratio, excellent corrosion resistance and high yield strength, and the Stavax steel grade were found to have good mechanical properties for use in flexures. Ultimately, Ti-6Al-4V was selected, because there were more literature sources available concerning fatigue stress for this alloy than for the Stavax. Amongst others, [7] and [8] report a fatigue stress of 432 MPa for Ti-6Al-4V.

Results

The first parasitic eigenfrequency gives an indication of the stiffness of a system. The first eigenfrequency of the flexure-based crank-slider manipulator is a mode in which the system is retracting and extending. The first parasitic eigenfrequency (second eigenfrequency) should then be as high as possible. These eigenfrequencies have been simulated in Ansys WorkBench.

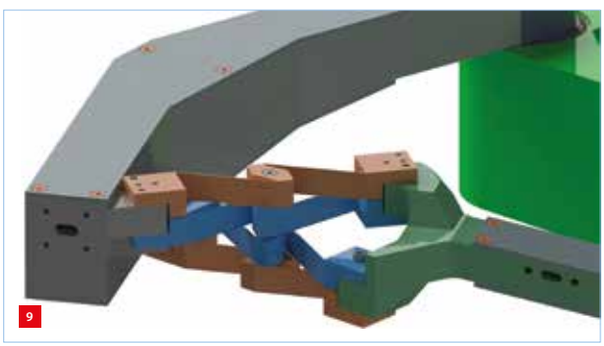

Detailed view of the flexure-based elbow hinge.

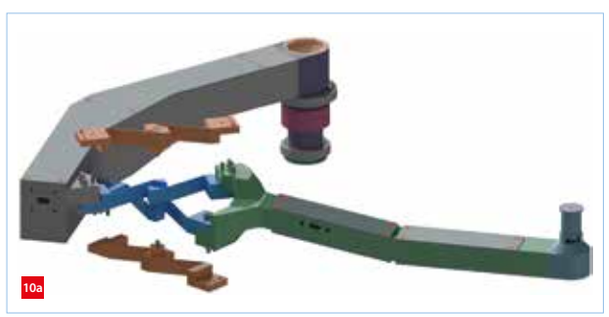

Flexure-based robot arm.
(a) Exploded design view.
(b) Produced version.

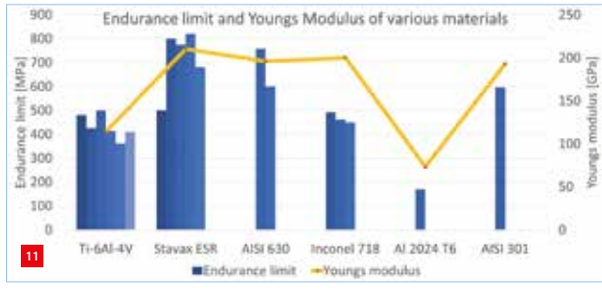

Endurance limit and Young's modulus of various materials, as reported by various sources in literature (indicated by different shades of blue for the endurance limit).

Figure 12a shows the first parasitic eigenfrequency of the fully extended crank-slider manipulator. The frequency f_2 = 74 Hz is caused by the elbow joint twisting and the membrane bending. This frequency is higher when the hinge is less deformed. Making the membrane stiffer increases the frequency aswell. A frequency of more than 100 Hz is then feasible.

Figure 12b shows the second parasitic eigenfrequency. This vibration is due to bending of the upper arm. The frequency f_3 = 80 Hz is independent of the angular rotation of the elbow hinge. With a lighter, stiffer redesign of the upper arm, a frequency of more than 100 Hz can be achieved. This has not yet been implemented, but is considered to be feasible.

Stresses

Stresses (in the hinge) have been calculated in Ansys WorkBench, while the average stresses had been calculated in SPACAR previously. In the retracted and extended positions, maximum mean stresses are 341 and 270 MPa, respectively (Figure 13). This corresponds to a hinge deformation angle of 45° and –37°, respectively, in these positions.

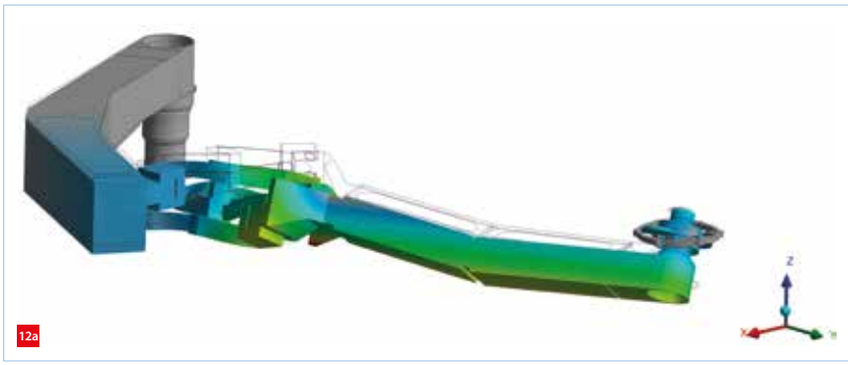

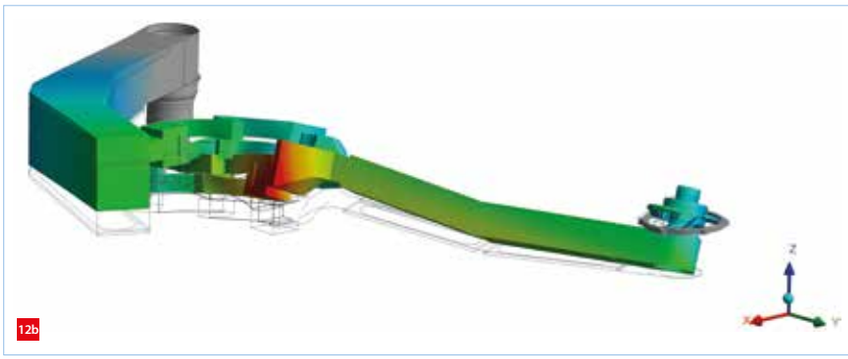

Parasitic eigenfrequencies of the fully extended flexure-based crank-slider mechanism.
(a) First.
(b) Second.

The influence of stress concentrations has been calculated in Ansys WorkBench. It was found that a radius of 0.5 mm (equal to the leafspring thickness) results in 35% higher stresses. As a result, maximal stresses are 341 MPa + 35% = 460 MPa, which exceeds the endurance limit. Fortunately, a radius of 2 mm instead of 0.5 mm decreases the concentration of stresses to +15% (Figure 14), which results in stresses not exceeding the fatigue limit anymore.

Validation of stiffness

Simulations of the crank-slider mechanisms in Ansys WorkBench will only ever be an approximation of reality. To estimate the accuracy, eigenfrequencies of the system from Figure 10b have been derived from modal analysis. Using an elastic band, the mechanism is deformed to measure eigenfrequencies with flexure deflection. Three accelerometers are used to measure the first four eigenfrequencies. Note that these eigenfrequencies are used to compare Ansys WorkBench simulations with results from practice. They do not offer information about the actual flexure-based slider-crank mechanism.

Figure 15 presents the eigenfrequencies of the mechanism from Figure 10b when deformed, as calculated by Ansys WorkBench and determined by experiment, respectively. Both methods exhibit the same trend of frequencies with flexure deformation and mutually deviate maximally 10%.

Conclusions

The work described in this article has demonstrated that it is feasible to meet the requirements of a wafer handler. The first two parasitic eigenfrequencies of the fully extended flexure-based crank-slider mechanism are 74 and 80 Hz, respectively. Using a stiffer membrane in the wrist joint can increase these frequencies to above 100 Hz. Stresses in the flexure mechanism are significant. However, it has been shown that it is feasible to reduce stresses to guarantee a 75 million cycles lifetime. SPACAR has proven to be a powerful tool for designing and simulating flexure mechanisms. To fully analyse a flexure mechanism, more advanced FEM software is required, such as Ansys WorkBench. The design of the flexure-based crank-slider mechanism has been produced and successfully validated. The design is directly industrially applicable as its interface is equal to a conventional interface.
To conclude, it is possible to design a flexure mechanism for a vacuum wafer-handling application.

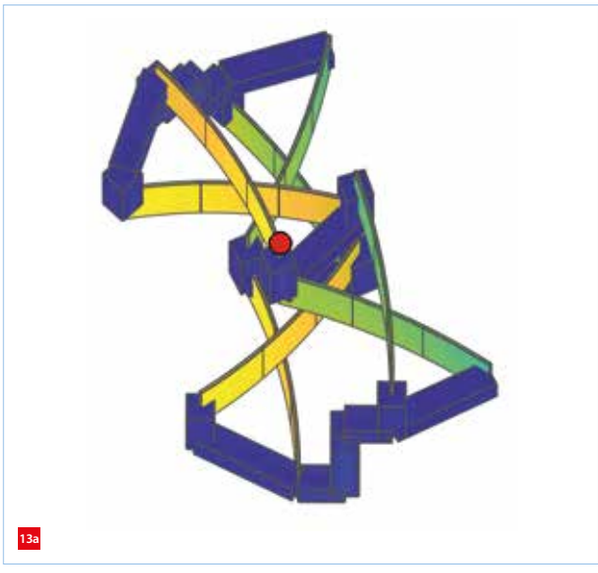

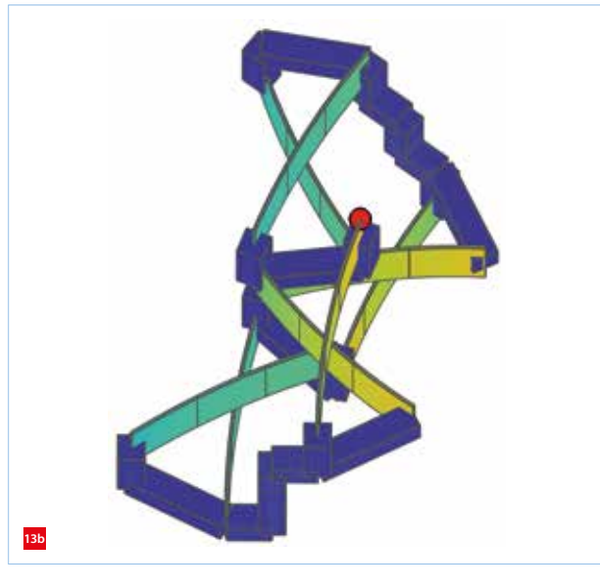

Average stresses (SPACAR) of the flexure mechanism.
(a) Fully retracted; max = 341 MPa.
(b) Fully extended; max = 270 MPa.

REFERENCES

[1] Koster, M.P., *Constructieprincipes voor het nauwkeurig bewegen en positioneren*, ThiemeMeulenhoff, 2008.

[2] Peijnenburg, A.Th.A., and Baade, R., "A magnetic bearing assembly as well as a linear guideway assembly implementing one or more such magnetic bearing assemblies", Patent NL2019812B1, May 2019.

[3] Naves, M., Brouwer, D.M., and Aarts, R.G.K.M., "Building Block-Based Spatial Topology Synthesis Method for Large-Stroke Flexure Hinges", *Journal of Mechanisms and Robotics*, 9(4), 041006, 2018.

[4] Barels, E., "Design of large stroke flexures for an in-vacuum wafer handler robot", M.Sc. thesis, University of Twente, 2018.

[5] *www.spacar.nl*

[6] Van Haaren, S.J., and Naves, M., "Metal additive manufacturing of flexure mechanisms through Selective Laser Melting", *internal report*, University of Twente, 2018.

[7] Kouters, M., Slot, H.M., Zwieten, W., and Veer, J., "The influence of hydrogen on the fatigue life of metallic leaf spring components in a vacuum environment", *International Journal of Fatigue*, 59, pp. 309-314, 2014.

[8] Morrissey, R., and Nicholas, Th., "Fatigue strength of Ti–6Al–4V at very long lives", *International Journal of Fatigue*, 27, pp. 1608-1612, (2005).

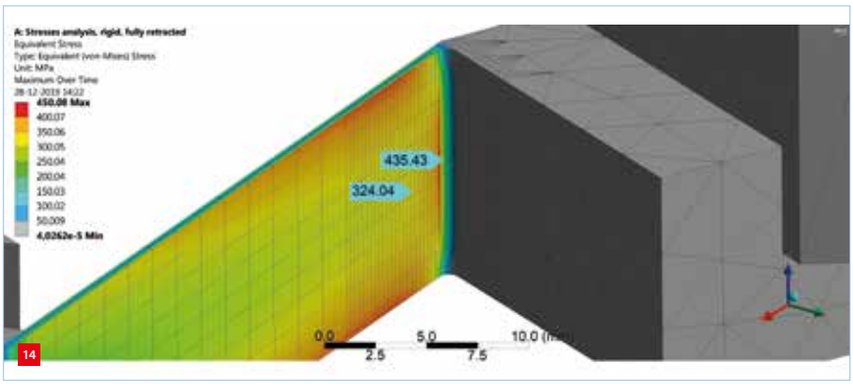

Concentration of stresses in the leafspring radius, as calculated in Ansys WorkBench; max = 460 MPa.

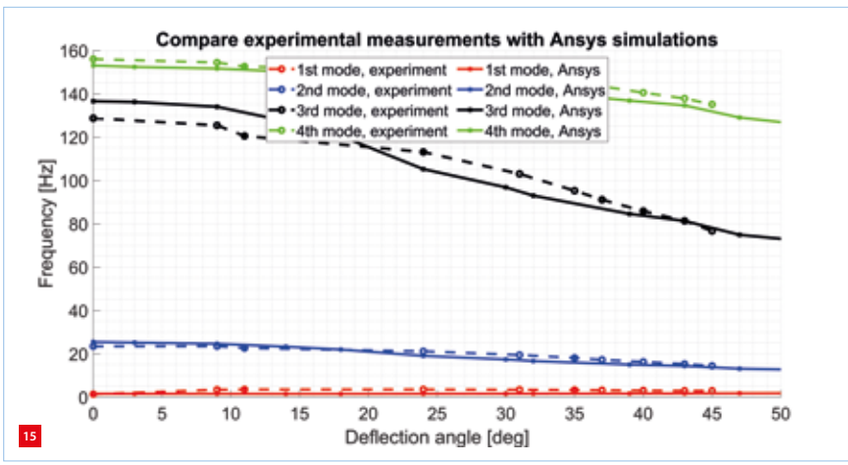

Comparison of the mechanism's eigenfrequencies between experiment and Ansys WorkBench simulation.

BALANCING BENEFITS AND DRAWBACKS

Fast-moving robots induce large dynamic reaction forces and moments at the base, resulting in disruptive vibrations and a loss of accuracy at the end-effector. By adding counter-masses and counter-inertias these shaking forces and moments may be reduced or even eliminated. However, current state-of-the-art approaches typically disregard the elasticity of the robot links, which potentially leads to undesirable parasitic dynamics, unbalance and loss of controller performance. In this article, the effect of link flexibility on the balance quality is investigated in a 2-DoF delta-type robot. It is demonstrated that a partial balancing solution accomplishes 80% shaking force reduction without the loss of controller bandwidth.

JAN DE JONG, BRAM SCHAARS AND DANNIS BROUWER

Introduction

Dynamic balance aims to eliminate the fluctuations in reaction forces and moments of high-speed robots by design of their kinematics and mass distribution [1], [2]. In theory, this leads to a dynamic decoupling of the robot and its surroundings, reducing the vibration propagation and potentially eliminating the need for vibration isolation measures such as force frames, soft mounts, and active vibration isolation [3]. In practice however, balancing leads to larger masses, increased motor torques and substantial bearing forces, since traditional balancing procedures rely on the addition of counter-masses. Although there are methods to mitigate these negative effects [3]-[6], in this article we focus on the effect of the traditional balancing procedure on the dynamic performance of robots with a finite stiffness.

This is especially of interest for the dynamic balance of delta-type robots. These parallel structures owe their high-speed motion capabilities in part to the lightweight design of their lower arms. Due to their particular kinematic structure, the lower arms are predominantly loaded in compression and tension, allowing for a slender design and high-speed motion. Adding counter-masses to these lower arms, as dictated by traditional balancing techniques, seems to be counterintuitive as it increases the moving mass and induces dynamic bending moments in the slender legs, thus requiring additional bending stiffness and even more mass.

Moreover, we expect that the added mass lowers the natural frequencies of the mechanisms leading to increased vibrations and lower controller bandwidth. This is confirmed by [7]-[10], where significant shaking forces are reported when considering link flexibility of a nominally balanced linkage. Yet, the exact nature and the impact of these lowered natural frequencies on the frequency response of multiple-degree-of-freedom (multi-DoF) robots has not been demonstrated. Moreover, it remains unclear under what conditions dynamic balancing of robots with realistic stiffness is beneficial.

In this article, we study the frequency response of a scaled-down planar robot that resembles an industrial delta-robot. We present an experimental set-up in combination with a flexible multi-body model in order to explain and quantify the effect of balancing on the shaking forces and controller performance of a finitely stiff manipulator.
In the following sections, the mechanism design and balancing solutions and the evaluation method for the balancing performance are presented. The resulting transfer functions are shown and qualitatively compared to a parametric model, leading to design criteria for optimising the dynamic balance of flexible robots.

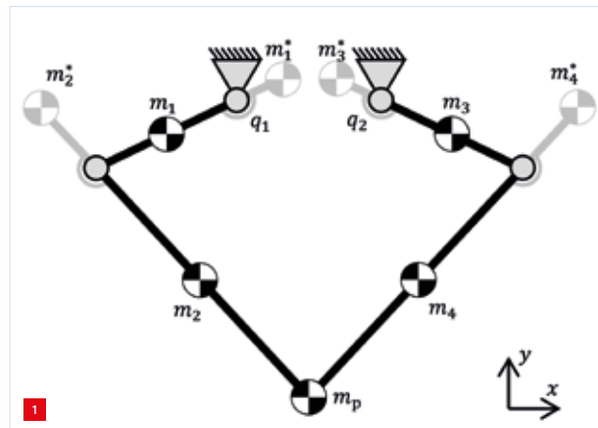

The 2-DoF planar mechanism with counter-masses in grey.

AUTHORS' NOTE

Jan de Jong (assistant professor) and Dannis Brouwer (professor) are associated with the chair of Precision Engineering in the Faculty of Engineering Technology at the University of Twente, Enschede (NL). In this group, Bram Schaars performed the M.Sc. thesis work described herein.
The authors would like to thank Leo Tiemersma, Wim Bartelds, Arnoud Domhof and Paul Stoffels for their practical work on the experimental set-up.

j.j.dejong@utwente.nl
www.utwente.nl/en/et/ms3/research-chairs/pe

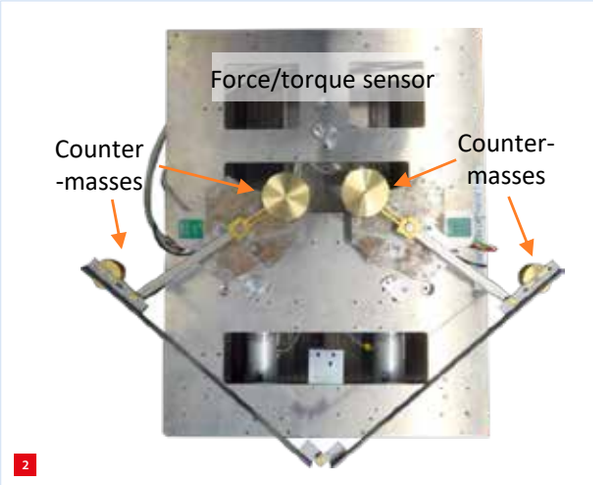

The force-balanced test set-up mounted on a 6-DoF force/torque sensor.

Three cases

The influence of flexibility on the force-balancing quality of a planar delta-robot mechanism is assessed for three cases: 1) unbalanced, 2) fully force-balanced, 3) partially balanced.

Unbalanced mechanism

The robotic system under evaluation is shown in Figure 1. The dimensions (Table 1) were chosen to resemble commercially available delta-robots [11] and scaled in order to fit on an available force/torque sensor. This resulted in a mechanism (Figure 2) with a workspace of approximately 200 mm x 200 mm. The upper arms are made of steel tubes with brass inserts, while the lower arms are made of steel sheet metal to resemble the stiffness properties of the carbon tubes that are used in most commercial delta-robots.

Force-balanced mechanism

A mechanism is force-balanced when the total centre of mass is stationary for all motion. A symmetric force-balanced solution with in-line counter-masses was chosen here. This places the following six conditions on the links' counter-masses m_i^* and counter-mass locations c_i^*:

Table 1
Robot design parameters.

Parameter	Symbol	Value	Unit
Base width	l_s	90	mm
Upper arm length	l_1, l_3	130	mm
Upper arm mass	m_1, m_3	93	g
Upper arm COM*	c_2, c_3	24	mm
Lower arm length	l_2, l_4	256	mm
Lower arm COM	c_1, c_4	90	mm
Lower arm mass	m_2, m_4	36	g
Payload	m_p	3	g

* COM = centre of mass

$$m_2^* c_2^* = m_2 c_2 + ½ m_p l_2 \quad (1)$$

$$m_1^* c_1^* = m_1 c_1 + (m_2 + m_2^* + ½ m_p) l_1 \quad (2)$$

$$m_1^* c_1^* = m_3^* c_3^*, \; m_1^* = m_3^* \quad (3, 4)$$

$$m_2^* c_2^* = m_4^* c_4^*, \; m_2^* = m_4^* \quad (5, 6)$$

From these equations a range of masses and their locations can be chosen. A solution with a minimal distance between a counter-mass and a joint is a common choice in literature [12]. Although this will result in large counter-masses, the moments of inertia and hence the motor torques are then minimal. Here we chose, based on practical considerations, c_i^* to be 30 mm and 39 mm for the upper and lower arms, respectively (Table 2). This resulted in counter-masses of 538 g for the upper arms and of 81 g for the lower arms.

Partially balanced mechanism

The large addition of mass can be mitigated by adopting a partial balance solution [13]. Here, only counter-masses on the two upper links are used. The location of the counter-masses is the same as for the previous case. The amount of added mass, however, is reduced by 50% (Table 2).

Evaluation of force-balance quality

The evaluation of the balance quality for these three cases was performed by simulation and experiments. A parametric model was used to interpret and explain the results.

Performance measures

Two performance measures were used to evaluate the three cases. The first measure relies on the comparison of the transfer functions $T(s)$ from an actuator angle q to the shaking forces F at the base:

$$T(s) = F(s) \,/\, q(s) \quad (7)$$

Here, s denotes the complex frequency. Transfer functions capture the frequency-dependent behaviour of a dynamic system. They therefore provide an excellent tool for studying the influence of stiffness on the balance quality.

Table 2
Counter-mass properties for the force-balanced (FB) and partially balanced (PB) case.

Property	Symbol	FB value	PB value	Unit
Upper arm counter-mass	m_1^*, m_3^*	538	306	g
Upper arm counter-mass location	c_1^*, c_3^*	32	32	mm
Lower arm counter-mass	m_2^*, m_4^*	81	-	g
Lower arm counter-mass location	c_2^*, c_4^*	37	-	mm

Here, a low magnitude of the shaking forces over a large frequency range indicates a high balancing quality. These transfer functions were obtained by modelling and linearisation of the mechanism in a numerically flexible multi-body software package [14]. Identification of the experimental set-up allowed for a verification of the results.

The second performance measure is related to the change in controller bandwidth of the balanced system. In most applications the performance of the controller is limited by the first parasitic frequency as stability issues limit the controller bandwidth to approximately 1/3 of this frequency. If, by addition of counter-masses, the first parasitic frequency drops, this would result in a decreased bandwidth and hence reduced system performance. The first parasitic frequency is therefore the second performance criterion for dynamic balance.

Experimental set-up
The set-up described in the previous section was built and placed on a 6-DoF force/torque sensor. A frequency identification of the set-up was performed by exciting the joints with a multisine signal and measuring the corresponding shaking forces in the *x*- and *y*-direction. Figure 2 shows the set-up in its balanced configuration.

Parametric model
The behaviour of the system is explained by a simplified analytic model of a balanced elastic beam. This beam is modelled as two spring-mass systems hinged at the base (Figure 3). The mass-spring on the right system represents the unbalanced mechanism and the system on the left represents the balance mass. The frequency transfer functions of the left (P_b) and right (P_a) mass-spring system from joint rotation to shaking force in the vertical direction then become (UB = unbalance):

$$P_{UB}(s) = P_a = m_a l_a k s^2 / (m_a s^2 + k) \quad (8)$$

$$P_b = m_b l_b k s^2 / (m_b s^2 + k) \quad (9)$$

Here, m_a, m_b, l_a and l_b are the masses and lengths. For convenience the same stiffness k is chosen for both systems. In the force-balanced as well as the partially balanced case, the two mass-spring systems are combined, leading to the following total transfer function (PB = partially balanced):

$$P_{PB} = P_a - P_b = \frac{(m_a l_a - m_b l_b) k^2 s^2 + m_a m_b (l_a - l_b) k s^4}{(m_a s^2 + k)(m_b s^2 + k)} \quad (10)$$

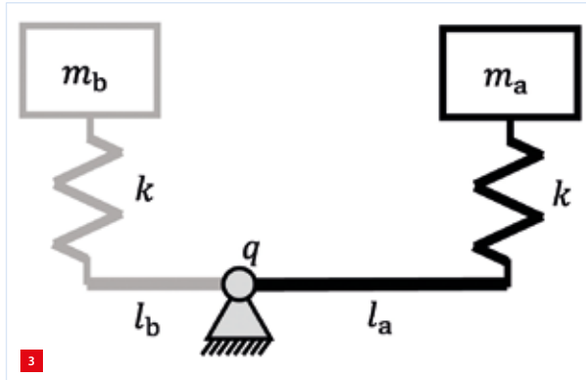

3

The parametric model of the dynamically balanced mechanism. The counter-mass is depicted in grey.

The force-balance condition of this beam is:

$$0 = m_a l_a - m_b l_b \quad (11)$$

Therefore, the transfer function of the force-balanced (FB) system becomes:

$$P_{FB} = m_a m_b (l_a - l_b) k s^4 / [(m_a s^2 + k)(m_b s^2 + k)] \quad (12)$$

Here, it can already be seen that force balance eliminates the s^2 component in the numerator of (10). This indicates the removal of a low-frequency component.

Results

The obtained transfer functions of the three cases and the measurement results are shown in Figure 4. Here, only the transfer function from the first motor to the forces in the *x*-direction is treated. The other transfer functions of the *y*-force and the second motor show comparable results. The parasitic frequencies and corresponding mode shapes are depicted in Figure 5.

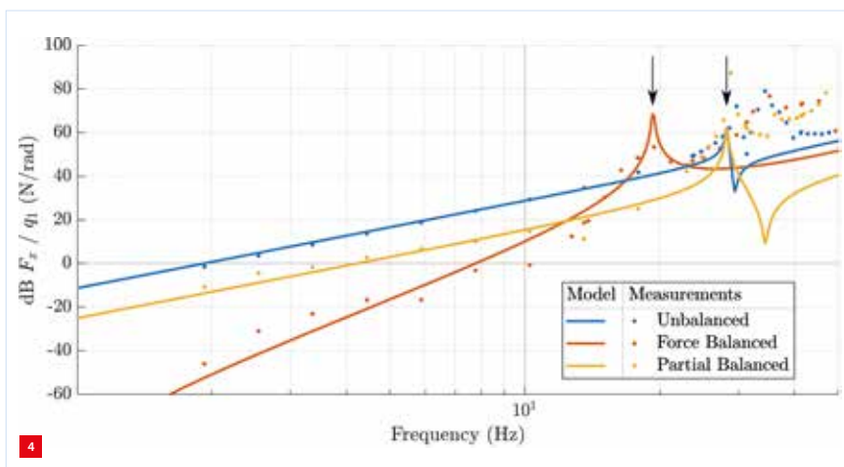

4

The shaking force frequency content of the 2-DoF mechanism in the horizontal x-direction due to actuation of joint 1. The dots indicate the results from the multisine identification. The arrows indicate the first peaks due to the natural frequencies of the system.

Unbalanced mechanism

The measurements and the model of the unbalanced robot both show a 40 dB/decade line up to the natural frequency at 28 Hz (Figure 4), while beyond this frequency the measurements and model start deviating. The slope in the low-frequency domain can be explained by Newton's laws. The shaking force induced by a moving rigid body corresponds to $F = m_{eq}\ddot{q}$. Here, m_{eq} is the equivalent mass of the motion. The corresponding Laplace transform is $T_{UB} \approx m_{eq}s^2$. This s^2 results in the observed 40 dB/decade line and is therefore termed the rigid-body effect.
This can also be seen if we apply a low-frequency approximation to the parametric model. In the frequency region far below the first natural frequency ($\omega << \omega_1$), the behaviour of the unbalanced mechanism (8) is approximately:

$$P_{UB} \approx m_a l_a s^2 = m_{eq} s^2 \tag{13}$$

It can be seen that here the rigid-body motion is dominant, corresponding to the 40 dB/decade line.
The differences between the model and the measurements in the higher-frequency region may be attributed to model simplifications, design tolerances and measurements errors. They are of less interest in the present context and are not discussed any further.

Force-balanced mechanism

For the fully force-balanced robot, the behaviour corresponds to an 80 dB/decade line up to the first natural frequency at 19 Hz (Figure 4). Again, this holds for both the model and the measurement results. Similarly, in the parametric model these effects are seen. Since (11) removes the s^2 contribution in (10), the low-frequency approximation of the parametric model (12) becomes:

$$P_{FB} \approx m_a m_b (l_a - l_b) s^4 / k \tag{14}$$

This fourth-order behaviour corresponds to the 80 dB/decade line as observed in the simulation and the measurements. Apparently, force balance removes the rigid-body effect, such that the function is characterised by $T(s) \approx m_{eq}s^4$. This m_{eq} is a different equivalent mass associated to the internal vibrations. This shows that dynamic balance results in a strong attenuation of the shaking forces in the frequency region well below the first natural frequency. On a side note, it might be theoretically possible to also remove this s^4 effect by design of the mode shapes, as shown in a recent study [15]. This would lead to even more attenuation in the low-frequency domain.

However, balancing also lowers the natural frequency of the system, from 28 to 19 Hz, indicating an approximate controller bandwidth loss of about 40%. Therefore, the force-balance quality of this flexible manipulator is improved in the low-frequency range up to 16 Hz; beyond this frequency, the performance is comparable if not worsened.

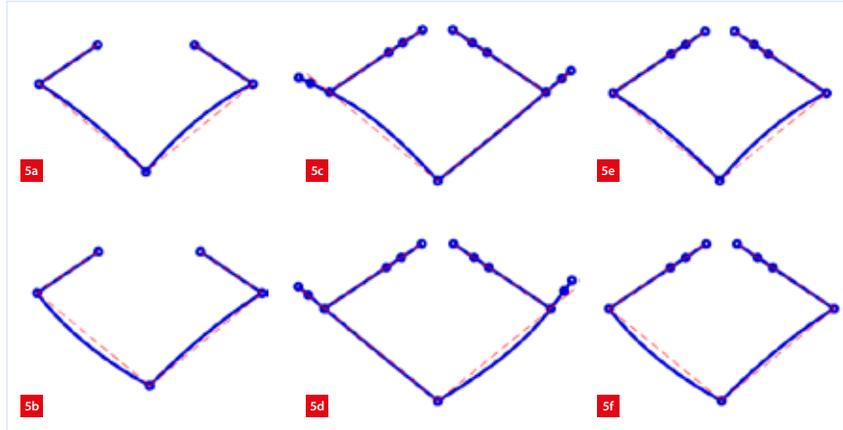

The first two mode shapes for the unbalanced (UB), force-balanced (FB), and partially balanced (PB) case.
(a) UB 1: 28 Hz *(c) FB 1: 19 Hz* *(e) PB 1: 28 Hz*
(b) UB 2: 28 Hz *(d) FB 2: 19 Hz* *(f) PB 2: 28 Hz*

Partially balanced mechanism

The partially balanced robot shares the 40 dB/decade line with the unbalanced mechanism. Yet, the magnitude of this line is significantly lower compared to the unbalanced case. Effectively, this results in approximately 15 dB or 80% reduction of the disruptive shaking forces in the lower frequency region.

In the parametric model, the shaking forces at the frequencies below the first natural frequency are dominated by the rigid-body effects as seen from the approximation of (10):

$$P_{PB} \approx (m_a l_a - m_b l_b) s^2 = m_{eq} s^2 \tag{15}$$

Here, also the rigid-body, second-order behaviour is found. The difference with the unbalanced case is a reduction of the effective mass by a suitable choice of the counter-mass ($m_b l_b$). Additionally, no noticeable change of the parasitic frequency is observed with respect to the unbalanced case. Since the counter-masses are placed at the base joints, solely the higher, non-critical modes are affected. This indicates that the controller bandwidth can be maintained with partial dynamic balance.

Concluding remarks

This work confirms that elasticity of the mechanism has a significant influence on the dynamic balance quality. It shows that force balance attenuates the shaking forces by 40 dB/decade in the lower-frequency domain by eliminating the rigid-body contribution. This is particularly helpful if a shaking force reduction is required in the frequency range far below the first parasitic frequency. However, around and beyond this frequency no clear improvement is observed.

It may be argued that for most applications the bulk of the motion energy is in the lower-frequency domain. However, the remaining high-frequency energy, the nonlinearities and possible external disruptions may excite internal vibrations that would result in substantial shaking forces in an otherwise force-balanced mechanism.

Moreover, the added balance mass may lower the first parasitic frequency of the mechanism. In the present case study, a reduction of 40%, from 28 to 19 Hz, was observed. This will result in a proportional loss of controller bandwidth and robot performance. Partial dynamic balance seems to be more advantageous in this case as it reduces the shaking forces by 80% without sacrificing the controllability of the robot.

REFERENCES

[1] V.H. Arakelian, and M.R. Smith, "Shaking Force and Shaking Moment Balancing of Mechanisms: A Historical Review With New Examples", *J. Mech. Des.*, vol. 127 (2), pp. 334-338, 2005, *doi: 10.1115/1.1829067*.

[2] V.H. Arakelian, and M.R. Smith, "Erratum: 'Shaking Force and Shaking Moment Balancing of Mechanisms: A Historical Review With New Examples", *J. Mech. Des.*, vol. 127 (5), pp. 1034-1035, 2005.

[3] V. van der Wijk, "Methodology for analysis and synthesis of inherently force and moment-balanced mechanisms - theory and applications", Ph.D. thesis, University of Twente (NL), 2014.

[4] J.-F. Collard, and C.M. Gosselin, "Optimal Synthesis of a Planar Reactionless Three-Degree-of-Freedom Parallel Mechanism", *J. Mech. Robot.*, vol. 3 (4), p. 041009, 2011, *doi: 10.1115/1.4004897*.

[5] I.S. Kochev, "General theory of complete shaking moment balancing of planar linkages: a critical review", *Mech. Mach. Theory*, vol. 35 (11), pp. 1501-1514, 2000, *doi: 10.1016/S0094-114X(00)00015-X*.

[6] M. Verschuure, B. Demeulenaere, J. Swevers, and J. De Schutter, "Counterweight Balancing for Vibration Reduction of Elastically Mounted Machine Frames: A Second-Order Cone Programming Approach", *J. Mech. Des.*, vol. 130 (2), p. 022302, 2008, *doi: 10.1115/1.2812420*.

[7] M.J. Walker, and R.S. Haines, "An experimental study of the effects of counterweights on a six-bar chain", *Mech. Mach. Theory*, vol. 17 (6), pp. 355-360, 1982, *doi: 10.1016/0094-114X(82)90027-1*.

[8] E. Raghu, and A. Balasubramonian, "Experimental study on the elastodynamic behavior of the unbalanced and the counterweighted four bar mechanisms", *J. Mech. Des.*, vol. 112 (3), pp. 271-277, 1990, *doi: 10.1115/1.2912604*.

[9] F. Xi, and R. Sinatra, "Effect of dynamic balancing on four-bar linkage vibrations", *Mech. Mach. Theory*, vol. 32 (6), pp. 715-728, 1997, *doi: 10.1016/s0094-114x(97)83005-4*.

[10] M.A.K. Zobairi, S.S. Rao, and B. Sahay, "Kineto-elastodynamic balancing of 4R-four bar mechanisms combining kinematic and dynamic stress considerations", *Mech. Mach. Theory*, vol. 21 (4), pp. 307-315, 1986.

[11] Codian Robotics, "Robots, Twee-dimensionale delta", *www.codian-robotics.com/d2-robots* (accessed Dec. 13, 2018).

[12] V. van der Wijk, and J.L. Herder, "Dynamic Balancing of Clavel's Delta Robot", *Computational Kinematics*, pp. 315-322, 2009.

[13] J.J. de Jong, J.P. Meijaard, and V. van der Wijk, "The Influence of Partial Force Balancing on the Shaking Moments, Contact Forces, and Precision of a Delta Robot-Like Manipulator in a Compliant Frame", *Proceedings 2018 ASME IDETC/CIE*, pp. 1-7, 2018, *doi: 10.1115/detc2018-86189*.

[14] J.B. Jonker, R.G.K.M. Aarts, and J. van Dijk, "A linearized input-output representation of flexible multibody systems for control synthesis", *Multibody Syst. Dyn.*, vol. 21 (2), pp. 99-122, 2009, *doi: 10.1007/s11044-008-9130-6*.

[15] J.P. Meijaard, and V. van der Wijk, "On the Dynamic Balance of a Planar Four-Bar Mechanism with a Flexible Coupler", *Advances in Mechanism and Machine Science*, vol. 73, pp. 2611-2620, 2019, *doi: 10.1007/978-3-030-20131-9*.

ADVANCED ROBOTICS, UNCERTAINTY STATEMENTS AND TRACEABILITY

This year should have marked a major milestone within euspen's heritage as its 20th international conference was to be held in conjunction with CERN. The euspen Annual Conference and Exhibition always attracts high-level interest from the precision engineering community and 2020 – whilst incredibly different, as a virtual online web-conference – was no exception.

DISHI PHILLIPS

The decision to originally hold the event in Geneva, Switzerland in conjunction with CERN, the largest particle physics laboratory in the world, was no coincidence. The intention was to let delegates and exhibitors experience impressive keynotes, workshops, tutorials, a sell-out exhibitor hall, a large-scale poster area and tours of CERN during the week of 8-12 June 2020.

In light of the global Covid-19 pandemic, changes were forced to the format of the conference. Delivering the euspen 2020 conference as a 'virtual online web-conference' ensured the participants remained safely connected. This decision was not easy to take and more challenging to implement than postponing or even cancelling the conference. The willingness to provide continuity in supporting the precision engineering community and spreading new ideas and findings prevailed.

AUTHOR'S NOTE

Dishi Phillips is the executive director of euspen (European Society for Precision Engineering and Nanotechnology).
The euspen community links industrialists, researchers, respected authorities, new, and established players worldwide. It is euspen's mission to advance the arts, sciences and technology of precision engineering, micro-engineering and nanotechnology; to promote its dissemination through education and training; and to facilitate its exploitation by science and industry.

dishi-phillips@euspen.eu
www.euspen.eu

Live workshops

The event started with two live interactive workshops taking place on Monday the 8th of June: "Ultra-precision high performance cutting" and "Uncertainty in dimensional X-ray computed tomography." These invited presentations were delivered live followed by an interactive Q&A between the presenters and attendees. The morning workshop was chaired by Prof. Richard Leach, University of Nottingham, UK, and assisted by Timo Dörgeloh, Leibniz-Institute for Materials Engineering IWT, Germany, and focused on X-ray computed tomography and its benefits over traditional contact and optical techniques for coordinate metrology.

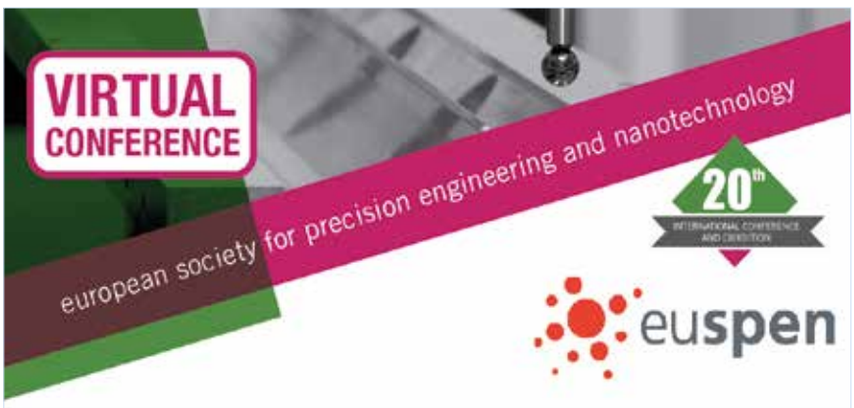

The afternoon workshop "Ultra-Precision High Performance Cutting", chaired by Dr.-Ing. Lars Schönemann (IWT), featured the research group "Ultra-Precision High Performance Cutting" (UP-HPC). This collaboration between the University of Bremen and the Leibniz University Hannover is funded by the German Research Foundation (DFG). Participating research institutes were the Laboratory for Precision Machining (LFM, Professor Ekkard Brinksmeier) from Bremen, the Bremen Institute for Mechanical Engineering (bime, Professor Bernd Kuhfuß) as well as the Institute of Production Engineering and Machine Tools (IFW, Professor Berend Denkena) from Hannover. The goal of UP-HPC *(www.up-hpc.de/index_en.html)* is to reduce the disproportionally long primary and secondary processing times in ultra-precision machining via scientific means, in order to leverage the economic applicability of this technology in the manufacturing industry. After two funding periods and six years of research in total, the UP-HPC research unit officially came to an end with a final colloquium and workshop at the euspen conference. There, a brief overview was given on the major outcomes of the five sub-projects of the research unit and this was accompanied by invited talks from industrial partners.

Keynotes

The technical element of the event continued with three days of presentations. Each day started with a keynote presentation

offering a broad perspective of high-precision engineering and nanotechnology, from robotics to a very comprehensive review of dimensional calibrated artefacts and a very complete state-of-the-art on uncertainty statements for topographic surface measurements. There were three conference keynotes.

Advanced robotics

Prof. Darwin Caldwell, Deputy Director of the Italian Institute of Technology and the Director of the Department of Advanced Robotics, presented "Advanced robotics and AI in 'demanding' industrial, and manufacturing environments".

Early robots were commonly used for tasks that were often described as dull, dirty and dangerous: essentially jobs that were unpopular with humans. After more than 50 years of development, robots are now common in industrial production, and they are increasingly seen in the domestic, service and transportation sectors. Indeed, the target applications in which robots may be used, now and in the future, is increasingly switching from the dull and repetitive, to the challenging and diverse. With these new operational demands, there is a need for new, increasingly sophisticated robots that combine advanced physical design and capabilities with enhanced cognitive capacities.

Caldwell considered the use of advanced robotic systems including 'general purpose' robots such as humanoids, centaurs and quadrupeds, and also more specialised crawler and snake-like robots. He explored some of the key aspects of the hardware and software design and showed how developments in these core technologies will move the use of robots from the dull and repetitive to the unexpected, unpredictable and challenging, where they can be effectively integrated into future designs for use in 'demanding' environments and advanced manufacturing (Industry 4.0).

Manufacturing metrology

Prof. Simone Carmignato, Professor of Manufacturing Engineering at the University of Padova, Italy, presented "Traceability in manufacturing metrology: do we still need artefacts?"

Today, dimensional artefacts – ranging from measurement standards to calibrated workpieces – might look dusty in comparison to some of the most evident innovations in advanced manufacturing, including cyber-physical systems and Industry 4.0 concepts that seem light years away from material artefacts. However, dimensional artefacts continue to play a fundamental role to establish the traceability of measurements in production, which is an essential prerequisite to control manufacturing processes and assure the quality of products, as well as for the comparability of the properties of components in global manufacturing environments. In fact, metrological traceability becomes even more important in today's manufacturing contexts, where reliable and accurate digital models of products, processes and production systems are needed.

Carmignato discussed dimensional artefacts, encompassing their characteristics, design, availability, selection and role in supporting production by establishing metrological traceability.

Uncertainty statements

Prof. Richard Leach, Professor of Metrology at the University of Nottingham, posed this question: "Why do we rarely see uncertainty statements with surface form and texture measurements?"

"We all understand the concept and need for measurement uncertainty. As educators, we often tell our students that a measurement is simply not complete without a quantitative statement about uncertainty. So, why do we rarely see uncertainty statements with surface topography (form and texture) measurements or specifications for engineering drawings? The only answer I have to this question is: "because it is a very tricky thing to do, especially if trying to follow international guidelines" (i.e. the GUM, Guide to the Expression of Uncertainty in Measurement)." Leach summarised the state-of-the-art in uncertainty quantification for surface topography measurement, laid out some of the issues that make it a tricky problem and presented some potential ways forward.

Oral sessions, poster pitches and exhibitor platform

The days were split into the usual oral sessions allowing delegates to listen to pre-recorded oral presentations on the latest advances in precision engineering and nanotechnologies, in non-mechanical and mechanical manufacturing processes, measuring instruments and machine tools, metrology, mechatronics, control and automation, with a dedicated session on precision manufacturing at CERN. Each author addressed a series of questions from the live Q&A session adding a small dimension of human reality into the virtual world.

Whilst there was not the opportunity for delegates to experience the buzz of the exhibition floor and the extensive A0 posters that would normally have occupied the same space, alternatives were offered. The poster presenters pre-recorded their poster pitches which delegates could access beforehand and then enter the virtual poster rooms for further discussions. Whilst this did not work as envisaged, improvements to a virtual platform event allows euspen to modify specific areas for better interaction and engagement for future practice. For the exhibitors, there was a social platform of pre-recorded soundbites as well as pre-recorded commercial presentations. The support from our regular and new sponsors was truly appreciated.

Scholarships

Finally, each year euspen hosts the Heidenhain Scholarships. The Heidenhain group of companies has been associated with the euspen annual event for over ten years, and has provided over 100 scholarships to date. The group was brought into a philanthropic foundation over 40 years ago with a philosophy to invest in research, development, social, and scientific projects.
Scholarships are available for students or researchers registered for Masters/Ph.D. or equivalent courses at a recognised international higher education institution.

Whilst the scholars could not receive their recognition in person, they have still been awarded this prestigious accolade. In light of this, euspen will be inviting the winners to its 21st international conference, next year.

Copenhagen

In 2021, the euspen annual event will be held in Copenhagen at the Technical University of Denmark (DTU) from 7-11 June, and all the indications are that the success of previous events, including this extraordinary one will carry forward significant momentum, and will continue in making this the largest ever euspen conference and exhibition. It is truly an exciting time in the precision engineering sector.

Technical University of Denmark, host of euspen's 21st International Conference & Exhibition in 2021. (Image: Thomas Hindsgaul, wikipedia)

ECP² COURSE CALENDAR

COURSE (content partner)	ECP² points	Provider	Starting date
FOUNDATION			
Mechatronics System Design - part 1 (MA)	5	HTI	28 September 2020
Mechatronics System Design - part 2 (MA)	5	HTI	5 October 2020
Fundamentals of Metrology	4	NPL	to be planned
Design Principles	3	MC	13 October 2020
System Architecting (S&SA)	5	HTI	28 September 2020
Design Principles for Precision Engineering (MA)	5	HTI	to be planned (2021)
Motion Control Tuning (MA)	6	HTI	23 November 2020
ADVANCED			
Metrology and Calibration of Mechatronic Systems (MA)	3	HTI	27 October 2020
Surface Metrology; Instrumentation and Characterisation	3	HUD	to be planned
Actuation and Power Electronics (MA)	3	HTI	16 November 2020
Thermal Effects in Mechatronic Systems (MA)	3	HTI	1 December 2020
Dynamics and Modelling (MA)	3	HTI	23 November 2020
Manufacturability	5	LiS	to be planned
Green Belt Design for Six Sigma	4	HI	21 September 2020
RF1 Life Data Analysis and Reliability Testing	3	HI	14 September 2020
Ultra-Precision Manufacturing and Metrology	5	CRANF	19 January 2021
SPECIFIC			
Applied Optics (T2Prof)	6.5	HTI	26 October 2020
Advanced Optics	6.5	MC	17 September 2020
Machine Vision for Mechatronic Systems (MA)	2	HTI	upon request
Electronics for Non-Electronic Engineers – Analog (T2Prof)	6	HTI	to be planned
Electronics for Non-Electronic Engineers – Digital (T2Prof)	4	HTI	to be planned
Modern Optics for Optical Designers (T2Prof) - part 1	7.5	HTI	to be planned (Q1 2021)
Modern Optics for Optical Designers (T2Prof) - part 2	7.5	HTI	to be planned (Q1 2021)
Tribology	4	MC	27 October 2020
Basics & Design Principles for Ultra-Clean Vacuum (MA)	4	HTI	2 November 2020
Experimental Techniques in Mechatronics (MA)	3	HTI	30 November 2020
Advanced Motion Control (MA)	5	HTI	26 October 2020
Advanced Feedforward & Learning Control (MA)	2	HTI	30 September 2020
Advanced Mechatronic System Design (MA)	6	HTI	to be planned (2020)
Passive Damping for High Tech Systems (MA)	3	HTI	17 November 2020
Finite Element Method	2	MC	29 October 2020
Design for Manufacturing (Schout DfM)	3	HTI	15 October 2020

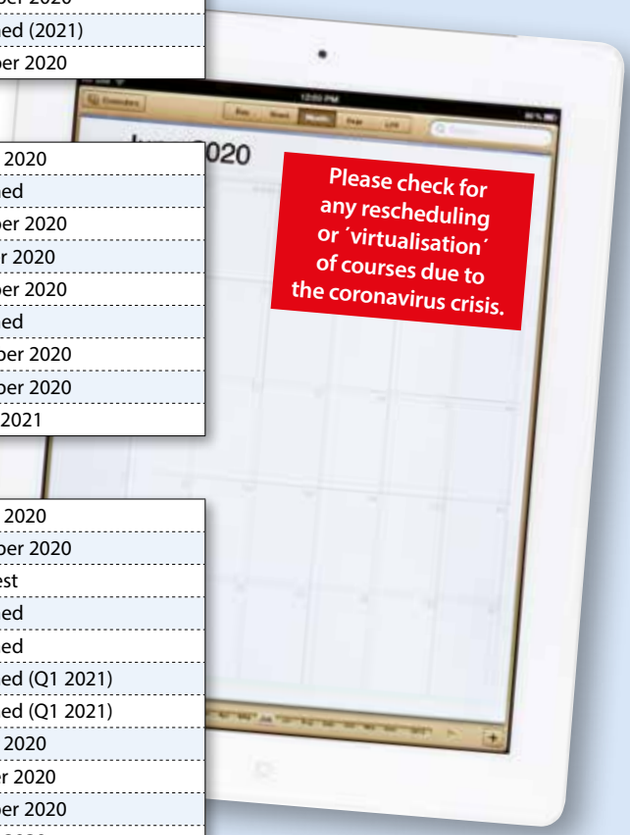

ECP² program powered by euspen

The European Certified Precision Engineering Course Program (ECP²) has been developed to meet the demands in the market for continuous professional development and training of post-academic engineers (B.Sc. or M.Sc. with 2-10 years of work experience) within the fields of precision engineering and nanotechnology. They can earn certification points by following selected courses. Once participants have earned a total of 45 points, they will be certified. The ECP² certificate is an industrial standard for professional recognition and acknowledgement of precision engineering-related knowledge and skills, and allows the use of the ECP² title.

WWW.ECP2.EU

Course providers

- High Tech Institute (HTI)
  WWW.HIGHTECHINSTITUTE.NL
- Mikrocentrum (MC)
  WWW.MIKROCENTRUM.NL
- LiS Academy (LiS)
  WWW.LISACADEMY.NL
- Holland Innovative (HI)
  WWW.HOLLANDINNOVATIVE.NL
- Cranfield University (CRANF)
  WWW.CRANFIELD.AC.UK
- Univ. of Huddersfield (HUD)
  WWW.HUD.AC.UK
- National Physical Lab. (NPL)
  WWW.NPL.CO.UK

Content partners

- DSPE
  WWW.DSPE.NL
- Mechatronics Academy (MA)
  WWW.MECHATRONICS-ACADEMY.NL
- Technical Training for Prof. (T2Prof)
  WWW.T2PROF.NL
- Schout DfM
  WWW.SCHOUT.EU
- Systems & Software Academy (S&SA)

DSPE Knowledge Day on Engineering for Contamination Control

On Tuesday 29 September 2020, the second edition of the DSPE Knowledge Day on Engineering for Contamination Control will be held. This afternoon event is devoted to design aspects aimed at dealing with contamination or minimising the implications of contamination. In addition, information will be shared regarding tools that support the design (and test) phase of a project. The first edition of the event, last summer, attracted some 30 attendees and featured a number of highly interesting presentations.

The event is highly relevant for precision engineers involved in designing advanced mechatronics systems. Presentations will be given by Paul Blom (senior system engineer at VDL ETG), Sven Pekelder (CTO at Settels Savenije), Cees van Duijn (contamination control expert at Omneo Systems), Rob Lansbergen (senior system engineer at Lans Engineering/Fast Micro) and Bert van der Zwan (senior project manager/business developer at Fast Micro). More information and registration on the DSPE website. The DSPE Knowledge Day on Engineering for Contamination Control is organised by DSPE in collaboration with VCCN, VDL ETG, Settels Savenije, Omneo Systems, Lans Engineering and Fast Micro, and will take place – with all due corona-related precautions – at the Aristo Meeting Center in the Eindhoven (NL) city centre.

WWW.DSPE.NL

Berliner Glas Group to become part of ASML

This summer, ASML, the world's leading manufacturer of lithography equipment for chip making, signed an agreement to acquire 100% of the shares of Berliner Glas. The two companies have been collaborating over the past 30 years. With this transaction, to be completed before the end of 2020, ASML will acquire technical capabilities that are important to support the future roadmap for its EUV and DUV products. ASML will also acquire business units that operate in other markets.

Berliner Glas, located in Berlin, Germany, integrates optics, mechanics and electronics to provide innovative system solutions, which are employed worldwide in light-using industries – from medical technology to the semiconductor industry (customer-specific electrostatic chucks, vacuum chucks, precision components, reference mirrors and stage modules), all the way to laser and space technologies.

WWW.ASML.COM

WWW.BERLINERGLASGROUP.COM

Video-recorder mechanism video

Many devices with moving parts have evolved over the last decades from an electromechanical solution to a mechatronic one, with software instead of hardware taking the lead. Sometimes it evolved even further, to fully solid-state electronics. However, some of the attraction of a beautifully designed mechanism was lost in the process. This certainly applies to the recording of video, which started with the video recorder using a magnetic tape cassette. It contained a particularly intricate mechanism for loading the tape, with a sequence of mechanical actions, from loading the cassette and guiding the tape around the head to pressing it against the drive spindle. After his old Philips VHS video recorder failed, Rini Zwikker opened it and discovered the beauty of this hidden mechanism. He decided to mount it vertically on a pedestal and actuate it using a microcontroller – a tribute to the ingenuity of the engineers of that time. The QR-code on the right contains a link to the 3-minute video of the result. It is a mechanical choreography of motions, driven by just one simple DC motor, with only a very basic position sensor. It contains a variety of mechanical components, like gears, levers and cam follower wheels, integrated in a compact construction.

Generally speaking, to this day it is certainly not true that a (closed-loop controlled) mechatronic solution is always better than an (electro-) mechanical one. When a fixed motion profile is to be generated repeatedly and fast, the use of a mechanism is still an efficient and robust method. This applies to both consumer devices like car engine camshafts and to production equipment like component pick & place handlers.

Design Concepts and Strategies for Precision Engineering

Recently, the publication of "Design Concepts and Strategies for Precision Engineering" was announced by the author, Susan van den Berg, lecturer at Fontys University of Applied Sciences (UAS) in Eindhoven (NL). This full-colour book (ISBN 978-90-829711-1-8) combines the earlier separate volumes, "Design Concepts for Precision Engineering" I and II, and has added chapters.

Noticing a mismatch between existing textbooks and the entry-level knowledge of the students in her class at Fontys, she decided to write a didactically sound textbook targeted specifically at UAS students and engineers who are novices to the field of precision engineering. Only prior knowledge of mechanics (statics, stress and deformation) and basic mathematics (trigonometry and calculus) is required.

WWW.BERGPRECISIONPUBLISHING.NL

BionicWheelBot

One of the natural models for the new projects from Festo's Bionic Learning Network is the flic-flac spider, which lives in a desert. It can walk like other spiders; however, it can also move with a combination of somersaulting and rolling on the ground. It is therefore ideally adapted to its surroundings: on even ground, it is twice as fast in rolling mode than when walking.

Ingo Rechenberg, a bionics professor at the TU Berlin, discovered the spider in 2008 and since then has been working on transferring its movement patterns to technological applications. With his team he first constructed a number of prototypes for the BionicWheelBot.

They now have further developed the kinematics and drive concept of the artificial spider together with Festo.

Just like a natural spider, the BionicWheelBot propels itself with a tripod gait, using six of its eight legs to walk. In order to start rolling, the BionicWheelBot bends three legs on each side of its body to make a wheel. The two legs that are folded up during walking are then extended, push the rolled-up spider off the ground, and continuously push it forward whilst rolling. This prevents the BionicWheelBot from grinding to a halt and ensures that it can keep moving forward even on rough terrain.

WWW.FESTO.COM/GROUP/EN/CMS/10156.HTM

Additive Manufacturing / 3D metal printing

Raytech
Dirk Martensstraat 3A
8200 Brugge
Belgium
T +32 (0)50 45 44 05
E info@raytech.be
W www.raytech.be

Raytech offers 3D metal printing (titanium & aluminium) with a strong focus on small and accurate components. Optional treatments after 3D printing: laser welding – laser engraving – cleaning – polishing.

Automation Technology

Festo BV
Schieweg 62
2627 AN DELFT
The Netherlands
T +31 (0)15-2518890
E sales@festo.nl
W www.festo.nl
Contact person:
Mr. Michiel Deen

Festo is a leading world-wide supplier of automation technology and the performance leader in industrial training and education programs.

member DSPE

Cleanrooms

Brecon Group
Droogdokkeneiland 7
5026 SP Tilburg
T +31 (0)76 504 70 80
E brecon@brecon.nl
W www.brecon.nl

Brecon Group can attribute a large proportion of its fame as an international cleanroom builder to continuity in the delivery of quality products within the semiconductor industry, with ASML as the most important associate in the past decades.

Brecon is active with cleanrooms in a high number of sectors on:
* Industrial and pharmaceutical
* Healthcare and medical devices

member DSPE

Connect 2 Cleanrooms BV
Newtonlaan 115
Zen Building
3584 BH Utrecht
Nederland
T +31 (0)30 210 60 51
E info@connect2cleanrooms.com
W www.connect2cleanrooms.nl

Developing the most appropriate cleanroom to transform your production is our passion. Our scalable and connected cleanrooms have been delivering regulatory compliance to our clients since 2002. We innovate to overcome your contamination control challenges – resulting in a new generation of scalable cleanrooms that set an unprecedented benchmark in the industry.

member DSPE

Development

TNO
T + 31 (0)88-866 50 00
W www.tno.nl

TNO is an independent innovation organisation that connects people and knowledge in order to create the innovations that sustainably boosts the competitiveness of industry and wellbeing of society.

member DSPE

Development and Engineering

Segula Technologies Nederland B.V.
De Witbogt 2
5652 AG Eindhoven
T +31 (0)40 8517 500
W www.segula.nl

SEGULA Technologies Nederland BV develops advanced intelligent systems for the High Tech and Automotive industry. As a project organisation, we apply our (engineering) knowledge to non-linear systems. This knowledge is comprised of systems architecture and modelling, analysis, mechanics, mechatronics, electronics, software, system integration, calibration and validation.

member DSPE

Education

Leiden school for Instrumentmakers (LiS)
Einsteinweg 61
2333 CC Leiden
The Netherlands
T +31 (0)71-5681168
E info@lis.nl
W www.lis.nl

The LiS is a modern level 4 MBO school with a long history of training Research instrumentmakers. The school establishes projects in cooperation with industry and scientific institutes thus allowing for professional work experience for our students. LiS TOP accepts contract work and organizes courses and summer school programs for those interested in precision engineering.

member DSPE

Electrical Discharge Machining (EDM)

CVT BV
Heiberg 29C
5504 PA Veldhoven
The Netherlands
T +31 (0)497 54 10 40
E info@cvtbv.nl
W www.cvtbv.nl

Partner high tech industry for wire EDM precision parts. Flexible during day shifts for prototyping. Outside office hours low cost unmanned machining. Call and enjoy our expertise!

member DSPE

Ter Hoek Vonkerosie
Propaanstraat 1
7463 PN Rijssen
T +31 (0)548 540807
F +31 (0)548 540939
E info@terhoek.com
W www.terhoek.com

INNOVATION OF TOMORROW, INSPIRATION FOR TODAY
Staying ahead by always going the extra mile. Based on that philosophy, Ter Hoek produces precision components for the high-tech manufacturing industry.

We support customers in developing high-quality, custom solutions that can then be series-produced with unparalleled accuracy. That is what makes us one of a kind.
It is in that combination of innovative customization and repeated precision that we find our passion. Inspired by tomorrow's innovation, each and every day.

member DSPE

Lasers, Light and Nanomotion

Laser 2000 Benelux C.V.
Voorbancken 13a
3645 GV Vinkeveen
Postbus 20, 3645 ZJ Vinkeveen
T +31(0)297 266 191
F +31(0)297 266 134
E info@laser2000.nl
W www.laser2000.nl

Laser 2000 Benelux considers it her mission to offer customers the latest photonics technologies available.
Our areas of expertise are:
- Lasers, scanners and laser machines for industry and research
- Light metrology instruments for LED and luminaire industries
- Light sources for scientific applications
- Piezo- and stepper motion products for nano- and micro positioning
- Inspection and research grade high speed cameras
- Laser safety certified products

Te Lintelo Systems B.V.
Mercurion 28A
6903 PZ Zevenaar
T +31 (0)316 340804
E contact@tlsbv.nl
W www.tlsbv.nl

Photonics is our passion!
Our experienced team is fully equipped to assist you with finding your best optical business solution.
For over 35 years TLS represent prominent suppliers in the photonics industry with well-educated engineers, experience and knowledge.
Over the years we became the specialist in the field of:
- Lasers
- Light metrology,
- Opto-electronic equipment,
- Positioning equipment
- Laser beam characterization and positioning,
- Interferometry,
- (Special) Optical components,
- Fiber optics,
- Laser safety

Together with our high end suppliers we have the answer for you!

member DSPE

Mechatronics Development

Sioux Mechatronics Competence Centre
De Pinckart 24
5674 CC Nuenen
T +31 (0)40 2635000
E info.ccm@sioux.eu
W www.sioux.eu

Sioux Technologies is a global technology partner that supports or acts as the R&D department for high-tech companies. We help leading companies with the development, industrialization and creation of their products, from concept stage to a prototype and/or delivery of series production. Commitment, motivation, education and skills of our employees are the solid basis for our business approach. Together with the customer, we bring high-tech to life.

member DSPE

MTA B.V.
Maisdijk 12
5704 RM Helmond
T +31 (0)492 474992
E info@m-t-a.nl
W www.m-t-a.nl

MTA is an high-tech system supplier specialized in the development and manufacturing of mechatronic machines and systems.
Our clients are OEM s in the Packaging, Food, Graphics and High-tech industries.

member DSPE

Mechatronics Development

MI-Partners
Habraken 1199
5507 TB Veldhoven
The Netherlands
T +31 (0)40 291 49 20
F +31 (0)40 291 49 21
E info@mi-partners.nl
W www.mi-partners.nl

MI-Partners is active in R&D of high-end mechatronic products and systems. We are specialised in concept generation and validation for ultra-fast (>10g), extremely accurate (sub-nanometers) or complex positioning systems and breakthrough production equipment.

member DSPE

Metal Precision Parts

Etchform BV
Arendstraat 51
1223 RE Hilversum
T +31 (0)35 685 51 94
F info@etchform.com
W www.etchform.com

Etchform is a production and service company for etched and electroformed metal precision parts.

member DSPE

Micro Drive Systems

maxon benelux
Josink Kolkweg 38
7545 PR Enschede
The Netherlands
F +31 53 744 0 713
E info@maxongroup.nl
W www.maxongroup.nl

maxon is a developer and manufacturer of brushed and brushless DC motors, as well as gearheads, encoders, controllers, and entire mechatronic systems. maxon drives are used wherever the requirements are particularly high: in NASA's Mars rovers, in surgical power tools, in humanoid robots, and in precision industrial applications, for example. To maintain its leadership in this demanding market, the company invests a considerable share of its annual revenue in research and development. Worldwide, maxon has more than 3000 employees at nine production sites and is represented by sales companies in more than 30 countries.

member DSPE

Micro Drive Systems

FAULHABER Benelux B.V.
Drive Systems
High Tech Campus 9
5656 AE Eindhoven
The Netherlands
T +31 (0)40 85155-40
E info@faulhaber.be
E info@faulhaber.nl
W www.faulhaber.com

FAULHABER specializes in the development, production and deployment of high-precision small and miniaturized drive systems, servo components and drive electronics with output power of up to 200 watts. The product range includes brushless motors, DC micromotors, encoders and motion controllers. FAULHABER also provides customer-specific complete solutions for medical technology, automatic placement machines, precision optics, telecommunications, aerospace and robotics, among other things.

Physik Instrumente (PI)
Benelux BV
Hertog Hendrikstraat 7a
5492 BA Sint-Oedenrode
The Netherlands
T +31 (0)499-375375
F +31 (0)499 375373
E benelux@pi.ws
W www.pi.ws

Stay ahead with drive components, positioners and systems by PI. In-depth knowledge, extensive experience and the broadest and deepest portfolio in high-end nanopositioning components and systems provide leading companies with infinite possibilities in motion control.

member DSPE

Motion Control Systems

Aerotech United Kingdom
The Old Brick Kiln
Ramsdell, Tadley
Hampshire RG26 5PR
UK
T +44 (0)1256 855055
F +44 (0)1256 855649
W www.aerotech.co.uk

Aerotech's motion control solutions cater a wide range of applications, including medical technology and life science applications, semiconductor and flat panel display production, photonics, automotive, data storage, laser processing, electronics manufacturing and testing.

Motion Control Systems

Newport Spectra-Physics B.V.
Vechtensteinlaan 12 - 16
3555 XS Utrecht
T +31 (0)30 6592111
E netherlands@newport.com
W www.newport.com

Newport Spectra-Physics B.V. is a subsidiary of Newport, a leader in nano and micro positioning technologies with an extensive catalog of positioning and motion control products. Newport is part of MKS Instruments Inc., a global provider of instruments, subsystems and process control solutions that measure, control, power, monitor, and analyze critical parameters of advanced processes in manufacturing and research applications.

member DSPE

Physik Instrumente (PI) Benelux BV
Hertog Hendrikstraat 7a
5492 BA Sint-Oedenrode
The Netherlands
T +31 (0)499-375375
F +31 (0)499 375373
E benelux@pi.ws
W www.pi.ws

Opt for state-of-the-art motion control systems from the world's leading provider PI. Developed, manufactured and qualified in-house by a dedicated and experienced team. Our portfolio includes a wide and deep range of components, drives, actuators and systems and offers infinite possibilities in motion control on a sub-micron and nanometer scale.

member DSPE

Optical Components

Molenaar Optics
Gerolaan 63A
3707 SH Zeist
T +31 (0)30 6951038
E info@molenaar-optics.nl
W www.molenaar-optics.eu

Molenaar Optics is offering optical engineering solutions and advanced products from world leading companies OptoSigma, Sill Optics and Graticules Optics.

member DSPE

Piezo Systems

HEINMADE BV
Heiberg 29C
NL - 5504 PA Veldhoven
T +31 (0)40 851 2180
E info@heinmade.com
W www.heinmade.com

As partner for piezo system solutions, HEINMADE serves market leaders in the high tech industry. Modules and systems are developed, produced and qualified in-house. HEINMADE distributes Noliac piezo components.

member DSPE

Piezo Systems

Physik Instrumente (PI) Benelux BV
Hertog Hendrikstraat 7a
5492 BA Sint-Oedenrode
The Netherlands
T +31 (0)499-375375
F +31 (0)499 375373
E benelux@pi.ws
W www.pi.ws

High-precision piezo systems and applications that perform on a sub-micron and nanometer scale: world leader PI develops, manufactures and qualifies these in-house. With a broad and deep portfolio with infinite possibilities in components, drives, actuators and systems at hand, our experienced team is dedicated to find the best solution for any motion control challenge.

member DSPE

Precision Electro Chemical Machining

Ter Hoek Vonkerosie
Propaanstraat 1
7463 PN Rijssen
T +31 (0)548 540807
F +31 (0)548 540939
E info@terhoek.com
W www.terhoek.com

As Application Centre we possess the required knowledge to support our clients in every phase of development and process selection.
With our own PEM800 machine we can also use PECM in-house for the benefit of our clients.

member DSPE

Ultra-Precision Metrology & Engineering

IBS Precision Engineering
Esp 201
5633 AD Eindhoven
T +31 (0)40 2901270
F +31 (0)40 2901279
E info@ibspe.com
W www.ibspe.com

IBS Precision Engineering delivers world class measurement, positioning and motion systems where ultra-high precision is required. As a strategic engineering partner to the world's best manufacturing equipment and scientific instrument suppliers, IBS has a distinguished track record of proven and robust precision solutions. Leading edge metrology is at the core of all that IBS does. From complex carbon-fibre jet engine components to semiconductor chips accurate to tens of atoms; IBS has provided and engineered key enabling technologies.

member DSPE

ADVERTISERS INDEX

Festo	Cover 2
www.festo.nl	
Heidenhain Nederland BV	Cover 4
www.heidenhain.nl	
High Tech Institute	49
www.hightechinstitute.nl	
Mikroniek Guide	51 - 54
NTS	Cover 2
www.nts-group.nl	
Oude Reimer BV	47
www.oudereimer.nl	
Ter Hoek Vonkerosie	44
www.terhoek.com	